SAPIENZA
UNIVERSITÀ DI ROMA

Dottorato di Ricerca in Energetica

– XXVI Ciclo –

Optimization of convection heat transfer in nanoparticle liquid suspensions (*nanofluids*)

Marta Cianfrini

Tutor: Prof. Massimo Corcione

Triennio accademico 2010/11 –2012/13

The present work has been possible thanks to the precious men I met during my PhD experience.

My most heartfelt thanks to prof. Massimo Corcione, for the time he devoted to convey to me his great knowledge with great generosity, and to make me see things from a new and ever more interesting point of view.

Many thanks also to Dr. Emanuele Habib and Dr. Alessandro Quintino for supporting me over the years and for making their high competence available to me with such kindness.

TABLE OF CONTENTS

INTRODUCTION

Effective cooling is one of the top challenges that high-tech manufacturing companies are continuously called to face in order to assure the reliability of their products. In fact, both the heat loads and the heat fluxes of modern devices are growing at an exponential pace as a consequence of the increasing demand for high performance and reduced size. Typical examples are represented by the microelectronics and automotive industries, just to name a few. In this connection, a considerable research effort has been dedicated to the development of advanced methods for heat transfer enhancement, such as those relying on new geometries and configurations, as well as those based on the use of extended surfaces and/or turbulators.

On the other hand, according to a wide number of recent studies, a further important contribution to the cooling issue may derive by the replacement of traditional heat transfer fluids, such as water, ethylene glycol and mineral oils, with nanofluids. These are a new type of heat transfer fluids consisting of colloidal suspensions of nanoparticles, whose effective thermal conductivity has been demonstrated to be higher than that of the corresponding pure base liquid. Actually, since their introduction, which officially occurred in 1995 at Energy Technology Division of Argonne National Laboratory (IL, USA), nanofluids have attracted the interest of an increasing number of scientists, as clearly reflected by the very large number of papers published on this topic in the last years.

However, it must be pointed out that the increase in effective thermal conductivity consequent to the dispersion of a given amount of nanoparticles into the pure base liquid is accompanied by a contemporary growth of the effective dynamic viscosity. Indeed,

although this occurrence was not often taken into due consideration, such a dynamic viscosity increase may represent a serious limitation to the energetic performance of nanofluids, either in terms of a drastic fluid motion decrease in natural convection flow situations or in terms of an exaggerated pressure drop increase in forced convection flow applications.

Accordingly, the possibility of accurately evaluating the effective thermal conductivity and dynamic viscosity of nanoparticle suspensions seems crucial to establish if their use is beneficial with respect to the pure base liquid. In fact, the equations originally developed for composites and mixtures with micro-sized and milli-sized inclusions tend to underestimate the nanofluid effective thermal conductivity and dynamic viscosity, mainly because they account only for the concentration effect. For this reason, in the last decade a number of new theoretical and empirical models have been introduced, yet most of them either fail more or less markedly in predicting the actual values of the nanofluid thermo-mechanical effective properties or have limited ranges of applicability. This has motivated the validation, in the first stage of my reserch program, of a pair of easy-to-apply empirical equations for predicting the effective thermal and mechanical properties of nanofluids, that, matching pretty well a sufficiently high number of experimental data readily available in the open literature, can be usefully employed for thermal engineering design tasks. The reliability of these correlating equations, developed by the research team I became part of during my PhD internship, has been tested by a comparative analysis with a number of relations from other authors and experimental data different from those used in generating them, showing a satisfactory degree of agreement, which will be the subject of chapter I.

Successively, studies on the energetic performance of nanofluids in natural convection internal and external flows, as well as in forced convection pipe flow, have been performed.

As regards the studies related to buoyancy-induced convection, it is worth noticing that, on the basis of the empirical equations mentioned earlier, the effective thermal conductivity increases with a slightly decreasing slope as the concentration of the suspended nanoparticles is increased, while the effective dynamic viscosity increases with a pronouncedly increasing slope. Thus, at small nanoparticle concentrations the positive effect arising from the increase of the thermal conductivity prevails upon the negative effect originating from the dynamic viscosity growth, whereas at large nanoparticle concentrations the situation is opposite. This would mean that an optimal particle loading for maximum heat transfer, that must obviously be a function of the system geometry, the operating conditions, the nanoparticle shape and size, and the solid-liquid combination, has reason to exist. Investigations have been carried out both theoretically for a differentially heated horizontal annulus and for a vertical plate and numerically for a differentially heated enclosure, with the main aim to determine the enhancement of heat transfer deriving from the dispersion of solid nanoparticles into the base liquid, as well as the optimal formulation of the nanofluid, which will be the subject of chapters II, and III, respectively.

As far as the energetic performance of nanofluids in pipe flow is concerned, it must be emphasized that all the experimental and numerical studies performed in this field by other research teams have reached the common conclusion that nanofluids offer better thermal performance than the corresponding base liquids at same Reynolds number, and that the heat transfer rate increases with increasing the concentration of the suspended nanoparticles. However, since the cited increase of the effective dynamic viscosity may imply an excessive increase in pressure drop, which, in turn, may result in an exaggerated

pumping power requirement, a better evaluation of the merits of nanofluids should be executed in terms of global energetic performance, rather than simply in terms of heat transfer enhancement. Actually, this overall point of view becomes absolutely relevant when the availability of electric energy for pumping purposes is limited or in case of battery-operated pumps. Such a topic has been treated following two options. The first option is aimed at determining how much the heat transfer rate changes as the nanoparticle concentration is increased, keeping constant the pumping power. The second option has the scope to evaluate in what measure the pumping power changes with increasing the nanoparticle concentration, for an assigned heat transfer rate. Of course, the addition of nanoparticles to the base liquid has to be considered as advantageous in all those cases in which either a heat transfer enhancement occurs at a fixed cost of operation or a lower amount of power is dissipated in friction at same thermal performance. Interestingly, also in this case optimal particle loadings are found to exist, contradicting the general belief that the more nanoparticles are dispersed into the base liquid, the better pipe flow performance is obtained. Theoretical investigations have been carried out for both laminar pipe flow and turbulent pipe flow, which will be the subject of chapter IV.

CHAPTER I
Nanofluid Effective Physical Properties

1.1 Effective thermal conductivity

The inadequacy of the traditional mean-field theories in predicting the effective thermal conductivity of nanofluids with a sufficiently good approximation, unless the temperature is about 20–25°C, has motivated the development of several new models. A number of these models assign a key role to the effect of the interfacial nanolayer, whose existence was suggested by Choi et al. [1] on the basis of the work of Yu et al. [2], [3] who reported the observation of molecular layering in a liquid at the solid/ liquid interface using X-ray reflectivity – see e.g. Yu and Choi [4], Xue [5], Xie et al. [6] and Leong et al. [7]. A second group of models incorporate two different contributions: one static and one dynamic. The former contribution depends on the composition of the nanofluid, whilst the latter contribution accounts for the effect of the micro-mixing convection caused by the Brownian motion of the nanoparticles, that is assumed to be a decisive mechanism of energy transfer – see e.g. Kumar et al. [8], Koo and Kleinstreuer [9], Jang and Choi [10], [11], Patel et al. [12], Ren et al. [13], Prasher et al. [14] and [15], Xuan et al. [16], Xu et al. [17], Prakash and Giannelis [18] and Murshed et al. [19]. Notice that the models discussed in refs. [10] and [11] and [14]-[16] consider also the role of the interfacial Kapitza resistance [20], whose temperature-discontinuity effect could degrade significantly the nanofluid heat transfer performance; in contrast, the combined effects of the Brownian motion and the interfacial nanolayer are taken into account in the models proposed in refs. [13] and [18], as well as in ref. [19] wherein the additional contributions of the nanoparticle surface chemistry and the interaction potential are also considered. Finally, other models take into account the nanoparticle aggregation that causes local percolation

effects–see e.g. Wang et al. [21], Prasher et al. [22] and Evans et al. [23]– or combine the effects of the micro-convection due to the nanoparticle Brownian motion with those due to the aggregation occurring among individual nanoparticles and/or nanoparticle clusters–see e.g. Xuan et al. [24] and Prasher et al. [25]. However, all these models exhibit large discrepancies among each other, which clearly represents a restriction to their safe applicability. Moreover, many of them include empirical constants whose values were often determined on the basis of a limited number of experimental data, or were not clearly defined.

Therefore, in the present work the nanofluid effective thermal conductivity, k_n, is calculated through the following empirical correlation derived by Corcione [26] on the basis of a wide variety of experimental data extracted from the sources listed in Table 1.1 [27], [28], [25]-[35], in which details on the nanofluid type, the size of the suspended nanoparticles, and the measuring method, are also reported:

$$\frac{k_n}{k_f} = 1 + 4.4 Re_p^{0.4} Pr_f^{0.66} \left(\frac{T}{T_{fr}} \right)^{10} \left(\frac{k_s}{k_f} \right)^{0.03} \varphi^{0.66}, \tag{1.1}$$

where k_f is the thermal conductivity of the base liquid, Re_p is the nanoparticle Reynolds number, Pr_f is the Prandtl number of the base liquid, T is the nanofluid temperature, T_{fr} is the freezing point of the base liquid, k_s is the thermal conductivity of the solid nanoparticles, and φ is the nanoparticle volume fraction.

The relationship existing between the nanoparticle volume fraction, φ, and the nanoparticle mass fractions, m, is

$$\rho_s \varphi = \rho_n m, \tag{1.2}$$

where ρ_s is the mass density of the solid nanoparticles.

Literature source	Nanofluid type	Nanoparticle size	Measuring method
Masuda et al.	TiO_2 + water	27 nm	transient hot-wire
Lee et al.	CuO + water	23.6 nm	transient hot-wire
	Al_2O_3 + water	38.4 nm	
	CuO + ethylene glycol	23.6 nm	
	Al_2O_3 + ethylene glycol	38.4 nm	
Eastman et al.	Cu + ethylene glycol	10 nm	transient hot-wire
Das et al.	CuO + water	28.6 nm	temperature oscillation
	Al_2O_3 + water	38.4 nm	
Chon et al.	Al_2O_3 + water	47 nm	transient hot-wire
Chon and Kihm	Al_2O_3 + water	47 nm	transient hot-wire
	Al_2O_3 + water	150 nm	
Murshed et al.	Al_2O_3 + water	80 nm	transient hot-wire
	Al_2O_3 + ethylene glycol	80 nm	
Mintsa et al.	CuO + water	29 nm	transient hot-wire
Duangthongsuk and Wongwises	TiO_2 + water	21 nm	transient hot-wire

Table 1.1 – Thermal conductivity experimental data used for deriving eq. (1.1).

The Reynolds number of the suspended nanoparticles is defined as

$$\mathrm{Re}_p = \frac{\rho_f u_B d_p}{\mu_f}, \tag{1.3}$$

where ρ_f and μ_f are the mass density and the dynamic viscosity of the base fluid, respectively, and d_p and u_B are the nanoparticle diameter and the nanoparticle Brownian velocity, respectively. The nanoparticle Brownian velocity u_B is calculated as the ratio between d_p and the time τ_D required to cover such a distance, that, according to Keblinski et al. [38], is

$$\tau_D = \frac{d_p^2}{6D_E} = \frac{\pi\mu_f d_p^3}{2k_b T}, \tag{1.4}$$

where D_E is the Einstein diffusion coefficient and $k_b = 1.38066\times10^{-23}$ J/K is the Boltzmann constant. Hence

$$u_B = \frac{2k_bT}{\pi\mu_f d_p^2}. \tag{1.5}$$

If we substitute eq. (1.5) into eq. (1.3), we obtain

$$Re_p = \frac{2\rho_f k_b T}{\pi\mu_f^2 d_p}. \tag{1.6}$$

Notice that in the preceding equations all the physical properties are calculated at the nanofluid temperature T.

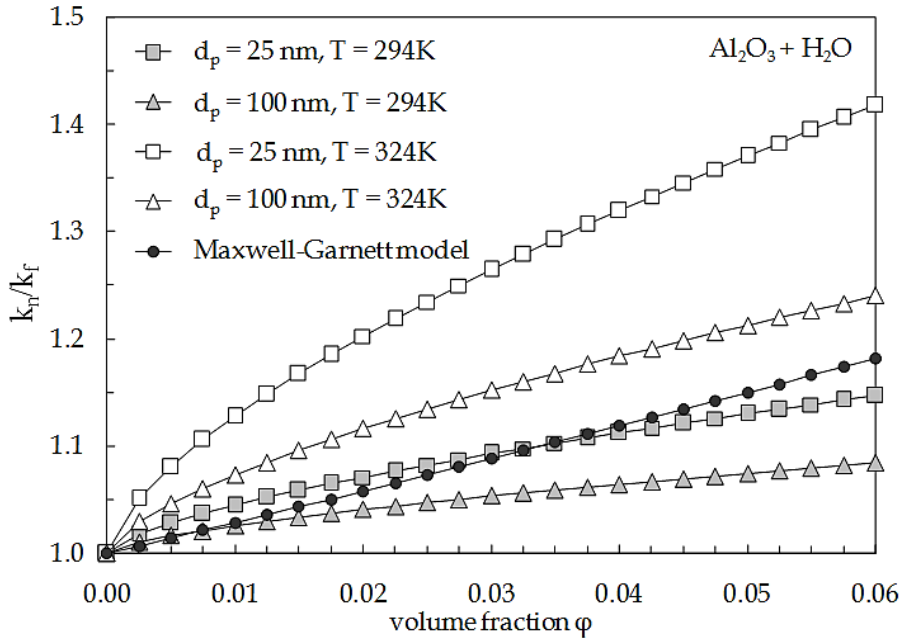

Fig. 1.1 – Distributions of k_n/k_f vs. φ for $Al_2O_3 + H_2O$, with d_p and T as parameters.

It is apparent that the thermal conductivity ratio, k_n/k_f, increases as φ and T increase, and d_p decreases. Moreover, k_n/k_f depends marginally on the solid–liquid combination, as denoted by the extremely small exponent of k_n/k_f. The distributions of k_n/k_f vs. φ that emerge from eq. (1.1) for e.g. $Al_2O_3 + H_2O$, with d_p and T as parameters, are displayed in

Fig. 1.1, where the prediction of the Maxwell-Garnett model [54] is also reported for comparison, showing that the degree of failure of this model applied to nanofluids increases as the temperature increases, and the nanoparticle size decreases.

Besides the fact that eq. (1.1) interpolates rather well a wide variety of literature data from different sources, its reliability is tested by a comparative analysis with a number of relations from other authors and experimental data different from those used in generating it [33], [51]-[53]. The results of such comparison are displayed in Figs. 1.2 and 1.3, showing a satisfactory degree of agreement.

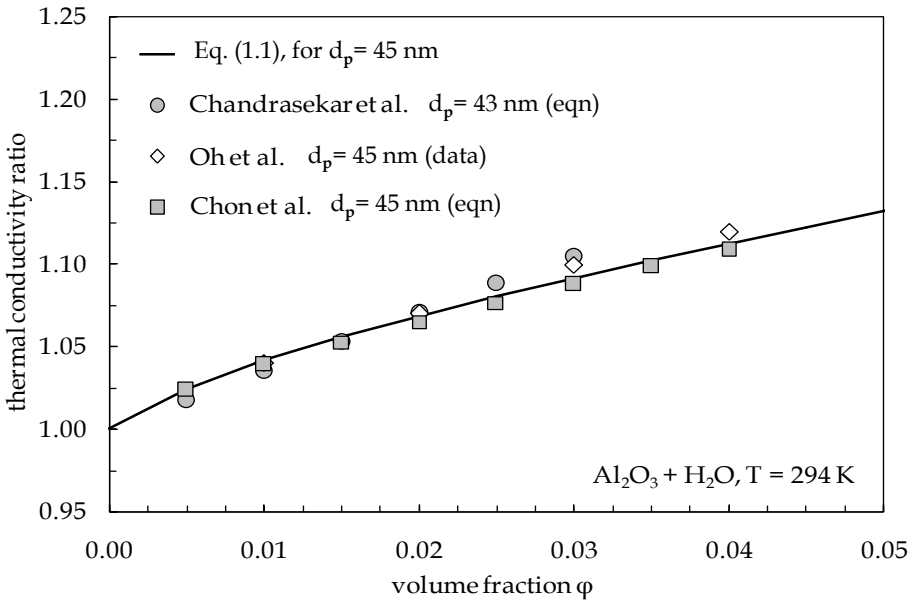

Fig. 1.2 – Comparison between the predictions of eq. (1.1) for Al_2O_3 (d_p = 45 nm) + H_2O at T = 294 K and some available literature correlations/data.

1.2 Effective dynamic viscosity

Although the traditional theories under predict significantly the effective dynamic viscosity of nanofluids, only few models have recently been proposed for describing their rheological behaviour. This is e.g. the case of the models developed by Koo [39] and Masoumi et al. [40], that account for the effects of the Brownian motion of the suspended nanoparticles, and the model proposed by Ganguly and Chakraborty [41], that is based on

the kinetics of the agglomeration–deagglomeration phenomena due to the interparticle interactions. However, as these models contain empirical correction factors based on an extremely small number of experimental data, their regions of validity are someway limited.

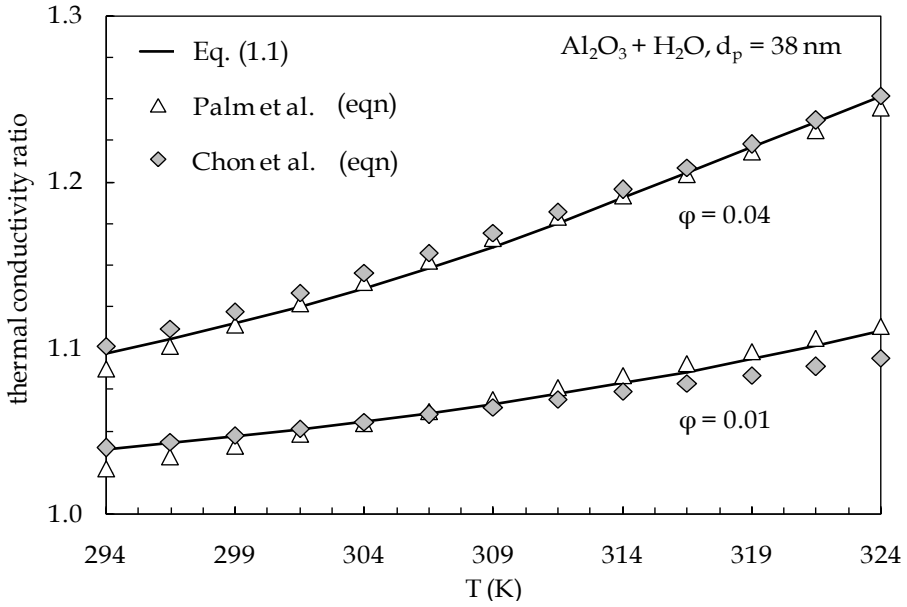

Fig. 1.3 – Comparison between the predictions of eq. (1.1) for Al_2O_3 (d_p = 38 nm) + H_2O at φ = 0.01–0.04 and some available literature correlations.

Hence, the effective dynamic viscosity, μ_n, is calculated through the following empirical correlation obtained by Corcione [26] on the basis of a large number of experimental data taken out of the studies listed in Table 1.2 [28]-[30], [42]-[50]wherein details on the nanofluid type, the size of the suspended nanoparticles, and the type of viscometer/rheometer used for measurements, are also reported:

$$\frac{\mu_n}{\mu_f} = \frac{1}{1-34.87(d_p/d_f)^{-0.3}\varphi^{1.03}}. \qquad (1.7)$$

In the above equation d_f is the equivalent diameter of a base fluid molecule calculated at the reference temperature T_0 = 293 K on the basis of the relation $M = \rho_{f0} V_m N$, where M, ρ_{f0} and V_m are the molar mass, the mass density at T_0 and the molecular volume

of the base fluid, whilst $N = 6.022 \cdot 10^{23}$ mol^{-1} is the Avogadro number. If we express V_m as $(4/3)\pi(d_f/2)^3$, we obtain:

$$d_f = 0.1\left[\frac{6M}{N\pi\rho_0}\right]^{1/3}. \tag{1.8}$$

Literature source	Nanofluid type	Nanoparticle size	Viscometer/Rheometer
Masuda et al.	TiO2 + water	27 nm	–
Pak and Cho	TiO2 + water	27 nm	cone/plate (Brookfield)
Wang et al.	Al2O3 + water	28 nm	–
Putra and co-workers	Al2O3 + water	38 nm	rotating disk-type
Prasher et al.	Al2O3 + propylene glycol	27 nm	controlled stress-type
	Al2O3 + propylene glycol	40 nm	
	Al2O3 + propylene glycol	50 nm	
He et al.	TiO2 + water	95 nm	Bohlin CVO (Malvern)
Chen et al.	TiO2 + ethylene glycol	25 nm	Bohlin CVO (Malvern)
Chevalier et al.	SiO2 + ethanol	35 nm	capillary-type
	SiO2 + ethanol	94 nm	
	SiO2 + ethanol	190 nm	
Lee et al.	Al2O3 + water	30 nm	VM-10A (CBC Co.)
Garg et al.	Cu + ethylene glycol	200 nm	AR-G2 (TA Instruments)

Table 1.2 – Dynamic viscosity experimental data used for deriving eq. (1.7).

It may be observed that the dynamic viscosity ratio, μ_n/μ_f, increases as d_p decreases and φ increases, whilst, within the limits of eq. (1.7), it is independent of both the solid–liquid combination and the temperature. The distributions of μ_n/μ_f vs. φ that emerge from eq. (1.7) for e.g. water-based nanofluids, with d_p as a parameter, are displayed in Fig. 1.4, where the predictions of the Brinkman equation [55] are additionally delineated, pointing out that the error deriving from its application to nanofluids increases remarkably with decreasing the nanoparticle size.

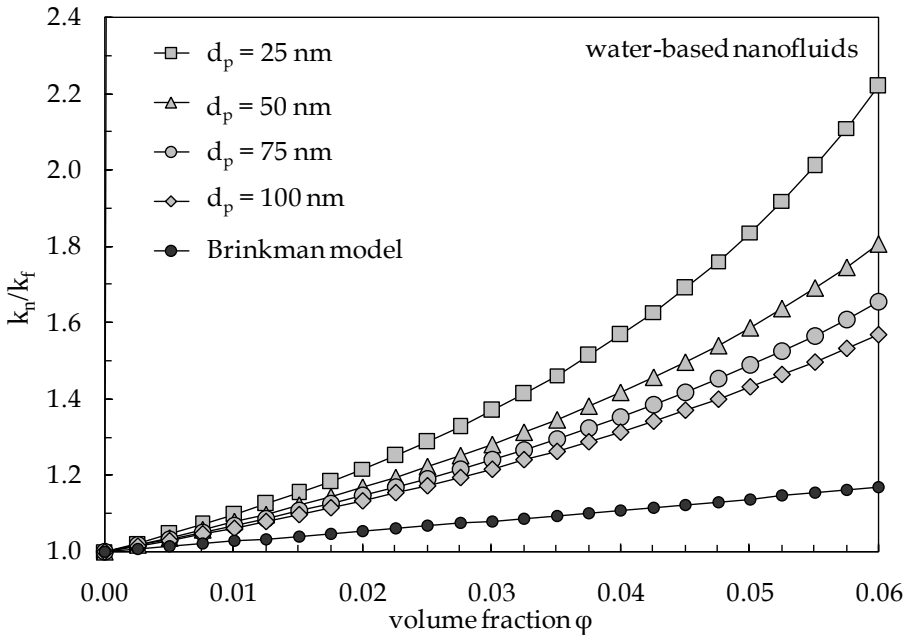

Fig. 1.4 – Distributions of μ_n/μ_f vs. φ for water-based nanofluids, with d_p as a parameter.

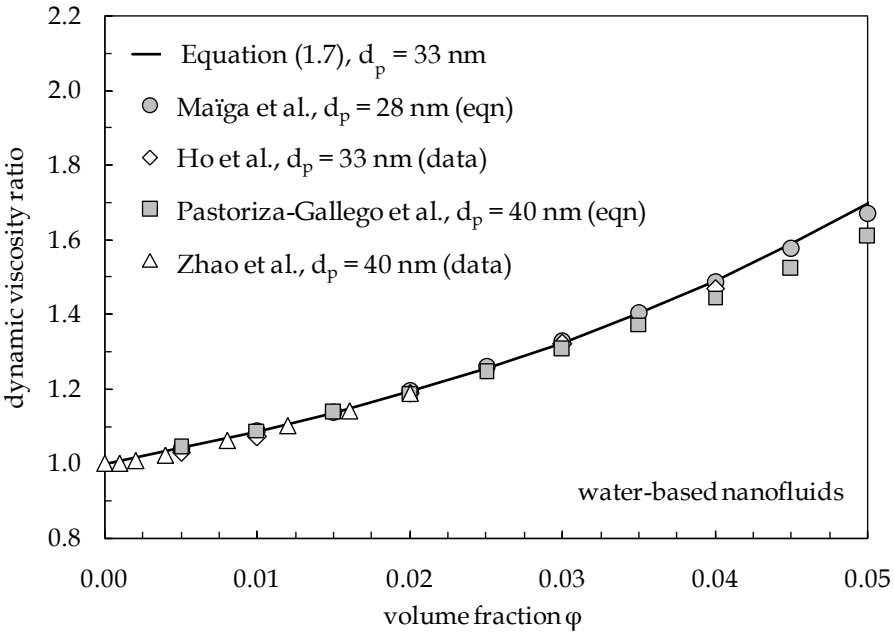

Fig. 1.5 – Comparison between the predictions of eq. (1.7) for water-based nanofluids containing nanoparticles with d_p = 33 nm and some available literature correlations/data.

As done for the effective thermal conductivity correlation, a comparative analysis is conducted to test the strength of eq. (1.7) using relations from other authors and experimental data from sources different from those listed in Table 1.2. According to such

comparative analysis, whose results are shown in Fig. 1.5, eq. (1.7) seems to be sufficiently reliable to be used for practical applications.

1.3 Other effective physical properties

The other effective physical properties of the nanofluid are calculated according to the mixing theory, as typically done in the majority of the studies performed in this field.

The effective mass density of the nanofluid, ρ_n, is given by

$$\rho_n = (1-\varphi)\rho_f + \varphi\rho_s, \tag{1.9}$$

where ρ_f and ρ_s are the mass densities of the base fluid and the solid nanoparticles, respectively.

The heat capacity at constant pressure per unit volume of the nanofluid, $(\rho c)_n$, is

$$(\rho c)_n = (1-\varphi)(\rho c)_f + \varphi(\rho c)_s, \tag{1.10}$$

where $(\rho c)_f$ and $(\rho c)_s$ are the heat capacities at constant pressure per unit volume of the base fluid and the solid nanoparticles, respectively. Accordingly, the effective specific heat at constant pressure of the nanofluid, c_n, is calculated as

$$c_n = \frac{(1-\varphi)(\rho c)_f + \varphi(\rho c)_s}{(1-\varphi)\rho_f + \varphi\rho_s}, \tag{1.11}$$

whose validity was confirmed experimentally by Zhou and Ni [56].

The effective coefficient of thermal expansion of the nanofluid, β_n, is defined by

$$(\rho\beta)_n = -\frac{d\rho_n}{dT}, \tag{1.12}$$

If we substitute eq. (1.9) into eq. (1.12), and replace the temperature derivatives of ρ_f and ρ_s with $(\rho\beta)_f$ and $(\rho\beta)_s$, respectively, we have

$$(\rho\beta)_n = (1-\varphi)(\rho\beta)_f + \varphi(\rho\beta)_s , \tag{1.13}$$

thus obtaining

$$\beta_n = \frac{(1-\varphi)(\rho\beta)_f + \varphi(\rho\beta)_s}{(1-\varphi)\rho_f + \varphi\rho_s} . \tag{1.14}$$

The distributions of the mass density ratio, ρ_n/ρ_f, the ratio between the specific heats at constant pressure, c_n/c_f, and the ratio between the coefficients of thermal expansion, β_n/β_f, plotted against the nanoparticle volume fraction for e.g. $Al_2O_3 + H_2O$ at T = 309 K, are shown in Fig. 1.6, where the distributions of the ratio between the heat capacities at constant pressure per unit volume, $(\rho c)_n/\rho_f c_f$, and the ratio between the derivatives of the mass density, $(\rho\beta)_n/(\rho\beta)_f$, are also represented.

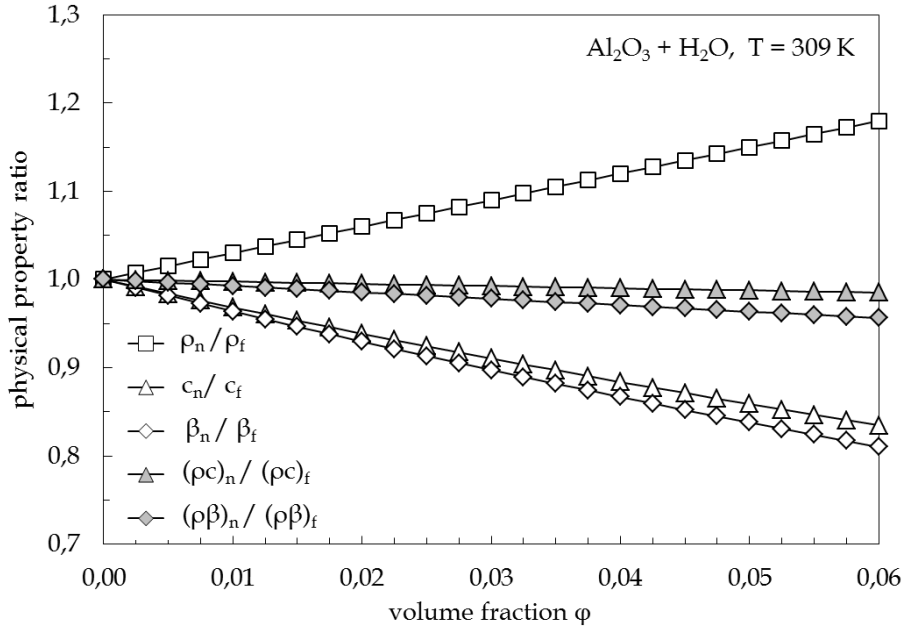

Fig. 1.6 – Distributions of the other property ratios vs. φ for $Al_2O_3 + H_2O$ at T = 309 K.

References

[1] S. U. S. Choi, Z. G. Zhang, W. Yu, F. E. Lockwood, E. A. Grulke, Anomalous thermal conductivity enhancement in nanotube suspensions, Appl. Phys. Lett. 79 (2001) 2252–2254.

[2] C.-J. Yu, A. G. Richter, A. Datta, M. K. Durbin, P. Dutta, Observation of molecular layering in thin liquid films using X-ray reflectivity, Phys Rev. Lett. 82 (1999) 2326–2329.

[3] C.-J. Yu, A. G. Richter, A. Datta, M. K. Durbin, P. Dutta, Molecular layering in a liquid on a solid substrate: an X-ray reflectivity study, Physica B 283 (2000) 27–31.

[4] W. Yu, S. U. S. Choi, The role of interfacial layers in the enhanced thermal conductivity of nanofluids: a renovated Maxwell model, J. Nanopart. Res. 5 (2003) 167–171.

[5] Xue, Q.-Z. (2003): Model for effective thermal conductivity of nanofluids. Phys. Lett. A, vol. 307, pp. 313-317.

[6] H. Xie, M. Fujii, X. Zhang, Effect of interfacial nanolayer on the effective thermal conductivity of nanoparticle-fluid mixture, Int. J. Heat Mass Transfer 48 (2005) 2926–2932.

[7] K. C. Leong, C. Yang, S. M. S. Murshed, A model for the thermal conductivity of nanofluids– the effect of interfacial layer, J. Nanopart. Res. 8 (2006) 245–254.

[8] D. H. Kumar, H. E. Patel, V. R. R. Kumar, T. Sundararajan, T. Pradeep, S. K. Das, Model for heat conduction in nanofluids, Phys. Rev. Lett. 93 (2004) 144301.

[9] J. Koo, C. Kleinstreuer, A new thermal conductivity model for nanofluids, J. Nanopart. Res. 6 (2004) 577–588.

[10] S. P. Jang, S. U. S. Choi, Role of Brownian motion in the enhanced thermal conductivity of nanofluids, Appl. Phys. Lett. 84 (2004) 4316–4318.

[11] S. P. Jang, S. U. S. Choi, Effects of various parameters on nanofluid thermal conductivity, J. Heat Transfer 129 (2007) 617–623.

[12] H. E. Patel, T. Sundararajan, T. Pradeep, A. Dasgupta, N. Dasgupta, S. K. Das, A micro-convection model for the thermal conductivity of nanofluids, Pramana – J. Phys. 65 (2005) 863–869.

[13] Y. Ren, H. Xie, A.Cai, Effective thermal conductivity of nanofluids containing spherical nanoparticles, J. Phys. D: Appl. Phys. 38 (2005) 3958–3961.

[14] R. Prasher, P. Bhattacharya, P. E. Phelan, Thermal conductivity of nanoscale colloidal solutions (nanofluids), Phys. Rev. Lett. 94 (2005) 025901.

[15] R. Prasher, P. Bhattacharya, P. E. Phelan, Brownian motion-based convective-conductive model for the effective thermal conductivity of nanofluids, J. Heat Transfer 128 (2006) 588–595.

[16] Y. Xuan, Q. Li, X. Zhang, M. Fujii, Stochastic thermal transport of nanoparticle suspensions, J. Appl. Phys. 100 (2006) 043507.

[17] J. Xu, B. Yu, M. Zou, P. Xu, A new model for heat conduction of nanofluids based on fractal distributions of nanoparticles, J. Phys. D: Appl. Phys. 39 (2006) 4486–4490.

[18] M. Prakash, E. P. Giannelis, Mechanism of heat transport in nanofluids, J. Computer-Aided Mater. Des. 14 (2007) 109–117.

[19] S. M. S. Murshed, K. C. Leong, C. Yang, A combined model for the effective thermal conductivity of nanofluids, Appl. Thermal Eng. 29 (2009) 2477–2483.

[20] P. L. Kapitza, The study of heat transfer in Helium II, J. Phys. USSR 4 (1941) 181–210.

[21] B.-X. Wang, L.-P. Zhou, X.-F. Peng, A fractal model for predicting the effective thermal conductivity of liquidwith suspension of nanoparticles, Int. J. Heat Mass Transfer 46 (2003) 2665–2672.

[22] R. Prasher, W. Evans, P. Meakin, J. Fish, P. Phelan, P. Keblinski, Effect of aggregation on thermal conduction in colloidalnanofluids, Appl. Phys. Lett. 89 (2006) 143119.

[23] W. Evans, R. Prasher, J. Fish, P. Meakin, P. Phelan, P. Keblinski, Effect of aggregation and interfacial thermal resistance on thermal conductivity of nanocomposites and colloidal nanofluids, Int. J. Heat Mass Transfer 51 (2008) 1431–1438.

[24] Y. Xuan, Q. Li, W. Hu, Aggregation structure and thermal conductivity of nanofluids, AIChE J. 49 (2003) 1038–1043.

[25] R. Prasher, P. E. Phelan, P. Bhattacharya, Effect of aggregation kinetics on the thermal conductivity of nanoscale colloidal solutions (nanofluid), Nano Letters 6 (2006) 1529–1534.

[26] M. Corcione, Empirical correlating equations for predicting the effective thermal conductivity and dynamic viscosity of nanofluids, Energy Conv. Manag. 52 (2011) 789–793.

[27] S. K. Das, N. Putra, P. Thiesen, W. Roetzel, Temperature dependence of thermal conductivity enhancement for nanofluids. J. Heat Transfer 125 (2003) 567–574.

[28] H. Masuda, A. Ebata, K. Teramae, N. Hishinuma, Alteration of thermal conductivity and viscosity of liquid by dispersing ultra-fine particles (dispersion of γ-Al_2O_3, SiO_2, and TiO_2 ultra-fine particles), NetsuBussei 4 (1993) 227–233.

[29] B. C. Pak, Y. I. Cho, Hydrodynamic and heat transfer study of dispersed fluids with submicron metallic oxide particles, Exp. Heat Transfer 11 (1998) 151–170.

[30] X. Wang, X. Xu, S. U. S. Choi, Thermal conductivity of nanoparticle-fluid mixture, J. Thermophys. Heat Transfer 13 (1999) 474–480.

[31] S. Lee, S. U. S. Choi, S. Li, J. A. Eastman, Measuring thermal conductivity of fluids containing oxide nanoparticles, J. Heat Transfer 121 (1999) 280–289.

[32] J. A. Eastman, S. U. S. Choi, S. Li, W. Yu, L. J. Thompson, Anomalously increased effective thermal conductivity of ethylene glycol-based nanofluids containing copper nanoparticles, Appl. Phys. Lett. 78 (2001) 718–720.

[33] C. H. Chon, K. D. Kihm, S. P. Lee, S. U. S. Choi, Empirical correlation finding the role of temperature and particle size for nanofluid (Al_2O_3) thermal conductivity enhancement, Appl. Phys. Lett. 87 (2005) 153107.

[34] C. H. Chon, K. D. Kihm, Thermal conductivity enhancement of nanofluids by Brownian motion, J. Heat Transfer 127 (2005) 810.

[35] S. M. S. Murshed, K. C. Leong, C. Yang, Investigations of thermal conductivity and viscosity of nanofluids, Int. J. Thermal Sciences 47 (2008) 560–568.

[36] H. A. Mintsa, G. Roy, C. T. Nguyen, D. Doucet, New temperature dependent thermal conductivity data for water-based nanofluids, Int. J. Thermal Sciences 48 (2009) 363–371.

[37] W. Duangthongsuk, S. Wongwises, Measurement of temperature-dependent thermal conductivity and viscosity of TiO_2-water nanofluids, Exp. Thermal Fluid Sciences 33 (2009) 706–714.

[38] P. Keblinski, S. R. Phillpot, S. U. S. Choi, J. A. Eastman, Mechanisms of heat flow in suspensions of nano-sized particles (nanofluids), Int. J. Heat Mass Transfer 45 (2002) 855–863.

[39] J. Koo, Computational nanofluid flow and heat transfer analyses applied to micro-systems, Dissertation Thesis, North Carolina State University, Rayleigh, NC, 2005.

[40] N. Masoumi, N. Sohrabi, A. Behzadmehr, A new model for calculating the effective viscosity of nanofluids, J. Phys. D: Appl. Phys. 42 (2009) 055501.

[41] S. Ganguly, S. Chakraborty, Effective viscosity of nanoscale colloidal suspensions, J. Appl. Phys. 106 (2009) 124309.

[42] N. Putra, W. Roetzel, S. K. Das, Natural convection of nano-fluids, Heat Mass Transfer 39 (2003) 775–784.

[43] S. K. Das, N. Putra, W. Roetzel, Pool boiling characteristics of nano-fluids, Int. J. Heat Mass Transfer 46 (2003) 851–862.

[44] Y. He, Y. Jin, H. Chen, Y. Ding, D. Cang, H. Lu, Heat transfer and flow behaviour of aqueous suspensions of TiO_2 nanoparticles (nanofluids) flowing upward through a vertical pipe, Int. J. Heat Mass Transfer 50 (2007) 2272–2281.

[45] R. Prasher, D. Song, J. Wang, P. Phelan, Measurements of nanofluid viscosity and its implications for thermal applications, Appl. Phys. Lett. 89 (2006) 133108.

[46] H. Chen, Y. Ding, Y. He, C. Tan, Rheological behaviour of ethylene glycol based titania nanofluids, Chem. Phys. Lett. 444 (2007) 333–337.

[47] H. Chen, Y. Ding, C. Tan, Rheological behaviour of nanofluids, New Journal of Physics 9 (2007) 367.

[48] J. Chevalier, O. Tillement, F. Ayela, Rheological properties of nanofluids flowing through microchannels, Appl. Phys. Lett. 91 (2007) 233103.

[49] J.-H. Lee, K. S. Hwang, S. P. Jang, B. H. Lee, J. H. Kim, S. U. S. Choi, C. J. Choi, Effective viscosities and thermal conductivities of aqueous nanofluids containing low volume concentrations of Al_2O_3 nanoparticles, Int. J. Heat Mass Transfer 51 (2008) 2651–2656.

[50] J. Garg, B. Poudel, M. Chiesa, J. B. Gordon, J. J. Ma, J. B. Wang, Z. F. Ren, Y. T. Kang, H. Ohtani, J. Nanda, G. H. McKinley, G. Chen, Enhanced thermal conductivity and viscosity of copper nanoparticles in ethylene glycol nanofluid, J. Appl. Phys. 103 (2008) 074301.

[51] M. Chandrasekar, S. Suresh, A. Chandra Bose, Experimental investigations and theoretical determinations of thermal conductivity and viscosity of Al_2O_3/water nanofluid, Exp. Thermal Fluid Sciences 34 (2010) 210-216.

[52] D. W. Oh, A. Jain, J. K. Eaton, K. E. Goodson, J. S. Lee, Thermal conductivity measurement and sedimentation detection of aluminium oxide nanofluids by using the 3ω method, Int. J. Heat Fluid Flow 29 (2008) 1456-1461.

[53] S. J. Palm, G. Roy, C. T. Nguyen, Heat transfer enhancement with the use of nanofluids in radial flow cooling systems considering temperature-dependent properties,Appl. Thermal Eng.26 (2006) 2209-2218.

[54] J. C. Maxwell-Garnett, Colours in metal glasses and in metallic films, Philos. Trans. Roy. Soc. A 203 (1904) 385–420.

[55] H. C. Brinkman, The viscosity of concentrated suspensions and solutions, J. Chem. Phys. 20 (1952) 571.

[56] S. Q. Zhou, R. Ni, Measurement of the specific heat capacity of water-based Al_2O_3nanofluid, Appl. Phys. Lett. 92 (2008) 093123.

CHAPTER II
Natural Convection in Nanofluids: Horizontal Annular Spaces and Vertical Plates. A Theoretical Approach

2.1 Introduction

Buoyancy-induced convection is the heat removal strategy often preferred by many thermal engineering designers, especially when a small power consumption, a negligible operating noise, and a high reliability of the system, are main concerns. However, the inherently poor energy efficiency of natural convection, in comparison with equivalent or similar forced convection cases, and the intrinsic low thermal conductivity of conventional coolants, such as water, ethylene glycol, and mineral oils, limit noticeably the amount of heat that can be dissipated via buoyancy-driven cooling.

In this context, in the past decades a considerable research effort has been dedicated to the development of new techniques for heat transfer enhancement, such as those based on the use of extended surfaces and/or turbulators, as well as to the study of new geometries and configurations, yet these remedies are not able to satisfy completely the severe cooling requirements of modern devices.

A possible solution to mitigate the problem is the replacement of traditional heat transfer fluids with nanofluids, i.e. liquid suspensions of nano-sized solid particles, whose effective thermal conductivity is known to be higher than that of the corresponding pure base liquid.

The majority of the papers available in the literature on convective heat transfer in nanofluids are related to forced convection flows, proving that nanoparticle suspensions have undoubtedly a great potential for heat transfer enhancement, as thoroughly discussed

in the review-articles recently compiled by Daungthongsuk and Wongwises [1], Murshed et al. [2], and Kakaç and Pramuanjaroenkij [3]. Conversely, the relatively few works performed on buoyancy-induced heat transfer in nanofluids, most of which are numerical studies dealing with enclosed flows, lead to contradictory conclusions, leaving still unanswered the question if the use of nanoparticle suspensions for natural convection applications is actually advantageous with respect to pure liquids. In fact, according to some authors, the addition of nanoparticles to a base liquid implies a more or less remarkable enhancement of the heat transfer rate, whilst, according to others, a deterioration may occur.

The reason for such conflicting results can be explained by considering that the heat transfer performance of nanofluids in natural convection flows is a strict consequence of the two opposite effects arising from the increase of the effective thermal conductivity and the increase of the effective dynamic viscosity that occur as the nanoparticle volume fraction is augmented. In other words, the dispersion of a given concentration of nanoparticles into a base liquid can bring to either an enhancement or a degradation of the heat transfer performance in buoyancy-induced flows, depending on whether the increased thermal conductivity effect is larger or smaller than the increased viscosity effect. Now, besides the experimental analysis, the approach commonly used to investigate the main heat transfer features of nanoparticle suspensions is based on the assumption that nanofluids behave more like single-phase fluids rather than like conventional solid–liquid mixtures, which means that the mass, momentum and energy transfer governing equations for pure fluids, as well as any heat transfer correlation available in the literature, can be directly extended to nanoparticle suspensions, provided that the thermophysical properties appearing in them are the nanofluid effective properties. Therefore, the use of robust theoretical models or empirical equations, capable to predict the nanofluid effective properties as more accurately as possible, is crucial for obtaining realistic data.

Unfortunately, most of the numerical studies on buoyancy-driven nanofluids based on the single-phase model miss this requirement, for one reason or another, thus leading to unreliable results. Typically, erroneous results may derive from the calculation of the effective thermal conductivity and dynamic viscosity by the Maxwell-Garnett model [4] and the Brinkman equation [5], which belong to the category of the traditional mean-field theories, originally developed for composites and mixtures with micro-sized and milli-sized inclusions. In fact, the Maxwell-Garnett model, and the other traditional models commonly used to predict the effective thermal conductivity, such as the Hamilton–Crosser model [6] and the Bruggemann model [7], appear to be suitable to this end when the nanofluid is at ambient temperature, see e.g. Eapen et al. [8] and Buongiorno et al. [9], but tend to fail dramatically when the temperature of the suspension is one or some degrees higher than 20–25°C, as e.g. shown experimentally by Das et al. [10], Li and Peterson [11], and Yu et al. [12]. On its turn, the Brinkman equation is known to underestimate the actual values of the dynamic viscosity of nanofluids, with a degree of underestimation that increases significantly as the nanoparticle diameter decreases and the nanoparticle concentration increases, as e.g. demonstrated in the experimental studies conducted by Chen et al. [13],[14] and Chevalier et al. [15]. Same considerations apply to the Einstein equation [16],[17], sometimes used instead of the Brinkman equation to evaluate the effective dynamic viscosity. Misleading conclusions may also be achieved when the nanofluid effective physical properties are evaluated by partly inconsistent semi-empirical models or by correlations based on experimental data that are inexplicably in contrast with the main body of the literature results.

In this chapter, the buoyancy-induced convection of nanofluids either confined or unconfined is studied theoretically. For the case of enclosed nanofluids, the geometry of a horizontal annular space is considered. Conversely, as far as a typical example of external configuration is concerned, the flow adjacent to a vertical plate is investigated.

In the field of natural convection of nanofluids inside the annular space existing between a pair of horizontal concentric cylinders maintained at different uniform temperatures, very few papers are readily available in the open literature, the first of which was published in 2008 by Abu-Nada et al. [32], who performed a numerical investigation reporting increased heat transfer with respect to the pure base liquid. In particular, the degree of enhancement was a function of both the Rayleigh number of the base fluid and the ratio between the thickness of the annular space and the diameter of the inner cylinder. However, the nanofluid thermal conductivity and dynamic viscosity were predicted by the Maxwell-Garnett model [4] and the Brinkman equation [5], respectively, which, as mentioned earlier, limits considerably the reliability of the results obtained.

Successively, two more numerical investigations were carried out by Abu-Nada [33], [34] for water-based nanofluids containing either Al_2O_3 or CuO suspended spherical nanoparticles having a diameter of 47 nm and 29 nm, respectively. In both studies, the nanofluid thermal conductivity was evaluated by the empirical correlation proposed by Chon et al. [35], whilst the effective dynamic viscosity was calculated by a correlation derived using the raw experimental data of Nguyen et al. [36], following the same approach previously used by Abu-Nada et al. [37] to study natural convection of nanofluids in side-heated enclosures. It was found that, for the convection dominated regime, the average Nusselt number substantially decreased with increasing the nanoparticle volume fraction, with a degree of deterioration depending on the Rayleigh number of the base fluid and the aspect ratio of the annulus, as well as on the nanoparticle material. Indeed, these results are seriously affected by an overestimation of the effective dynamic viscosity, which makes them somehow unrealistic. In fact, the dynamic viscosities measured by Nguyen and colleagues for Al_2O_3 (d_p = 47 nm) + H_2O were higher than those detected for Al_2O_3 (d_p = 36 nm) + H_2O, that is in contrast with most results available in the literature, according to which the effective dynamic viscosity is inversely

proportional to the size of the suspended nanoparticles, as e.g. found experimentally by Prasher et al. [38], and Chevalier et al. [15]. On the other hand, since the data relative to d_p= 36 nm are in substantial good agreement with the results obtained by Chevalier and co-workers for d_p = 35 nm, the data reported for Al_2O_3 (d_p = 47 nm) + H_2O tend necessarily to be overstimated. In addition, also the values of viscosity of CuO (d_p = 29 nm) + H_2O detected by Nguyen and colleagues are larger than those available in the literature for nanofluids containing nanoparticles having a similar size, which is the case of the data reported by Masuda et al. [39] for d_p = 27 nm, Pak and Cho [40] for d_p = 27 nm, and Wang et al. [41] for d_p = 28 nm. The reasons behind such overestimated values are difficult to understand, although a possible explanation may be searched in the use of an unknown surfactant which could have unusually affected the mechanical behavior of the suspensions prepared for experiments.

In the field of external natural flows in nanoparticle suspensions only three papers dealing with the basic geometry of a vertical flat plate are currently available in the literature, the first of which was published in 2007 by Polidori et al. [18], who executed a theoretical study based on the boundary layer approach. Both conditions of uniform heat flux and uniform wall temperature at the plate surface were considered. The nanofluid investigated was Al_2O_3 + H_2O, whose effective thermal conductivity was calculated by the Maxwell-Garnett model [4]. The effective dynamic viscosity was evaluated using either the Brinkman equation [5] or the equation derived by Maïga et al. [19] by way of regression analysis of the experimental data reported by Wang et al. [20] for Al_2O_3 (d_p = 28 nm) + H_2O, with the main aim to emphasize the key role of viscosity in determining the heat transfer performance of nanofluids in free convection laminar flows. It resulted that these of the Brinkman equation yielded a heat transfer enhancement for both UHF and UWT boundary conditions. In contrast, the use of the empirical correlation developed by Maïga and co-workers brought to a very slight heat transfer enhancement, around 0.6%, for

a 2.5% volume fraction of the suspended nanoparticles, followed by a deterioration trend, which was ascribed to the dominant effect of the kinematic viscosity. However, owing to the smoothness of the maximum, the authors did not give much importance to this result. Actually, as it will be shown further on, if the thermal conductivity had been calculated by a model more adherent to reality than the traditional Maxwell-Garnett model, the maximum of the heat transfer enhancement would have been much more accentuated.

Kuznetsov and Nield [21] found the similarity solutions of the boundary-layer flow using the two-phase, four-equation, nonhomogeneous equilibrium model developed by Buongiorno [22],that incorporates the effects of Brownian motion and thermophoresis. The results were presented in the form of dimensionless correlations expressing the reduced Nusselt number, i.e. the ratio between the Nusselt number and the Rayleigh number raised to the one-fourth power, as a function of a buoyancy-ratio parameter, a Brownian motion parameter, and a thermophoresis parameter, for different values of the Prandtl and Lewis numbers. In particular, for any investigated pair of the Prandtl and Lewis numbers, the reduced Nusselt number was found to be a decreasing function of each of the other three independent dimensionless parameters.

Finally, in a work based on the same theoretical approach previously used by Polidori et al. [18], Popa et al. [23] extended the investigation to the turbulent regime, and to CuO + H_2O. In this case, the effective thermal conductivity of the nanofluids was calculated by a pair of empirical correlations proposed by Mintsa et al. [24] for water-based nanofluids containing either Al_2O_3 or CuO nanoparticles having a diameter of 36–47 nm or 29 nm, respectively. As regards the prediction of the effective dynamic viscosity, the cited equation derived by Maïga et al. [19] was used for Al_2O_3 + H_2O, whereas the correlation developed by Nguyen et al. [25] on the basis of their own experimental data was adopted for CuO + H_2O. It was found that the heat transfer performance of the

nanofluid decreased with increasing the nanoparticle concentration, in both laminar and turbulent flows, much more for $CuO + H_2O$ than for $Al_2O_3 + H_2O$, which can basically be imputed to an overestimation of the viscosity effects. In this regard, it must be observed that the experimental correlation proposed by Mintsa and colleagues for predicting the thermal conductivity of $Al_2O_3 + H_2O$ was obtained using nanoparticles with an average size of 36–47 nm, whilst the viscosity equation developed by Maïga and co-workers is relative to a water suspensions of Al_2O_3 nanoparticles having a diameter of 28 nm, which necessarily implied a certain overestimation of the viscosity effects. In fact, for the same nanoparticle concentration, the overall contact surface area between smaller nanoparticles and base fluid is wider than that existing between larger nanoparticles and base fluid, thus meaning that the nanofluid containing smaller nanoparticles is characterized by a larger amount of friction occurring at the solid/liquid interface and, correspondingly, a higher effective dynamic viscosity. Notice that the increase of the effective dynamic viscosity with decreasing the diameter of the suspended nanoparticles, and then increasing the area of the solid/liquid contact surface, is largely demonstrated by a number of experimental studies readily available in the literature, such as those performed by Prasher et al. [26] and Chevalier et al. [15]. Furthermore, an additional contribution to the overestimation of the viscosity effects may originate from the fact that the effective thermal conductivities measured by Mintsa and collaborators are slightly lower than those reported by other authors for liquid suspensions of nanoparticles having a similar diameter, that is e.g. the case of the data published by Das et al. [10] and Lee et al. [29] for Al_2O_3 (d_p = 38.4 nm) + H_2O, and by Das et al. [10] for CuO (d_p = 28.6 nm) + H_2O.

Framed in this general background, the aim of the present chapter is to undertake a comprehensive theoretical studies on natural convection heat transfer in nanofluids both contained inside the horizontal annular space existing between two long concentric cylinders, whose surfaces are maintained at different uniform temperatures, and adjacent to

a vertical flat plate, whose surface is maintained at a uniform temperature, with the primary scope to determine the main heat transfer features for different operating conditions, nanoparticle diameters, and solid–liquid combinations.

2.2 Theoretical formulation of the problem

Although strictly speaking a nanofluid is a solid–liquid mixture, the approach conventionally used in most studies on this subject handles the nanofluid as a single-phase fluid. In fact, since the suspended nanoparticles have usually small size and concentration, the hypothesis of a solid–liquid mixture statistically homogeneous and isotropic can reasonably be advanced. This means that, under the further assumptions that the nanoparticles and base liquid are in local thermal equilibrium, and no slip motion occurs between the solid and liquid phases, to all intents and purposes the nanofluid can be treated as a pure fluid. Therefore, as discussed above, any single-phase heat transfer correlation available in the literature can be employed for the corresponding nanofluid application by simply replacing the thermophysical properties of the pure fluid with the nanofluid effective properties calculated at the reference temperature. Notice that a similar approach was previously used by Kim et al. [42] and Hwang et al. [43] for investigating the Rayleigh-Bénard convection of nanofluids, and later by Corcione [44], [45] for studying the main heat transfer features of buoyancy-driven nanofluids inside rectangular enclosures.

2.2.1 Horizontal annular space

For natural convection heat transfer in the annular space between long horizontal concentric cylinders maintained at different uniform temperatures, the Raithby–Hollands correlation [46], based on a large number of experimental data obtained from other authors, is usually recommended – see e.g. Bejan [47] and Incropera et al. [48]:

$$q = 0.386\frac{2\pi Lk(T_i - T_o)}{b^{3/4}\left(1/D_i^{3/5} + 1/D_o^{3/5}\right)^{5/4}}\left[\frac{Pr\,Ra_b}{0.861 + Pr}\right]^{1/4}, \qquad (2.1)$$

$$0.7 \le Pr \le 6000, \quad \frac{\left[\ln(D_o/D_i)\right]^4}{b^3\left(1/D_i^{3/5} + 1/D_o^{3/5}\right)^5} Ra_b \le 10^7,$$

where q is the heat transfer rate between the two cylinders of length L, k is the thermal conductivity of the fluid, D_i is the diameter of the inner cylinder at temperature T_i, D_o is the diameter of the outer cylinder at temperature T_o, and $b = (D_o - D_i) / 2$ is the gap width. The Rayleigh number Ra_b is based on the cylinder-to-cylinder temperature difference, $T_i - T_o$, and on the gap width, b. The fluid properties are evaluated at the reference average temperature $T_{ref} = (T_i + T_o)/2$.

Notice that eq. (2.1) may be expressed in dimensionless form by dividing q by the heat transfer rate that the motionless fluid would transmit across the gap via radial thermal conduction:

$$Nu = 0.386\frac{\ln(D_o/D_i)}{(b/D_i)^{3/4}\left[1 + (D_o/D_i)^{-3/5}\right]^{5/4}}\left[\frac{Pr\,Ra_b}{0.861 + Pr}\right]^{1/4}. \qquad (2.2)$$

If the characteristic length in the Rayleigh number is assumed to be the diameter of the inner cylinder instead of the gap width between the two cylinders, eq. (2.2) becomes:

$$Nu = 0.386\frac{\ln(D_o/D_i)}{\left[1 + (D_o/D_i)^{-3/5}\right]^{5/4}}\left[\frac{Pr\,Ra}{0.861 + Pr}\right]^{1/4}, \qquad (2.3)$$

$$\frac{\left[\ln(D_o/D_i)\right]^4}{\left[1 + (D_o/D_i)^{-3/5}\right]^5} Ra \le 10^7, \quad 0.7 \le Pr \le 6000$$

in which the Rayleigh number is $Ra = g\beta(T_i - T_o)D_i^3 / \nu\alpha$.

The Raithby–Hollands heat transfer correlation introduced above will be used to assess the effect of the nanoparticle volume fraction on the heat transfer enhancement, E, defined as

$$E = \frac{q_n}{q_f} - 1 = \frac{k_n}{k_f} \times \frac{Nu_n}{Nu_f} - 1 \quad , \tag{2.4}$$

where q_f, k_f and Nu_f are the heat transfer rate, the thermal conductivity and the Nusselt number of the base fluid, respectively, and q_n, k_n and Nu_n are the corresponding effective quantities of the nanoparticle suspension. Recall that Nu_n is the outcome of eq. (2.3), in which the Rayleigh and Prandtl numbers of the pure fluid are replaced by the nanofluid effective Rayleigh and Prandtl numbers, Ra_n and Pr_n, calculated at temperature T_{ref}.

2.2.2 Vertical plate

For natural convection heat transfer occurring between a vertical flat plate at uniform temperature T_w and the adjacent undisturbed fluid reservoir at temperature T_∞, the Churchill–Chu correlation [28], based on a large number of experimental data obtained from other authors, is usually recommended – see e.g. Bejan [29], Martynenko and Khramtsov [30], and Incropera et al. [31]:

$$Nu^{1/2} = 0.825 + 0.387 Ra^{1/6} \left[1 + \left(\frac{0.492}{Pr} \right)^{9/16} \right]^{-8/27} \quad , \; Ra \le 10^{12} \tag{2.5}$$

where the characteristic dimension in the Nusselt and Rayleigh numbers is the plate length, and the thermophysical properties are calculated at the average reference temperature

$T_{ref} = (T_w + T_\infty) / 2$.

The Churchill–Chu heat transfer correlation expressed by eq. (2.5) will then be used to assess the effect of the nanoparticle volume fraction on the heat transfer enhancement, E, defined above in eq. (2.4).

2.3 Results and discussion

The effect of the nanoparticle volume fraction, φ, on the heat transfer enhancement, E, is calculated for different values of the nanoparticle diameter, d_p, the average reference temperature of the nanofluid, T_{ref}, and the Rayleigh number of the base fluid, Ra_f, as well as for a number of combinations of solid and liquid phases.

2.3.1 Horizontal annular space

The effects of the size of the suspended nanoparticles and the nanofluid average temperature are pointed out in Figs. 2.1 and 2.2 where the distributions of the percentage heat transfer enhancement are plotted versus the solid-phase volume fraction, for different nanoparticle diameters, and different average temperatures of the nanofluid, respectively. In the same figures, the distributions of E vs. φ obtained by using the Maxwell-Garnett and Brinkman models for calculating the nanofluid effective thermal conductivity and dynamic viscosity, respectively, are also reported, confirming the weakness of these models in capturing the main features of the thermal and rheological behaviors of nanoparticle suspensions.

It may be seen that, owing to the dispersion of a progressively larger amount of nano-sized solid particles into the base liquid, the heat transfer enhancement increases up to a point, which is due to the increased effective thermal conductivity of the nanofluid. Notice that the impact of the increased effective thermal conductivity is higher when the diameter of the suspended nanoparticles is smaller and the nanofluid average temperature is higher.

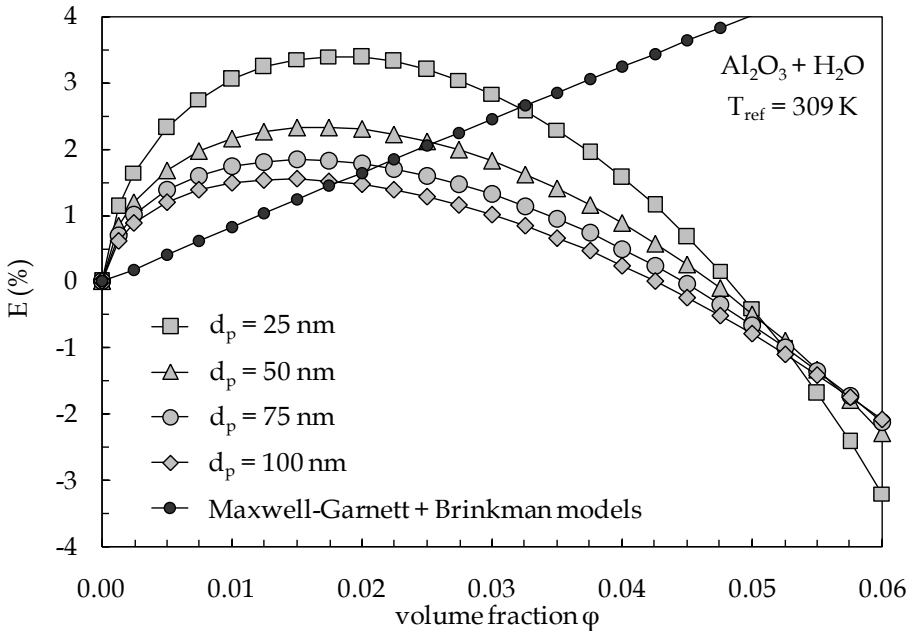

Fig. 2.1 – Distributions of E (%) vs. φ for $Al_2O_3 + H_2O$ at T_{ref} = 309 K, with d_p as a parameter.

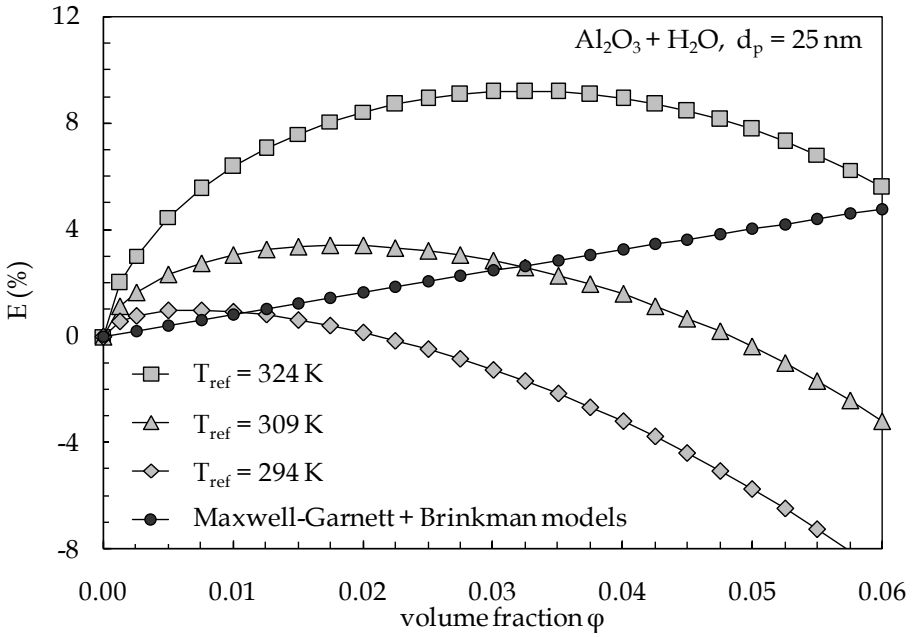

Fig. 2.2 – Distributions of E (%) vs. φ for Al_2O_3 (d_p = 25 nm) + H_2O, with T_{ref} as a parameter.

The value of φ corresponding to the peak of E is defined as the optimal particle loading φ_{opt}. As the volume fraction is further increased above φ_{opt}, the heat transfer enhancement decreases, which is due to the excessive growth of the nanofluid effective viscosity. In fact, as discussed earlier, the nanofluid behavior in natural convection flows is a consequence of the two opposite effects that originate from the contemporary increase of

the effective thermal conductivity and dynamic viscosity occurring as the nanoparticle concentration increases. The first effect, which tends to enhance the heat transfer performance, prevails at small volume fractions, whilst the second effect, which tends to degrade the heat transfer performance, prevails at large volume fractions. Obviously, when the increased viscosity effect outweighs the increased thermal conductivity effect, the heat transfer enhancement becomes negative, thus meaning that the convective thermal performance of the nanofluid is lower than that of the pure base liquid. This aspect must be taken into account should the nanofluid average temperature drop significantly below the design reference value, due to drastic climatic changes or operation in colder environments.

As far as the optimal particle loading is concerned, a set of distributions of φ_{opt} vs. T_{ref} are represented in Fig. 2.3 for different values of d_p. It may be noticed that φ_{opt} depends very slightly on the nanoparticle size, whilst it increases notably as the average temperature of the nanofluid is increased. In fact, both k_n/k_f and μ_n/μ_f increase as d_p is reduced, which entails that the effect of the nanoparticle size on φ_{opt} is quite moderate. Conversely, since k_n/k_f enhances significantly when T_{ref} is increased, whilst μ_n/μ_f keeps constant, the nanoparticle concentration at which the increase in viscosity becomes excessive magnifies with increasing the nanofluid average temperature.

Typical distributions of the percentage heat transfer enhancement at the optimal particle loading, E_{max}, are reported in Fig. 2.4, that illustrates the dependence of E_{max} on d_p with T_{ref} as a parameter, and in Fig. 2.5, that illustrates the dependence of E_{max} on T_{ref} with d_p as a parameter.

Finally, the distributions of E versus φ for different solid–liquid combinations are plotted in Fig. 2.6, showing that the effect of the base fluid is more remarkable than that of the nanoparticle material. This can be justified by considering that for many liquids the

Prandtl number is generally much larger than 0.861, which implies that, on the basis of eq. (2.3), E is a primary function of the thermal conductivity ratio, k_n/k_f, and the Rayleigh number ratio, Ra_n / Ra_f.

On the other hand, the Rayleigh number ratio is given by the ratio between $[(\rho\beta)_n / (\rho\beta)_f] \times [(\rho c_p)_n /(\rho c_p)_f]$ and $(k_n/k_f) \times (\mu_n /\mu_f)$. Thus, since both $(\rho\beta)_n / (\rho\beta)_f$ and $(\rho c_p)_n /(\rho c_p)_f$ remain practically constant with increasing φ (as previously shown in Figs. 2.8 and 2.9), the heat transfer enhancement, E, is essentially a function of the thermal conductivity ratio, k_n/k_f, and the dynamic viscosity ratio, μ_n /μ_f. Hence, taking into account that k_n/k_f depends very few on the nanoparticle material, and μ_n /μ_f is completely independent of the nanoparticle material, we can conclude that E is affected much more by the liquid phase than by the solid phase. Obviously, since the thermal conductivity of water is more than the double of the thermal conductivity of ethylene glycol, the heat transfer enhancement produced by the addition of nanoparticles to the base liquid is less marked for water than for ethylene glycol.

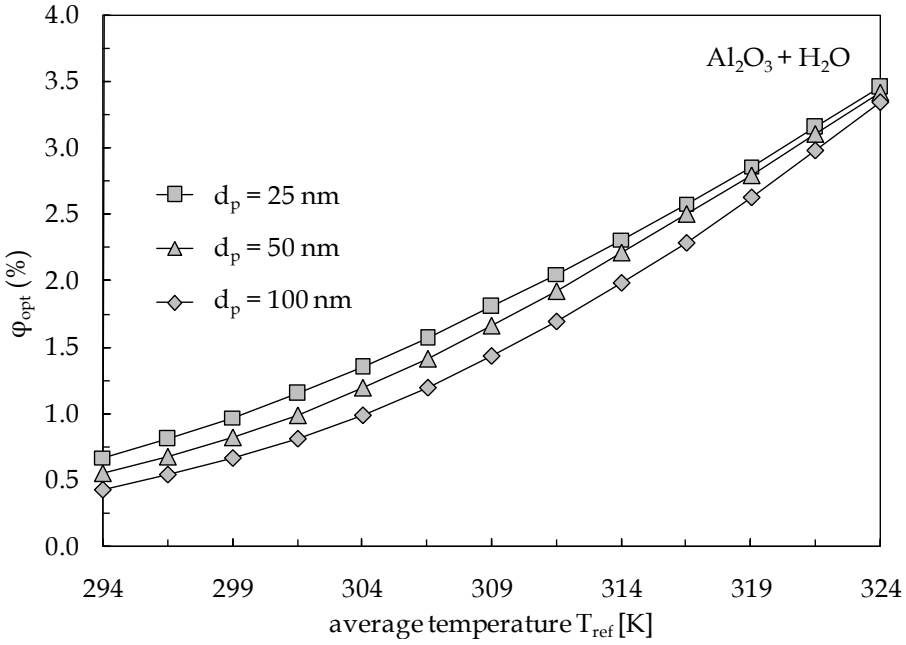

Fig. 2.3 – Distributions of φ_{opt} (%) vs. T_{ref} for $Al_2O_3 + H_2O$, with d_p as a parameter.

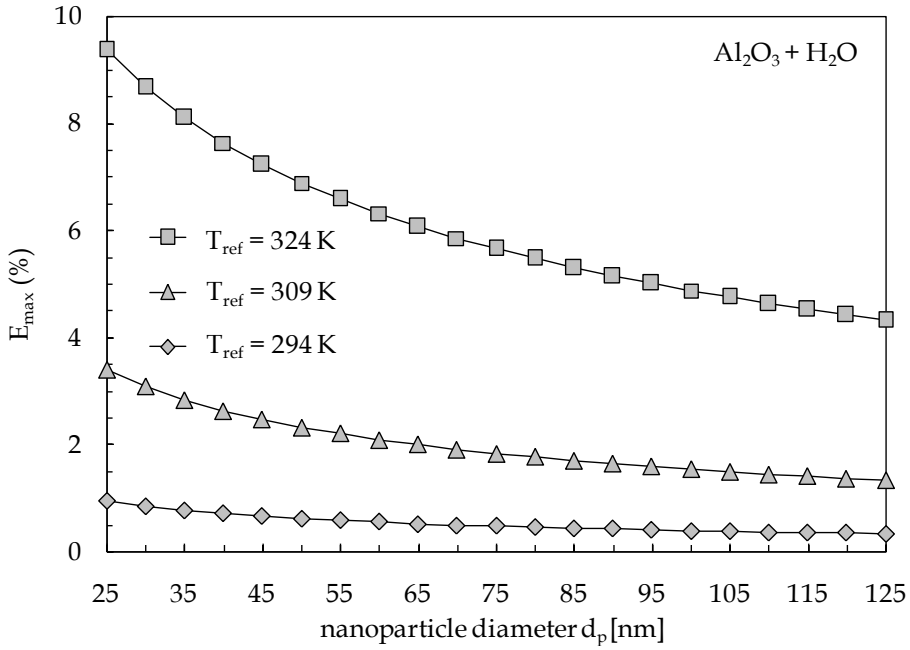

Fig. 2.4 – Distributions of E_{max} (%) vs. d_p for $Al_2O_3 + H_2O$, with T_{ref} as a parameter.

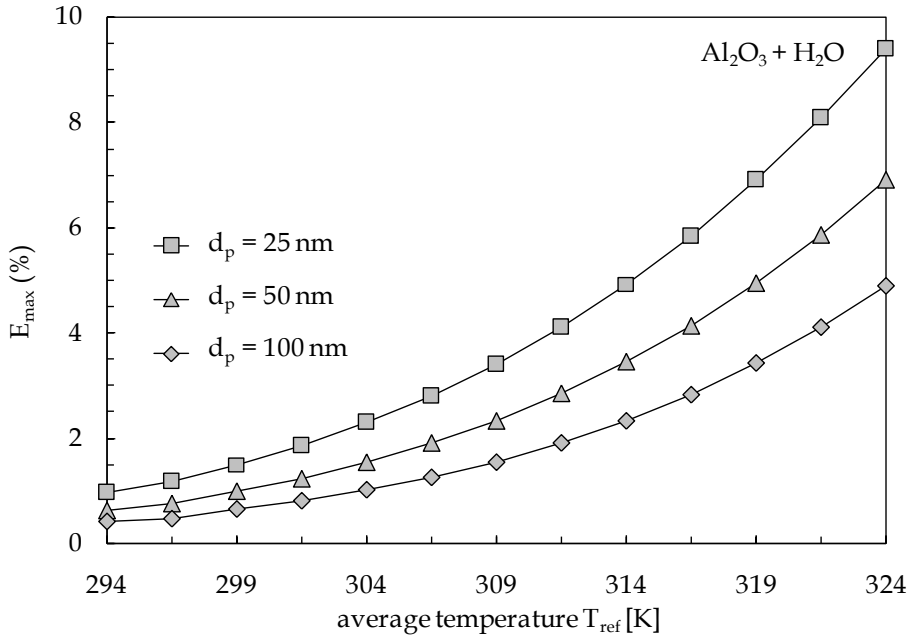

Fig. 2.5 – Distributions of E_{max} (%) vs. T_{ref} for $Al_2O_3 + H_2O$, with d_p as a parameter.

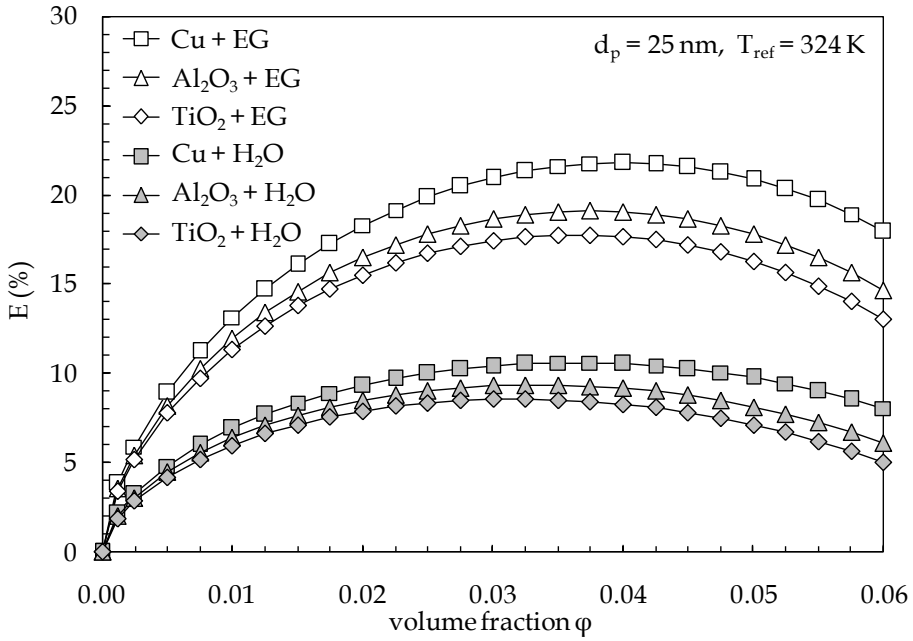

Fig. 2.6 – Distributions of E (%) vs. φ for different nanofluids, assumed d_p=25 nm and T_{ref} =324 K.

For the specific case of an annular space filled with Al_2O_3 + H_2O (that, according to literature, seems to be the nanofluid most frequently studied), a multiple regression analysis of the results obtained for the percentage optimal particle loading φ_{opt} produces the following empirical dimensional algebraic equations (see Fig. 2.7):

$$\varphi_{opt}(\%) = 0.0020\left[t_{ref}(°C)\right]^{2.093}\left[d_p(nm)\right]^{-0.2085}, \qquad (2.6)$$

$$21°C < t_{ref} \le 36°C,\ 25\,nm < d_p \le 100\,nm$$

with a 3.4% standard deviation of error and a ±6% percent range of error, and

$$\varphi_{opt}(\%) = 0.0012\left[t_{ref}(°C)\right]^{2.072}\left[d_p(nm)\right]^{-0.0560}, \qquad (2.7)$$

$$36°C < t_{ref} \le 51°C,\ 25\,nm < d_p \le 100\,nm$$

with a 2.9% standard deviation of error and a ±5% percent range of error. In the above equation, t_{ref} (°C) = T_{ref} − 273.15 is the reference average temperature of the nanofluid in Celsius degrees, and d_p (nm) is the nanoparticle diameter in nm.

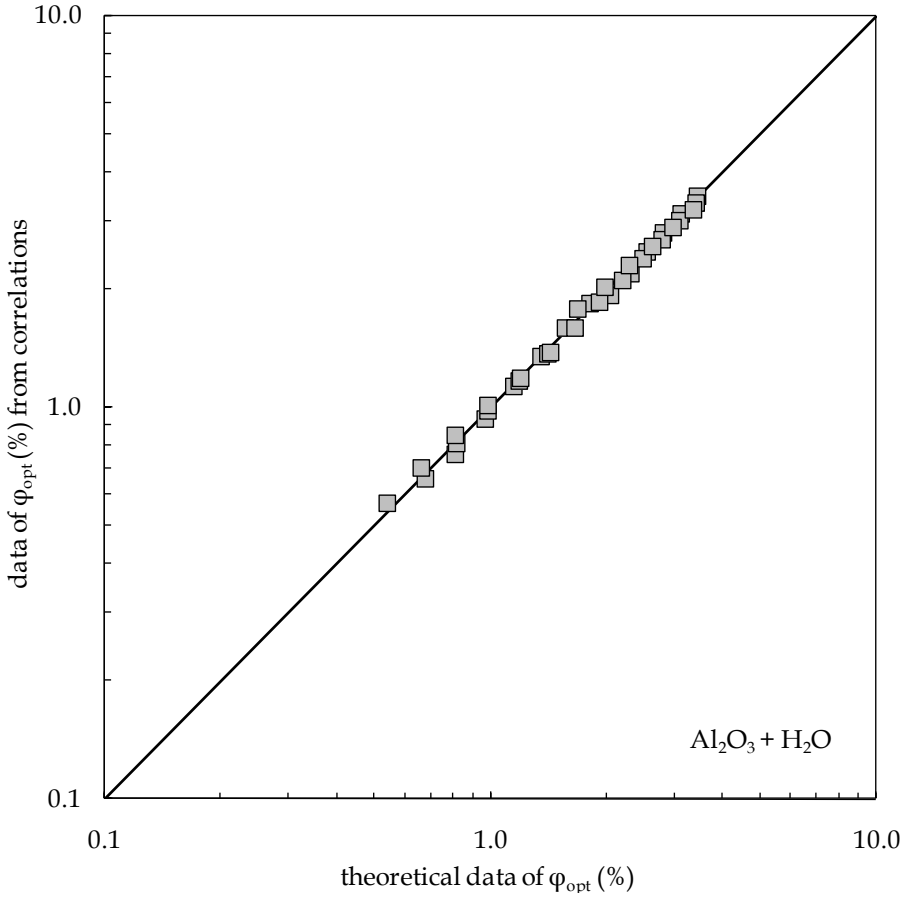

Fig. 2.7 – Comparison between eqs. (2.6)–(2.7) and the theoretical data of φ_{opt} (%).

2.3.2 Vertical plate

The distributions of the percentage heat transfer enhancement are plotted versus the solid-phase volume fraction, for different nanoparticle diameters (Fig. 2.8) and different average temperatures of the nanofluid (Fig. 2.9), pointing out the effects of the size of suspended nanoparticles and the nanofluid average temperature.

It may be seen that the curves have same trends of those reported for an annular space. Ttherefore, also for a vertical plate, it is possible to determine the optimal particle loading φ_{opt} that corresponds to the peak of E.

Distributions of E vs. φ with same trend of those reported in Figs. 2.8 and 2.9 are obtained for any other investigated Rayleigh number of the base liquid, as displayed in Fig. 2.10.

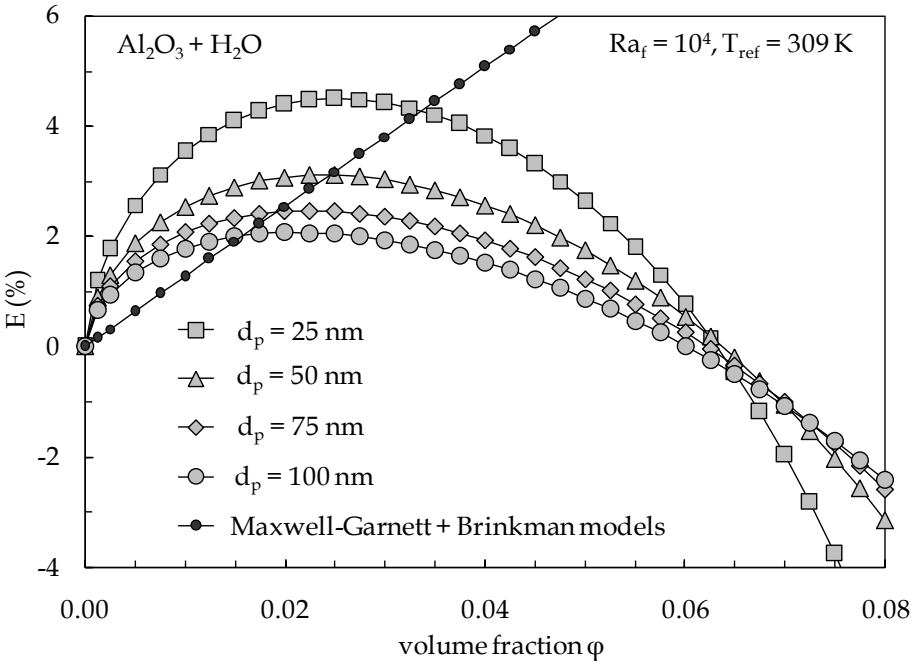

Fig. 2.8 – Distributions of E (%) vs. φ for $Al_2O_3 + H_2O$ at $Ra_f = 10^4$ for $T_{ref} = 309$ K and different values of d_p.

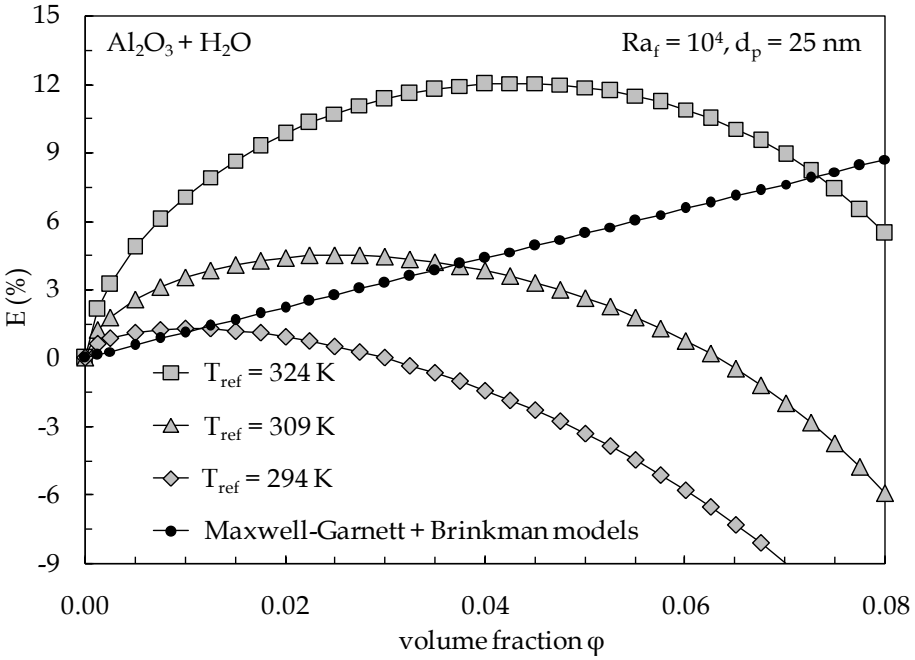

Fig. 2.9 – Distributions of E (%) vs. φ for $Al_2O_3 + H_2O$ at $Ra_f = 10^4$ for $d_p = 25$ nm and different values of T_{ref}.

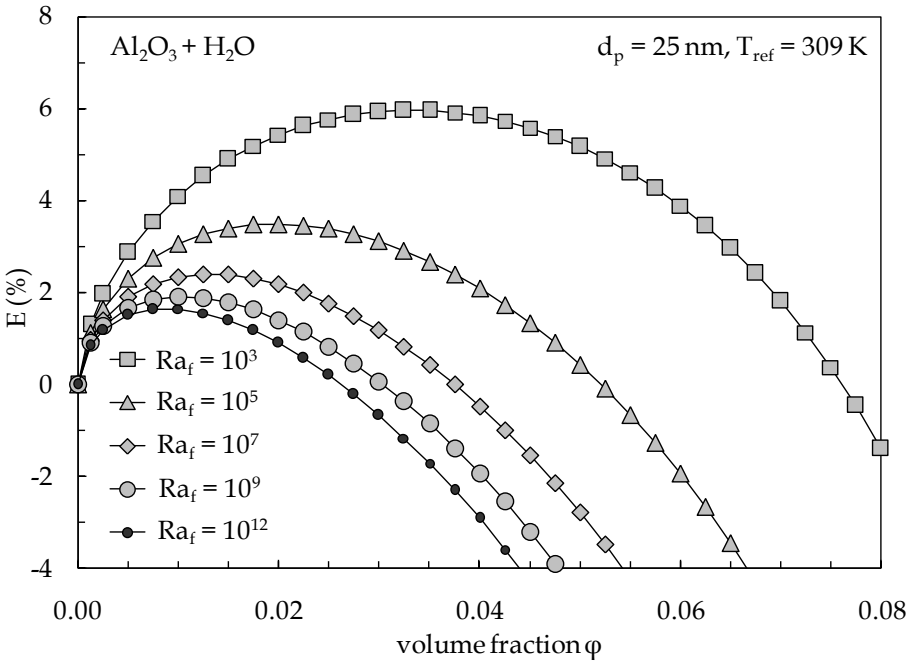

Fig. 2.10 – Distributions of E (%) vs. φ for Al_2O_3 (d_p = 25 nm) + H_2O at T_{ref} = 309 K, with Ra_f as a parameter.

It is apparent that the smaller is the Rayleigh number of the base liquid, the more pronounced is the heat transfer enhancement produced by the addition of solid nanoparticles to the base liquid. In fact, at small Rayleigh numbers the flow is featured by a low heat and momentum transfer performance, which implies that the addition of nanoparticles to the base fluid results in an increased thermal conductivity effect that prevails on the increased viscosity effect. On the contrary, at large Rayleigh numbers the flow is characterized by a high heat and momentum transfer performance, thus implying that the dispersion of nano-sized particles into the base fluid results in a more significant increased viscosity effect, that may even predominate on the increased thermal conductivity effect, especially at high volume fractions, with a consequent deterioration of the heat transfer performance.

The set of distributions of φ_{opt} vs. Ra_f reported in Fig. 2.11, for different combinations of values of d_p and T_{ref}, confirms that φ_{opt} depends very slightly on the nanoparticle size, whilst it increases as the average temperature of the nanofluid is

increased, as for an annular space. In particular, above $Ra_f = 10^4–10^5$ such weak dependence of φ_{opt} on d_p is almost linear, as e.g. shown in Fig. 2.12 for $T_{ref} = 309$ K.

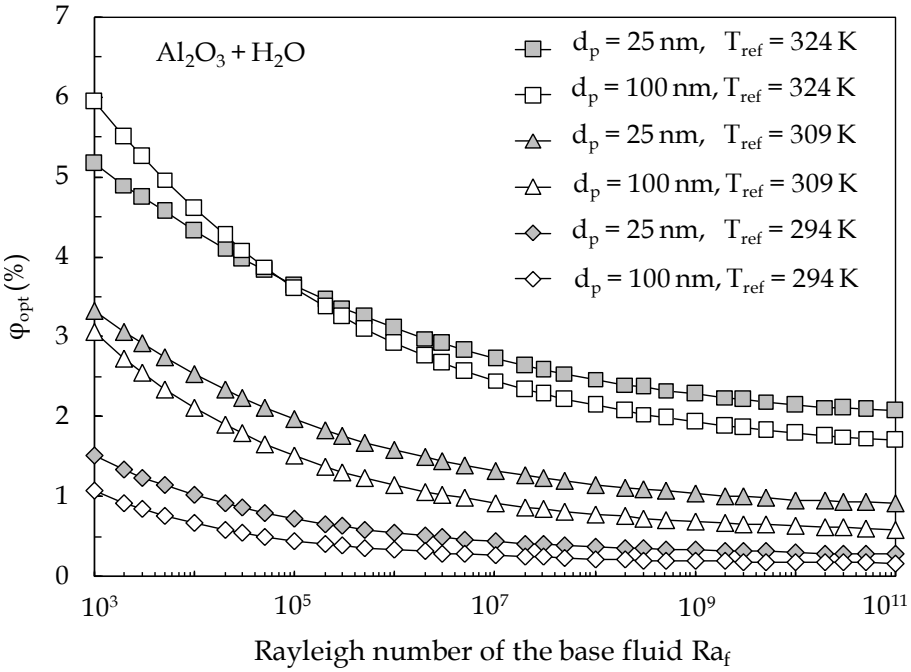

Fig. 2.11 – Distributions of φ_{opt} (%) vs. Ra_f for $Al_2O_3 + H_2O$, with d_p and T_{ref} as parameters.

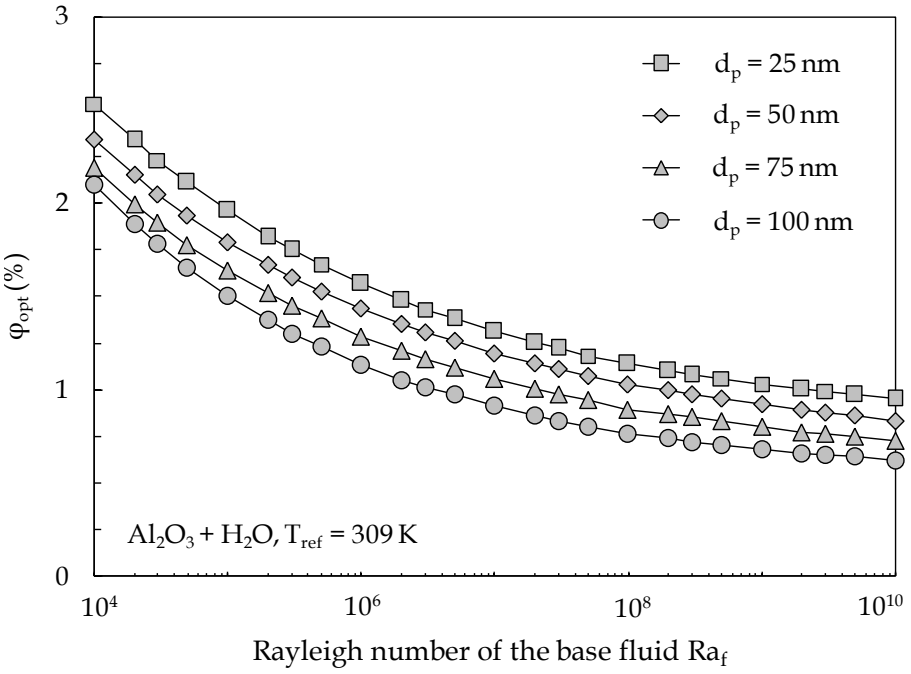

Fig. 2.12 – Distributions of φ_{opt} (%) vs. Ra_f for $Al_2O_3 + H_2O$ at $T_{ref} = 309$ K, with d_p as a parameter.

The distributions of the percentage heat transfer enhancement at the optimal particle loading, E_{max}, plotted versus the Rayleigh number of the base fluid, Ra_f, are reported in Figs. 2.13 and 2.14 for the same values of d_p and T_{ref} used in Fig. 2.11. Again, it is clear that the heat transfer enhancement consequent to the addition of nanoparticles to a base fluid is much more remarkable at small Rayleigh numbers rather than at large Rayleigh numbers of the base fluid.

Same type of conclusions related to the effects of solid–liquid combinations earlier reached for an annular space, are obtained for a vertical plate, as shown in Fig. 2.15.

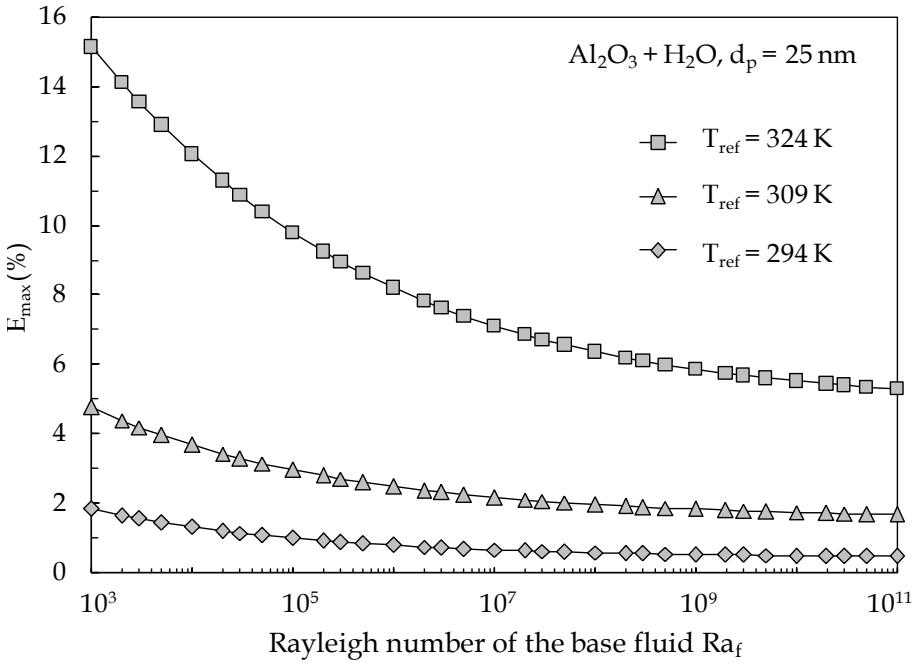

Fig. 2.13 – Distributions of E_{max} (%) vs. Ra_f for $Al_2O_3 + H_2O$ with d_p = 25 nm and different values of T_{ref}.

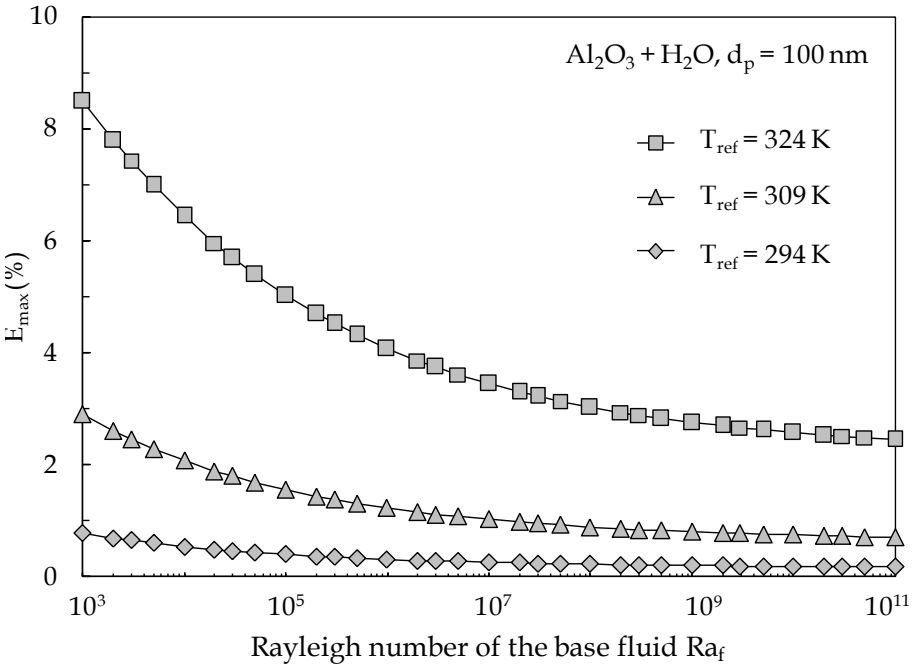

Fig. 2.14 – Distributions of E_{max} (%) vs. Ra_f for $Al_2O_3 + H_2O$ with d_p = 100 nm and different values of T_{ref}.

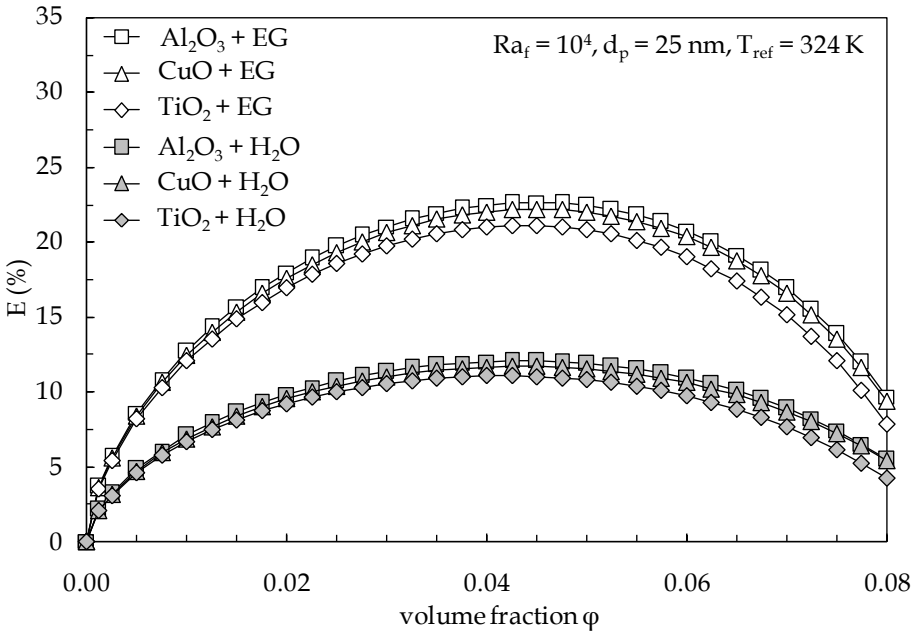

Fig. 2.15 – Distributions of E(%) vs. φ for different nanofluids, assumed $Ra_f = 10^4$, d_p = 25 nm and T_{ref} = 324 K.

For the specific case of natural convection in $Al_2O_3 + H_2O$ flowing past an isothermal vertical plate, a multiple regression analysis of the results obtained for the

percentage optimal particle loading φ_{opt} produces the following empirical dimensional equation:

$$\varphi_{opt}(\%) = \varphi_{opt-25}(\%) + [\varphi_{opt-100}(\%) - \varphi_{opt-25}(\%)] \times [d_p(\text{nm}) - 25]/75 \tag{2.8}$$

where

$$\varphi_{opt-25}(\%) = \left\{-0.00595 \times [t(°C)]^2 + 0.64178 \times t(°C) - 5.10505\right\} \times \times [\text{Log}(\text{Ra})]^{[0.01881 \times t(°C) - 1.71732]}, \tag{2.9}$$

$$\varphi_{opt-100}(\%) = \left[0.47270 \times t(°C) - 5.44482\right] \times \times [\text{Log}(\text{Ra})]^{\left\{0.00024 \times [t(°C)]^2 - 0.00241 \times t(°C) - 1.51256\right\}}. \tag{2.10}$$

The range of error of the above equation, in which d_p (nm) is the nanoparticle diameter in nm and t (°C) = T_{ref} − 273.15 is the average reference temperature of the nanofluid in Celsius degrees, is ±10%, as shown in Fig. 2.16.

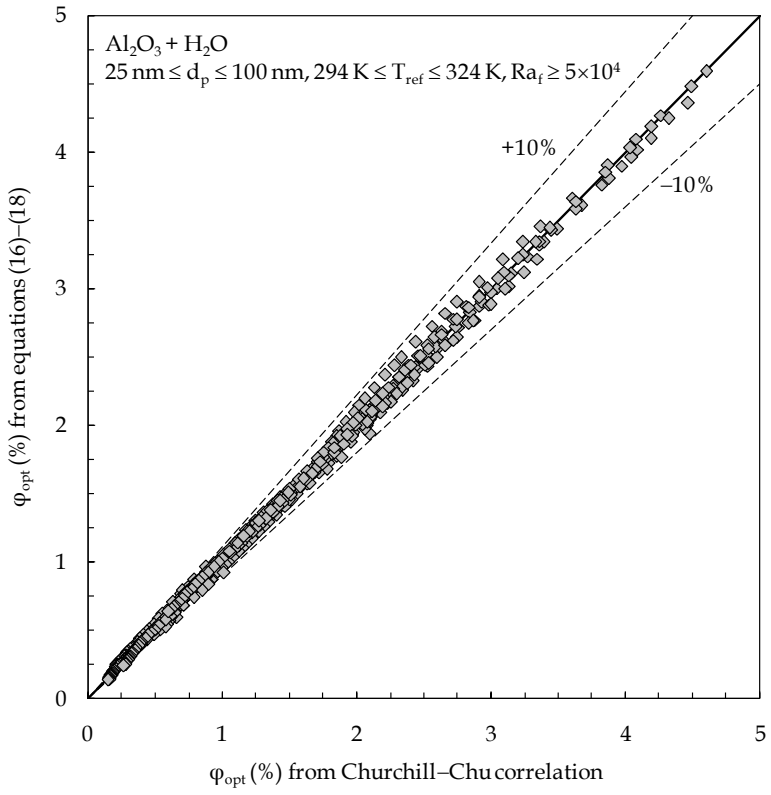

Fig. 2.16 – Comparison between eqs. (2.8)–(2.10) and the theoretical data of φ_{opt} (%).

2.4 Summary of the main results

The main results obtained may be summarized as follows:

(a) The heat transfer enhancement increases with increasing the nanoparticle volume fraction up to an optimal particle loading; excessive increases of the volume fraction above such optimal value may bring to remarkable deteriorations of the heat transfer rate at the plate surface with respect to the reference case of pure base liquid.

(b) The optimal particle loading, and the corresponding maximum heat transfer enhancement, increase as the average temperature of the nanofluid increases, and the size of the suspended nanoparticles decreases.

(c) For the vertical plate, the heat transfer enhancement is much more remarkable at small Rayleigh numbers than at large Rayleigh numbers of the base fluid.

(d) When different nanofluids are considered, the heat transfer enhancement and the optimal particle loading depend much more by the base liquid than by the nanoparticle material.

References

[1] Duangthongsuk, W., and Wongwises, S., 2007, "A critical review of convective heat transfer in nanofluids", Renewable Sustainable Energy Rev., 11, pp. 797-817.

[2] Murshed, S. M. S., Leong, K. C., and Yang, C., 2008, "Thermophysical and electrokinetic properties of nanofluids– A critical review", Applied Thermal Eng., 28, pp. 2109-2125.

[3] Kakaç, S., and Pramuanjaroenkij, A., 2009, "Review of convective heat transfer enhancement with nanofluid", Int. J. Heat Mass Transfer, 52, pp. 3187-3196.

[4] Maxwell-Garnett, J. C., 1904, "Colours in metal glasses and in metallic films", Philos. Trans. Roy. Soc. A, 203, pp. 385-420.

[5] Brinkman, H. C., 1952, "The viscosity of concentrated suspensions and solutions", J. Chem. Phys., 20, p. 571.

[6] Hamilton, R.L., and Crosser, O.K., 1962, "Thermal conductivity of heterogeneous two component systems", Ind. Eng. Chem. Fundam., 1, pp. 187 – 191.

[7] Bruggemann, D.A.G., 1935, "Berechnung Verschiedener Physikalischer Konstanten von Heterogenen Substanzen, I. Dielektrizitatskonstanten und Leitfahigkeiten der Mischkorperaus Isotropen Substanzen", Ann. Phys., 24, pp. 636 –679.

[8] Eapen, J., Williams, W. C., Buongiorno, J., Hu, L.-W., Yip, S., Rusconi, R., and Piazza, R., 2007, "Mean-field versus microconvection effects in nanofluid thermal conduction", Phys. Rev. Lett., 99, paper No. 095901.

[9] Buongiorno, J., Venerus, D. C., Prabhat, N., McKrell, T., Townsend, J., Christianson, R., Tolmachev, Y. V., Keblinski, P., Hu, L.-W., Alvarado, J. L., Bang, I. C., Bishnoi, S. W., Bonetti, M., Botz, F., Cecere, A., Chang, Y., Chen, G., Chen, H., Chung, S. J., Chyu, M. K., Das, S. K., Di Paola, R., Ding, Y., Dubois, F., Dzido, G., Eapen, J., Escher, W., Funfschilling, D., Galand, Q., Gao, J., Gharagozloo, P. E., Goodson, K. E., Gutierrez, J. G., Hong, H., Horton, M., Hwang, K. S., Iorio, C. S., Jang, S. P., Jarzebski, A. B., Jiang, Y., Jin, L., Kabelac, S., Kamath, A., Kedzierski, M. A., Kieng, L. G., Kim, C., Kim, J.-H., Kim, S., Lee, S. H., Leong, K. C., Manna, I., Michel, B., Ni, R., Patel, H. E., Philip, J., Poulikakos, D., Reynaud, C., Savino, R., Singh, P. K., Song, P., Sundararajan, T., Timofeeva, E., Tritcak, T., Turanov, A. N., Van Vaerenbergh, S., Wen, D., Witharana, S., Yang, C., Yeh, W.-H., Zhao, X.-Z.,

and Zhou, S.-Q., 2009, "A benchmark study on the thermal conductivity of nanofluids", J. Appl. Phys., 106, paper No. 094319.

[10] Das, S. K., Putra, N., Thiesen, P., and Roetzel, W., 2003, "Temperature dependence of thermal conductivity enhancement for nanofluids", J HEAT TRANS-T ASME, 125, pp. 567-574.

[11] Li, C. H., and Peterson, G. P., 2006, "Experimental investigation of temperature and volume fraction variations on the effective thermal conductivity of nanoparticle suspensions (nanofluids)", J. Appl. Phys., 99, paper No. 084314.

[12] Yu, W., Xie, H., Chen, L., and Li, Y., 2010, "Investigation on the thermal transport properties of ethylene glycol-based nanofluids containing copper nanoparticles", Powder Tecnology, 197, pp. 218-221.

[13] Chen, H., Ding, Y., and Tan, C., 2007, "Rheological behaviour of nanofluids", New J. of Physics, 9, paper No. 367.

[14] Chen, H., Ding, Y., He, Y., and Tan, C., 2007, "Rheological behaviour of ethylene glycol based titania nanofluids", Chem. Phys. Lett., 444, pp. 333-337.

[15] Chevalier, J., Tillement, O., and Ayela, F., 2007, "Rheological properties of nanofluids flowing through microchannels", Appl. Phys. Lett., 91, paper No. 233103.

[16] Einstein, A., 1906, "Eine neue Bestimmung der Molekuldimension", Ann. Phys., 19, pp. 289-306.

[17] Einstein, A., 1911, "Berichtigung zu meiner Arbeit: Eine neue Bestimmung der Molekuldimension", Ann. Phys., 34, pp. 591-592.

[18] Polidori, G., Fohanno, S., and Nguyen, C. T., 2007, "A note on heat transfer modelling of Newtonian nanofluids in laminar free convection", Int. J. Thermal Sciences, 46, pp. 739-744.

[19] Maiga, S. E. B., Nguyen, C. T., Galanis, N., and Roy, G., 2004, "Heat transfer behaviours of nanofluids in a uniformly heated tube", Superlattices and Microstruttures, 35, pp. 543-557.

[20] Wang, X., Xu, X., and Choi, S. U. S., 1999, Thermal conductivity of nanoparticle-fluid mixture", J. Thermophys. Heat Transfer, 13, pp. 474-480.

[21] Kuznetsov, A. V., and Nield, D. A., 2010, "Natural convective boundary-layer flow of a nanofluid past a vertical plate", Int. J. Thermal Sciences, 49, pp. 243-247.

[22] Buongiorno, J., 2006, "Convective transport in nanofluids", J HEAT TRANS-T ASME, 128, pp. 240-250.

[23] Popa, C.,Fohanno, S., Nguyen, C. T., and Polidori, G., 2010, "On heat transfer in external natural convection flows using two nanofluids", Int. J. Thermal Sciences, 49, pp. 901-908.

[24] Mintsa, H. A., Roy, G., Nguyen, C. T., and Doucet, D., 2009, "New temperature dependent thermal conductivity data for water-based nanofluids", Int. J. Thermal Sciences, 48, pp. 363-371.

[25] Nguyen, C.T., Desgranges, F., Roy, G., Galanis, N., Maré, T., Boucher S., and Mintsa H. A., 2007, "Temperature and particle-size dependent viscosity data for water-based nanofluids – Hysteresis phenomenon", Int. J. Fluid Flow, 28, pp. 1492-1506.

[26] Prasher, R., Song, D., Wang, J., and Phelan, P., 2006, "Measurements of nanofluid viscosity and its implications for thermal applications", Appl. Phys. Lett., 89, paper No. 133108.

[27] Lee, S., Choi, S. U. S., Li, S., and Eastman, J. A., 1999, "Measuring thermal conductivity of fluids containing oxide nanoparticles", J HEAT TRANS-T ASME, 121, pp. 280-289.

[28] Churchill, S. W., and Chu, H. H. S., 1975, "Correlating equations for laminar and turbulent free convection from a vertical plate", Int. J. Heat Mass Transfer, 18, pp. 1323-1329.

[29] Bejan, A., 2004, Convection Heat Transfer, 3rd ed., John Wiley & Sons, Inc., Hoboken, New Jersey, p. 215.

[30] Martynenko, O. G., and Khramtsov, P. P., 2005, Free-Convective Heat Transfer, Springer-Verlag, Berlin, p. 89.

[31] Incropera, F. P., DeWitt, D. P., Bergman, T. L., and Lavine, A. S., 2007, Fundamentals of Heat and Mass Transfer, 6th ed., John Wiley & Sons, Inc., Hoboken, New Jersey, p. 571.

[32] E. Abu-Nada, Z. Masoud, A. Hijazi, Natural convection heat transfer enhancement in horizontal concentric annuli using nanofluids, Int. Comm. Heat Mass Transfer 35 (2008) 657–665.

[33] E.Abu-Nada, Effects of variable viscosity and thermal conductivity of Al_2O_3-water nanofluid on heat transfer enhancement in natural convection. Int.J. Heat Fluid Flow 30 (2009) 679–690.

[34] E. Abu-Nada, Effects of variable viscosity and thermal conductivity of CuO-water nanofluid on heat transfer enhancement in natural convection: mathematical model and simulation, J. Heat Transfer 132 (2010) 052401.

[35] C. H. Chon, K. D. Kihm, S. P. Lee, S. U. S. Choi, Empirical correlation finding the role of temperature and particle size for nanofluid (Al_2O_3) thermal conductivity enhancement, Appl. Phys. Lett. 87 (2005) 153107.

[36] C. T. Nguyen, F. Desgranges, G. Roy, N. Galanis, T. Maré, S. Boucher, H. A. Mintsa, Temperature and particle-size dependent viscosity data for water-based nanofluids – Hysteresis phenomenon, Int. J. Fluid Flow 28 (2007) 1492–1506.

[37] E. Abu-Nada, Z. Masoud, H. F. Oztop, A. Campo, Effects of nanofluid variable properties on natural convection in enclosures, Int. J. Thermal Sciences 49 (2010) 479–491.

[38] R. Prasher, D. Song, J. Wang, P. Phelan, Measurements of nanofluid viscosity and its implications for thermal applications, Appl. Phys. Lett. 89 (2006) 133108.

[39] H. Masuda, A. Ebata, K. Teramae, N. Hishinuma, Alteration of thermal conductivity and viscosity of liquid by dispersing ultra-fine particles (dispersion of γ-Al_2O_3, SiO_2, and TiO_2 ultra-fine particles), NetsuBussei 4 (1993) 227–233.

[40] B. C. Pak, Y. I. Cho, Hydrodynamic and heat transfer study of dispersed fluids with submicron metallic oxide particles, Exp. Heat Transfer 11 (1998) 151–170.

[41] X. Wang, X. Xu, S. U. S. Choi, Thermal conductivity of nanoparticle-fluid mixture, J. Thermophys. Heat Transfer 13 (1999) 474–480.

[42] J. Kim, Y. T. Kang, C. K. Choi, Analysis of convective instability and heat transfer characteristics of nanofluids, Phys. Fluids 16 (2004) 2395–2401.

[43] K. S. Hwang, J.-H. Lee, S. P. Jang, Buoyancy-driven heat transfer of water-based Al_2O_3nanofluids in a rectangular cavity, Int. J. Heat Mass Transfer 50 (2007) 4003–4010.

[44] M. Corcione, Heat transfer features of buoyancy-driven nanofluids inside rectangular enclosures differentially heated at the sidewalls, Int. J. Thermal Sciences 49 (2010) 1536–1546.

[45] M. Corcione, Rayleigh-Bénard convection heat transfer in nanoparticle suspensions, Int. J. Heat Fluid Flow 32 (2011) 65–77.

[46] G. D. Raithby, K. G. T. Hollands, A general method of obtaining approximate solutions to laminar and turbulent free convection problems. In T. F. Irvine and J. P. Hartnett, Eds., Advances in Heat Transfer, vol. 11, Academic Press, New York, 1975, pp. 265–315.

[47] A. Bejan, Convection Heat Transfer, 3rd ed., John Wiley & Sons, Inc., Hoboken, New Jersey, 2004, pp. 288–290.

[48] F. P. Incropera, D. P. DeWitt, T. L. Bergman, A. S. Lavine, Fundamentals of Heat and Mass Transfer, 6th ed., John Wiley & Sons, Inc., Hoboken, New Jersey, 2007, pp. 590–591.

CHAPTER III
Natural Convection in Nanofluids: Differentially Heated Square Enclosure. An Heterogeneous Two-Phase Numerical Approach

3.1 Introduction

Natural convection of nanoparticle suspensions in enclosed spaces has recently attracted a great deal of interest in both academia and industry, as reflected by the extensive research performed in this area, mainly numerically – see, e. g., the review article recently published by Godson et al. [1].

The numerical works executed on this topic are typically based on two different approaches. The first approach is the so-called homogeneous or single-phase approach, in which nanofluids are treated as pure fluids, assuming that the solid and liquid phases are in local thermal equilibrium and no slip motion occurs between them. The second approach is known as heterogeneous or two-phase approach, wherein the effects of possible slip mechanisms occurring between suspended particles and base liquid are accounted for, which may result in a non-uniform distribution of the solid phase concentration throughout the mixture. In the two-phase approach the liquid phase is modeled using the conventional Eulerian approach, while the solid phase may be described either as a continuous phase (Eulerian–Eulerian formulation) or as a discrete phase (Eulerian–Lagrangian formulation). In the Eulerian–Eulerian formulation, one calculates the average local particle concentration and slip velocity. In the Eulerian–Lagrangian formulation, the Newton's equation of motion is solved for each individual particle.

The majority of the papers readily available in the literature are based on the single-phase approach, according to which the mass, momentum and energy transfer governing

equations for pure fluids are extended to nanofluids by simply replacing the physical properties appearing in them with the nanofluid effective properties. Moreover, in most studies such effective properties are assumed to be constant, except for the density variation in the buoyancy force term, which is calculated through the Boussinesq approximation.

In contrast, the papers based on the two-phase approach are relatively few, with a definite predominance of those relying on the transport model proposed by Buongiorno [2], which is a four-equation model (two mass equations, one momentum equation, and one energy equation) taking into account the effects of Brownian diffusion and thermophoresis as primary slip mechanisms. Also in this case, most studies are based on the assumption of constant physical properties.

Addressing our attention to natural convection in enclosures differentially heated at sides, which is undoubtedly the most investigated configuration, a summary of the numerical studies performed on this subject is reported in Table 3.1. It may be seen that only papers by Esfahani and Bordbar [8] and Bennacer [9] are based on the two-phase approach; however, in both papers the physical properties are assumed to be independent of temperature. On the other hand, the only two studies by Abu-Nada and Chamkha [6] and Abu-Nada et al. [7] wherein the temperature-dependence of the physical properties is accounted for, rely on the single-phase approach. Another observation deemed to be mentioned is that in many papers the effective thermal conductivity and dynamic viscosity are calculated by the Maxwell-Garnett model [3] and the Brinkman equation [4], respectively, which can lead to erroneous results. In fact, unless the nanofluid is at ambient temperature, the Maxwell-Garnett model tend to under-predict the increased thermal conductivity of the suspension, as e.g. shown in Das et al. [10], Li and Peterson [11], and Yu et al. [12]. Similarly, the effective dynamic viscosity of nanofluids is notably

underestimated by the Brinkman equation, as e.g. demonstrated experimentally by Chen et al. [13] and Chevalieret al. [14].

Notice that an incorrect evaluation of the effective physical properties, especially the exponential increase of the effective dynamic viscosity that occurs as the nanoparticle volume fraction is increased, leads to miss the existence of an optimal particle loading for maximum heat transfer, detected experimentally by Nnanna [15], and Ho et al. [16], and later calculated by Corcione [17] in a first-approach theoretical work. Finally, it is worth pointing out that most studies do not take into account the effects of the nanoparticle size.

Framed in this general background, a comprehensive numerical study on natural convection of alumina−water nanofluids in differentially heated square cavities is executed by a two-phase model based on Buongiorno's double-diffusion approach [2], in the hypothesis of temperature-dependent effective physical properties. Simulations are performed for different nanoparticle diameters and average concentrations, as well as different cavity sizes and wall temperatures. Primary scope of the chapter is to investigate in what measure the non-uniform distributions of both temperature and particle concentration affect the heat transfer performance of the enclosure, as well as to develop accurate correlations for predicting the heat transfer rate across the cavity and the optimal particle loading.

Year	Author(s)	Model	Properties	Nanofluid	Volume fraction	k_n (eqn / data)	μ_n (eqn / data)
2003	Khanafer et al.	single-phase	constant	Cu (d_p = 10 nm) + H_2O	0–25%	Maxwell-Garnett + Amiri and Vafai	Brinkman
2006	Jou and Tzeng	single-phase	constant	Cu (d_p = 10 nm) + H_2O	0–20%	Maxwell-Garnett + Amiri and Vafai	Brinkman
2008	Ho et al.	single-phase	constant	Al_2O_3 + H_2O	0–4%	Maxwell-Garnett or Maxwell-Garnett + Charuyakorn	Brinkman or Maïga et al.
2008	Santra et al.	single-phase	constant	Cu (d_p = 100 nm) + H_2O	0–2%	Patel et al.	Brinkman or Kwak and Kim
2008	Santra et al.	single-phase	constant	Cu (d_p = 100 nm) + H_2O	0–5%	Patel et al.	Putra et al.
2009	Abu-Nada and Oztop	single-phase	constant	Cu + H_2O	0–10%	Maxwell-Garnett	Brinkman
2009	Ghasemi and Aminossadati	single-phase	constant	CuO (d_p = 10 nm) + H_2O	0–10%	Koo and Kleistreuer	Brinkman
2010	Abu-Nada and Chamkha	single-phase	f (T)	CuO (d_p = 29 nm) + EG/H_2O	0–6%	Jang and Choi	Namburu et al.
2010	Abu-Nada et al.	single-phase	f (T)	Al_2O_3 (d_p = 47 nm) + H_2O CuO (d_p = 29 nm) + H_2O	0–6%	Chon et al.	Nguyen et al.
2010	Kahveci	single-phase	constant	Cu + H_2O Ag + H_2O Al_2O_3 + H_2O CuO + H_2O TiO_2 + H_2O	0–20%	Yu and Choi	Brinkman
2010	Lin and Violi	single-phase	constant	Al_2O_3 (d_p = 5–250 nm) + H_2O	0–5%	Xu et al.	Jang et al.
2010	Jahanshahi et al.	single-phase	constant	SiO_2 (d_p = 12 nm) + H_2O	0–4%	Maxwell-Garnett + Amiri and Vafai	Brinkman
2011	Esfahani and Bordbar	two-phase	constant	Cu + H_2O Ag + H_2O Al_2O_3 + H_2O TiO_2 + H_2O	0–10%	Maxwell-Garnett	Brinkman
2011	He et al.	single-phase	constant	Al_2O_3 + H_2O	0–4%	Maxwell-Garnett	Brinkman
2011	Kefayati et al.	single-phase	constant	SiO_2 + H_2O	0–4%	Maxwell-Garnett	Brinkman
2011	Lai and Yang	single-phase	constant	Al_2O_3 (d_p = 47 nm) + H_2O	0–4%	Mintsa et al.	Nguyen et al.
2011	Oueslati and Bennacer	two-phase	constant	Cu + H_2O Al_2O_3 + H_2O TiO_2 + H_2O	0–10%	Maxwell-Garnett	Maiga et al.
2011	Qi et al.	single-phase	constant	Cu + Ga	0–9%	Maxwell-Garnett	Brinkman
2011	Rashmi et al.	single-phase	constant	Al_2O_3 (d_p = 131.2 nm) + H_2O	0–4%	Maxwell-Garnett + Kumar et al.	Einstein
2011	Saleh et al.	single-phase	constant	Cu + H_2O Al_2O_3 + H_2O	0–5%	Maxwell-Garnett	Brinkman
2011	Yu et al.	single-phase	constant	CuO + H2O	0–4%	Koo and Kleistreuer	Koo and Kleistreuer
2012	Alloui et al.	single-phase	constant	Cu + H_2O Al_2O_3 + H_2O TiO_2 + H_2O	0–20%	Maxwell or Yu and Choi	Brinkman or Maiga et al. or Pak and Cho

Table 3.1 – Summary of the numerical studies performed on natural convection of nanofluids in enclosures differentially heated at sides.

3.2 Mathematical formulation of the problem

A square enclosure of width W filled with Al_2O_3 + H_2O is differentially heated at the vertical walls, as shown in Fig. 3.1, where the reference Cartesian coordinate system (x,y) is also represented.

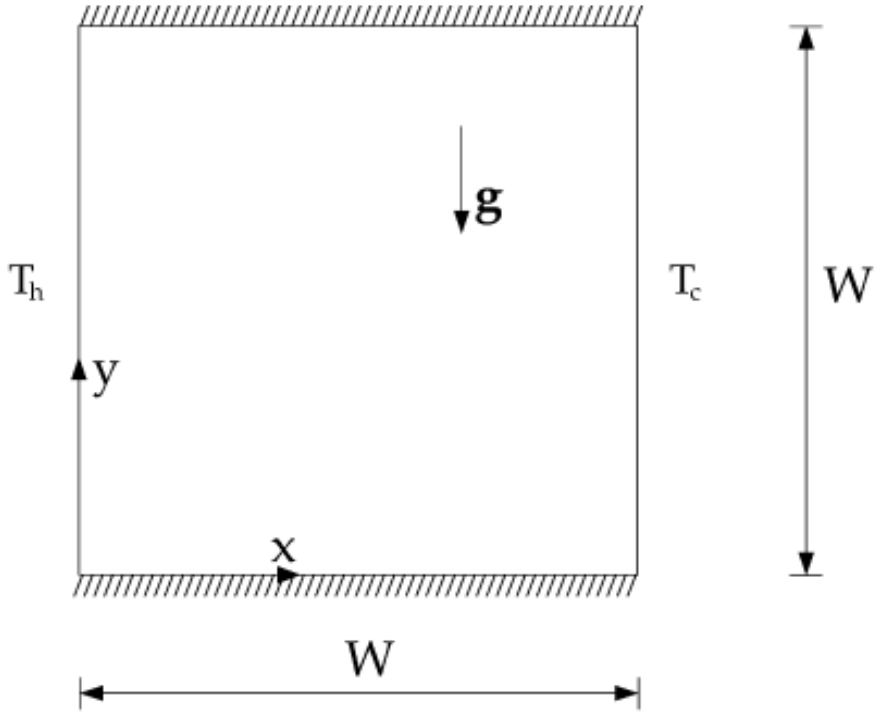

Fig. 3.1 – Sketch of the geometry and coordinate system.

The heated side is kept at a uniform temperature T_h, while the opposite cooled side is maintained at a uniform temperature T_c. The top and bottom walls are assumed to be perfectly insulated. The consequent buoyancy-induced flow is considered to be two-dimensional, laminar and incompressible, with negligible viscous dissipation and pressure work. It is assumed that the suspended nanoparticles and the base liquid are in local thermal equilibrium, and that Brownian diffusion and thermophoresis are the only slip mechanisms by which the nanoparticles can develop a significant relative velocity with respect to the base liquid (Brownian motion occurs from high to low nanoparticle concentrations, whereas thermophoresis occurs in the direction from hot to cold). Thus,

any particle-related effect is not accounted for. Actually, in elaborating his model, Buongiorno [2] considered seven different slip mechanisms: inertia, Brownian diffusion, thermophoresis, diffusiophoresis, Magnus effect, fluid drainage, and gravity settling. Yet, after a detailed analysis of the relative importance of each of them, he concluded that in the absence of turbulent effects just Brownian diffusion and thermophoresis may play an important role. Another assumption made in the derivation of the model is that the effective properties of the nanofluid vary with temperature, other than being locally dependent on the nanoparticle concentration. Finally, the heat transfer associated with the nanoparticle motion relative to the base fluid, as well as radiative heat transfer, are neglected.

In these hypotheses, the governing equations of continuity, momentum and energy for the nanofluid, and the equation of continuity for the nanoparticles, reduce to

$$\frac{\partial \rho_n}{\partial t} + \nabla \cdot (\rho_n \mathbf{V}) = 0 \tag{3.1}$$

$$\frac{\partial (\rho_n \mathbf{V})}{\partial t} + \nabla \cdot (\rho_n \mathbf{V}\mathbf{V}) = \nabla \cdot \boldsymbol{\tau} + \rho_n \mathbf{g} \tag{3.2}$$

$$\frac{\partial (\rho_n c_n T)}{\partial t} + \nabla \cdot (\rho_n \mathbf{V} c_n T) = \nabla \cdot (k_n \nabla T) \tag{3.3}$$

$$\frac{\partial (\rho_n m)}{\partial t} + \nabla \cdot (\rho_n \mathbf{V} m) = -\nabla \cdot \mathbf{J}_p \,, \tag{3.4}$$

where t is the time, **V** is the velocity vector having horizontal and vertical components U and V, $\boldsymbol{\tau}$ is the stress tensor, **g** is the gravity vector, $\mathbf{J}_p$ is the nanoparticle diffusion mass flux, T is the temperature, m is the mass fraction (also called concentration) of the suspended nanoparticles, ρ_n is the effective mass density, c_n is the effective specific heat at constant pressure, and k_n is the effective thermal conductivity. Assuming that the nanofluid has a Newtonian behaviour (see, e.g., Putra and co-workers [5], [18], Prasher et al. [19],

He et al. [20], Chen et al. [13] and Chevalier et al. [14]), the stress tensor can be expressed as

$$\boldsymbol{\tau} = -(p + \frac{2}{3}\mu_n \nabla \cdot \mathbf{V})\mathbf{I} + \mu_n[\nabla \mathbf{V} + (\nabla \mathbf{V})^t], \tag{3.5}$$

where p is the pressure, μ_n is the effective dynamic viscosity, and **I** is the unit tensor. Superscript *t* indicates the transpose of $\nabla\mathbf{V}$. The nanoparticle diffusion mass flux is calculated as the sum of the Brownian and thermophoretic diffusion terms in the hypothesis of dilute mixture (i.e., low mass fraction), thus obtaining:

$$\mathbf{J}_p = -\rho_n (D_B \nabla m + D_T \frac{\nabla T}{T}), \tag{3.6}$$

where D_B and D_T are the Brownian and thermophoretic diffusion coefficients, respectively.

The Brownian diffusion coefficient, D_B, is given by the Einstein–Stoke's equation [33]:

$$D_B = \frac{k_b T}{3\pi\mu_f d_p}, \tag{3.7}$$

in which $k_b = 1.38066 \times 10^{-23}$ J/K is the Boltzmann constant, μ_f is the dynamic viscosity of the base fluid, and d_p is the diameter of the suspended nanoparticles. The thermophoretic diffusion coefficient, D_T, can be calculated using the McNab–Meisen relationship for the thermophoretic velocity of particles dispersed in liquids [21], which leads to:

$$D_T = 0.26 \frac{k_f}{2k_f + k_s} \frac{\mu_f}{\rho_f} m, \tag{3.8}$$

where k_f is the thermal conductivity of the base fluid, k_s is the thermal conductivity of the solid nanoparticles, and ρ_f is the mass density of the base fluid. It is worth pointing out that the results obtained by MacNab and Meisen are relative to particles having diameters of 0.79 μm and 1.011 μm, which means at least one order of magnitude higher than the typical size of nanoparticles (i.e., 10–100 nm). On the other hand, as proposed by

Buongiorno [2], in the absence of thermophoretic data for nanoparticles it seems reasonable enough to extend the validity of the McNab–Meisen data to liquid suspensions of nanoparticles.

The assigned boundary conditions are: (a) $T = T_h$, $\mathbf{V} = 0$ and $\mathbf{J}_p = 0$ at the heated sidewall; (b) $T = T_c$, $\mathbf{V} = 0$ and $\mathbf{J}_p = 0$ at the cooled sidewall; and (c) $\partial T/\partial y = 0$, $\mathbf{V} = 0$ and $\mathbf{J}_p = 0$ at the top and bottom walls. The initial conditions assumed throughout the whole cavity are: (a) nanofluid at rest, i.e., $\mathbf{V} = 0$; (b) assigned uniform average mass fraction of the suspended nanoparticles, m_{av}; and (c) uniform average temperature of the nanofluid, $T_{av} = (T_c + T_h) / 2$.

3.3 Computational procedure

The system of governing equations (3.1)–(3.4) in conjunction with the boundary and initial conditions stated earlier is solved through a control-volume formulation of the finite-difference method. The pressure-velocity coupling is handled through the SIMPLE-C algorithm described by Van Doormaal and Raithby [22], which is essentially a more implicit variant of the SIMPLE algorithm developed by Patankar and Spalding [23], whose details are thoroughly described in Patankar [24]. The advection fluxes are evaluated by the QUICK discretization scheme proposed by Leonard [25]. A second-order backward scheme is used for time stepping. The computational spatial domain is filled with a non-uniform grid, having a higher concentration of grid lines near the boundary walls, and a lower uniform spacing throughout the remainder interior of the cavity. Time discretization is chosen uniform. Starting from the assigned initial fields of the dependent variables across the cavity, at each time-step the system of discretized algebraic governing equations is solved iteratively by way of a line-by-line application of the Thomas algorithm. A standard under-relaxation technique is enforced in all steps of the computational procedure to ensure adequate convergence. Within each time-step, the spatial numerical solution of

the velocity, temperature and concentration fields is considered to be converged when the maximum absolute values of the mass source, as well as the relative changes of the dependent variables at any grid-node between two consecutive iterations, are smaller than the pre-specified values of 10^{-6} and 10^{-7}, respectively. Time-integration is stopped once steady-state is reached. This means that the simulation procedure ends when the relative difference between the incoming and outgoing heat transfer rates at the heated and cooled sidewalls, and the relative changes of the time-derivatives of the dependent variables at any grid-node between two consecutive time-steps, are smaller than the pre-assigned values of 10^{-6} and 10^{-8}, respectively.

Once steady-state is reached, the heat fluxes at the heated and cooled sidewalls, Q_h and Q_c, are obtained using the following expressions

$$Q_h = -(k_n)_h \cdot \left.\frac{\partial T}{\partial x}\right|_{x=0} \tag{3.9}$$

$$Q_c = -(k_n)_c \cdot \left.\frac{\partial T}{\partial x}\right|_{x=W}, \tag{3.10}$$

wherein$(k_n)_h$ and $(k_n)_c$ are the values of the effective thermal conductivity of the nanofluid calculated at temperatures T_h and T_c, respectively. The temperature gradients in eqs. (3.9) and (3.10) are evaluated by a second-order temperature profile embracing the wall-node and the two adjacent fluid-nodes. The heat transfer rates added to the nanofluid by the heated sidewall and withdrawn from the nanofluid by the cooled sidewall, q_h and q_c, arethen calculated as

$$q_h = \int_0^W -(k_n)_h \cdot \left.\frac{\partial T}{\partial x}\right|_{x=0} dy \tag{3.11}$$

$$q_c = \int_0^W -(k_n)_c \cdot \left.\frac{\partial T}{\partial x}\right|_{x=W} dy, \tag{3.12}$$

in which the integrals are computed numerically by means of the trapezoidal rule.

The corresponding average Nusselt numbers for the heated and cooled sidewalls, Nu_h and Nu_c, are

$$Nu_h = \frac{h_h W}{(k_n)_h} = \frac{q_h}{(k_n)_h \cdot (T_h - T_c)} \tag{3.13}$$

$$Nu_c = \frac{h_c W}{(k_n)_c} = \frac{q_c}{(k_n)_c \cdot (T_c - T_h)}, \tag{3.14}$$

where h_h and h_c are the average coefficients of convection at the heated and cooled sidewalls.

Of course, since at steady-state the incoming and outgoing heat transfer rates are the same, i.e.,$q_h = -q_c = q$, the following relationship between Nu_h and Nu_c holds:

$$Nu_h (k_n)_h = Nu_c (k_n)_c . \tag{3.15}$$

Numerical tests related to the dependence of the results on the mesh spacing and time stepping have been methodically performed for several combinations of the five controlling parameters, namely m_{av}, d_p,T_c, T_h, and W. Of course, the nanofluid average temperature, T_{av}, in conjunction with the temperature difference between the cavity sides, ΔT, may be taken as independent variables instead of T_c and T_h. Additionally, the average nanoparticle volume fraction, φ_{av}, may be used as an independent variable instead of m_{av}:

$$\varphi_{av} = \left[\left(\frac{1}{m_{av}} - 1 \right) \frac{\rho_s}{\rho_f} + 1 \right]^{-1}, \tag{3.16}$$

in which the values of the mass densities ρ_s and ρ_f are calculated at temperature T_{av}.

The discretization grids and time-steps used for computations are chosen in such a way that further refinements do not produce noticeable modifications either in the heat transfer rates or in the flow and volume fraction fields. Specifically, the percentage changes of the heat transfer rates q_h and q_c, those of the maximum velocity components

U_{max} and V_{max} on the vertical and horizontal midplanes of the enclosure, and those of the maximum and minimum nanoparticle volume fractions φ_{max} and φ_{min}on the horizontal midplane of the enclosure, must be smaller than the pre-established accuracy value of 1%. The typical number of nodal points and time-step used for simulations lie in the ranges between 60× 60 and 120×120, and between 5×10^{-4} s and 10^{-2} s, respectively. Selected results of the grid sensitivity analysis are presented in Tables 3.2 and 3.3, in which the values of q_h, φ_{max}, φ_{min}, U_{max} and V_{max} relative to consecutive mesh sizes, are reported for d_p = 25 nm, T_{av} = 310 K, ΔT = 10 K and $\Delta t = 5\times10^{-3}$ s, and for φ_{av} = 0.01, T_{av} = 310 K, W = 0.015 m and $\Delta t = 5\times10^{-3}$ s, respectively.

W (m)	φ_{av}	Mesh size	q_h(W)	φ_{max}	φ_{min}	$U_{max}\times10^3$(m/s)	$V_{max}\times10^3$(m/s)
0.005	0.01	40 x 40	23.20	0.01095	0.00938	0.830	1.389
		60 x 60	23.19	0.01106	0.00932	0.833	1.403
		80 x 80	23.19	0.01110	0.00931	0.834	1.406
0.015	0.01	40 x 40	61.87	0.01128	0.00917	0.826	2.546
		60 x 60	61.75	0.01110	0.00927	0.829	2.556
		80 x 80	61.73	0.01104	0.00930	0.831	2.564
		100 x 100	61.72	0.01104	0.00932	0.832	2.571
0.015	0.04	40 x 40	60.61	0.04520	0.03678	0.790	2.272
		60 x 60	60.64	0.04475	0.03706	0.795	2.302
		80 x 80	60.66	0.04461	0.03710	0.796	2.309
		100 x 100	60.68	0.04454	0.03712	0.797	2.314

Table 3.2 – Grid sensitivity analysis for d_p = 25 nm, T_{av} = 310 K, ΔT = 10 K, $\Delta t = 5\times10^{-3}$ s.

It may be seen that a denser grid is required at larger widths of the enclosure, temperature differences between the cavity sides, and diameters of the suspended nanoparticles. Conversely, the grid-spacing is almost insensitive to the particle concentration. As far as the time stepping is concerned, its effects are displayed in Table 3.4 for φ_{av} = 0.01, d_p = 25 nm, T_{av} = 310 K, ΔT = 10 K and W = 0.015 m showing that

$\Delta\tau=5\times10^{-3}$ s represents a good compromise between solution accuracy and computation time.

Moreover, a number of test runs were also executed with the initial uniform temperature of the nanofluid set to T_c or T_h, rather than T_{av}, with the scope to determine what effect these initial conditions could have on the steady-state flow, temperature and concentration patterns. Solutions practically identical to those obtained assuming $T = T_{av}$ throughout the enclosure at time t = 0 were derived for all the configurations examined.

ΔT (K)	d_p(nm)	Mesh size	q_h(W)	φ_{max}	φ_{min}	$U_{max}\times10^3$(m/s)	$V_{max}\times10^3$(m/s)
10	25	40 x 40	61.87	0.01128	0.00917	0.826	2.546
		60 x 60	61.75	0.01110	0.00927	0.829	2.556
		80 x 80	61.73	0.01104	0.00930	0.831	2.564
		100 x 100	61.72	0.01104	0.00931	0.832	2.571
30	25	60 x 60	250.25	0.01503	0.00844	1.176	4.611
		80 x 80	250.09	0.01480	0.00848	1.174	4.627
		100 x 100	250.00	0.01462	0.00850	1.173	4.637
		120 x 120	249.93	0.01460	0.00851	1.173	4.639
30	100	80 x 80	243.37	0.01911	0.00562	1.164	4.703
		100 x 100	244.16	0.01687	0.00613	1.162	4.668
		120 x 120	244.77	0.01560	0.00639	1.161	4.647
		140 x 140	245.23	0.01557	0.00641	1.161	4.637

Table 3.3 – Grid sensitivity analysis for $\varphi_{av} = 0.01$, $T_{av} = 310$ K, W = 0.015 m, $\Delta t = 5\times10^{-3}$ s.

Mesh size	Δt (s)	q_h(W)	φ_{max}	φ_{min}	$U_{max}\times10^3$(m/s)	$V_{max}\times10^3$(m/s)
100 x 100	5×10^{-2}	61.86	0.01128	0.00917	0.831	2.546
	10^{-2}	61.73	0.01110	0.00927	0.832	2.571
	5×10^{-3}	61.72	0.01104	0.00932	0.832	2.571
	10^{-3}	61.72	0.01104	0.00935	0.832	2.571

Table 3.4 – Time-step sensitivity analysis for $\varphi_{av} = 0.01$, $d_p = 25$ nm, $T_{av} = 310$ K, ΔT = 10 K, W = 0.015 m.

Moreover, a number of test runs were also executed with the initial uniform temperature of the nanofluid set to T_c or T_h, rather than T_{av}, with the scope to determine what effect these initial conditions could have on the steady-state flow, temperature and concentration patterns. Solutions practically identical to those obtained assuming $T = T_{av}$ throughout the enclosure at time $t = 0$ were derived for all the configurations examined.

Finally, with the aim to validate the numerical code used for the present study, three different tests have been carried out.

In the first test, the steady-state solutions obtained for an air-filled differentially heated square cavity assuming $m_{av} = 0$ and constant physical properties have been compared with the benchmark results derived by de Vahl Davis [26] through a standard finite-difference method, as shown in Table 3.5.

Quantities	Present study	de Vahl Davis (BM1)	Mahdi and Kinney (BM2)	Wan et al. – FEM (BM3)	Wan et al. – DSC (BM4)
$Ra = 10^3$					
U_{max}	3.654	3.649	3.649	3.489	3.643
V_{max}	3.708	3.697	3.690	3.686	3.686
Nu	1.116	1.118	1.113	1.117	1.073
$Ra = 10^4$					
U_{max}	16.242	16.178	16.180	16.122	15.967
V_{max}	19.714	19.617	19.629	19.790	19.980
Nu	2.254	2.243	2.244	2.254	2.155
$Ra = 10^5$					
U_{max}	35.008	34.730	34.739	33.390	33.510
V_{max}	68.109	68.590	68.639	70.630	70.810
Nu	4.506	4.519	4.521	4.598	4.352
$Ra = 10^6$					
U_{max}	65.226	64.630	64.836	65.400	65.550
V_{max}	221.598	219.360	220.461	227.110	227.240
Nu	8.879	8.800	8.825	8.976	8.632

Table 3.5 – Comparison of the present solutions with the benchmark solutions of de Vahl Davis, Mahdi and Kinney + Hortman et al., Wan et al. by FEM, and Wan et al. by DSC for a differentially heated square cavity at steady state.

It may be seen that the average Nusselt numbers as well as the maximum horizontal and vertical dimensionless velocity components, on the vertical and horizontal midplanes of the enclosure, respectively, are well within 1% of the benchmark data listed in column BM1. The following extra benchmark solutions are also reported for further comparison: (a) the results obtained through finite-volume methods by Mahdi and Kinney [27] for Ra = 10^3 and by Hortman et al. [28] for Ra = 10^4–10^6 are listed in column BM2; (b) the results obtained through a finite-element method by Wan et al. [29] are listed in column BM3; (c) the results obtained through a discrete singular convolution algorithm by Wan et al. [29] are listed in column BM4.

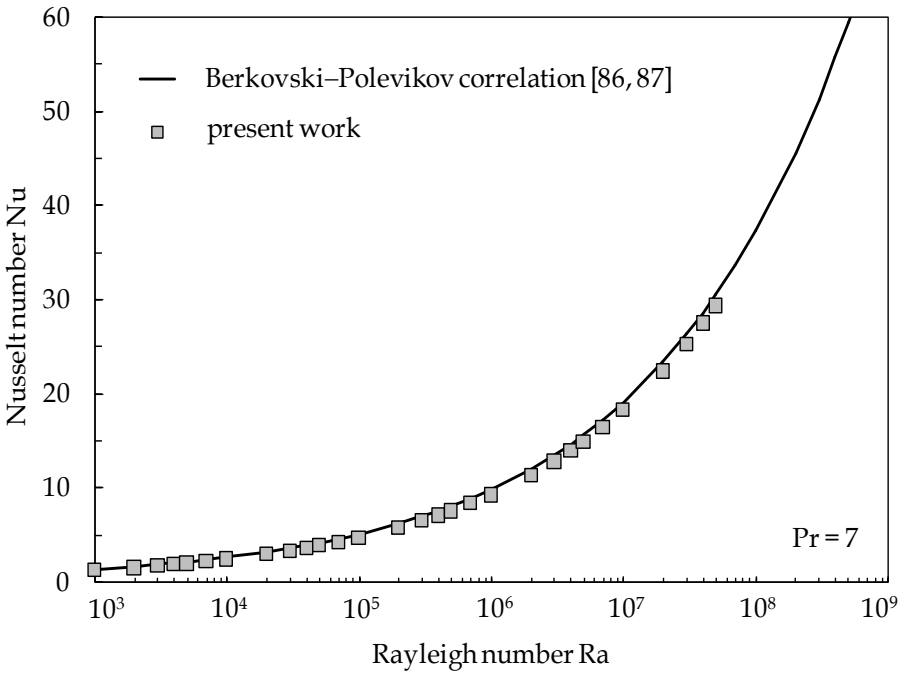

Fig. 3.2 – Comparison between the present numerical results and the Berkovsky–Polevikov correlation for a water-filled square enclosure differentially heated at sides.

In the second test, the values of the average Nusselt number computed numerically for Pr = 7 (which corresponds to water at T_{av} = 293 K) and Rayleigh numbers in the range 10^3–5×10^7 (calculated using a fixed ΔT = 20 K) have been compared with the usually recommended Berkovsky–Polevikov correlating equation based on experimental and

numerical data of laminar natural convection in a rectangular cavity heated and cooled from the side with an aspect ratio near unity (see, e.g., Bejan [30] and Incropera et al. [31]). The comparative analysis, displayed in Fig. 3.2, demonstrates that the correspondence between numerical results and literature data is widely satisfactory.

In the third test, the solutions obtained for the steady-state double-diffusive convection occurring in a square cavity filled with an air–pollutant mixture having constant physical properties, submitted to horizontal temperature and concentration gradients, have been compared with the numerical data published by Béghein et al. [32], as reported in Tables 3.6 –3.8. Also in this case, a good agreement between the present results and the literature data is apparent.

$Ra_T = 10^7$, Le = 1, Pr = 0.71, opposing flows		
Ra_S	Nu, Sh (Present study)	Nu, Sh (Béghein et al.)
10^5	16.47	16.40
10^6	16.04	16.00
5×10^6	13.63	13.60
5×10^7	23.80	23.70

Table 3.6 – Comparison of the present solutions with the solutions of Béghein et al. [32]: average Nusselt and Sherwood numbers at the hot sidewall for different values of the solutal Rayleigh number Ra_S.

$Ra_T = 10^7$, $Ra_S = 10^5$, Pr = 0.71, opposing flows		
Le	Nu, Sh (Present study)	Nu, Sh (Béghein et al.)
0.5	10.70	11.00
1	16.47	16.40
5	29.20	28.70

Table 3.7 – Comparison of the present solutions with the solutions of Béghein et al. [32]: average Nusselt and Sherwood numbers at the hot sidewall for different values of the Lewis number Le.

	$Ra_T = Ra_S = 10^4$, Le = 1, Pr = 0.71, aiding flows	
y / W	Nu, Sh (Present study)	Nu, Sh (Béghein et al.)
0.001	4.20	4.18
0.009	4.20	4.18
0.022	4.22	4.21
0.039	4.26	4.26
0.062	4.33	4.33
0.089	4.38	4.39
0.120	4.42	4.43
0.155	4.41	4.42
0.193	4.37	4.36
0.235	4.28	4.25
0.279	4.14	4.09
0.326	3.94	3.89
0.374	3.72	3.65
0.424	3.44	3.39
0.475	3.18	3.11
0.525	2.88	2.82
0.576	2.58	2.52
0.624	2.31	2.22
0.674	1.95	1.93
0.721	1.63	1.65
0.765	1.37	1.39
0.807	1.15	1.16
0.845	0.97	0.97
0.880	0.84	0.83
0.911	0.74	0.74
0.938	0.68	0.68
0.961	0.65	0.66
0.978	0.64	0.64
0.991	0.63	0.64
0.999	0.63	0.64

Table 3.8 – Comparison of the present solutions with the solutions of Béghein et al. [32]: local Nusselt and Sherwood numbers along the hot sidewall.

3.4 Results and discussion

Numerical simulations are performed for different values of (a) the average nanoparticle volume fraction, φ_{av}, in the range between 0 and 0.06, (b) the diameter of the suspended nanoparticles, d_p, in the range between 25 nm and 100 nm, (c) the temperature of the cooled sidewall, T_c, in the range between 295 K and 315 K, (d) the temperature of the heated sidewall, T_h, in the range between 300 K and 345 K (correspondingly, the temperature difference between the sidewalls, ΔT, spans from 5 K to 50 K), and (e) the width of the enclosure, W, in the range between 0.002 m and 0.05 m. Notice that, fixed T_c

= 295–315 K and T_h= 300–345 K, the width interval 0.002–0.05 m corresponds to Rayleigh numbers of the order 10^4–10^7; just to make an example, for T_c = 300 K and T_h= 310 K, the cavity width W = 0.01 m corresponds to a Rayleigh number of the pure base fluid, Ra_f, equal to 2.5×10^5 (using T_c for the calculation of the physical properties).

Typical local results are presented in Fig. 3.3, in which the streamline, isotherm, and concentration contours are plotted for φ_{av} = 0.04 (i.e., $m_{av}\cong$ 0.143), d_p = 25 nm, T_c = 305 K, T_h = 315 K, and W = 0.01 m.

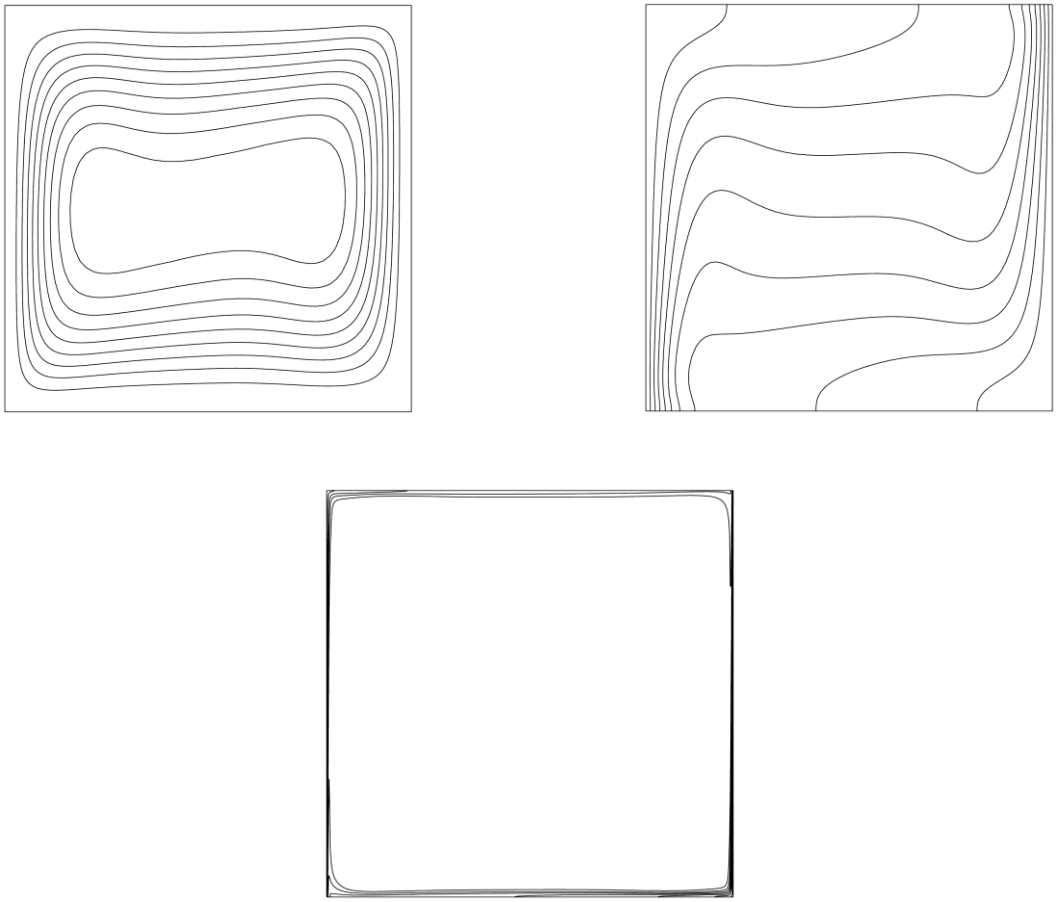

Fig. 3.3 – Streamline, isotherm and concentration contours for φ_{av} = 0.04, d_p = 25 nm, T_c = 305 K, T_h = 315 K and W = 0.01 m.

As expected, for all the configurations examined the flow field consists of a single roll-cell that derives from the rising of the hot fluid adjacent to the heated sidewall and its

descent along the opposite cooled sidewall, which leads to the distinctive temperature distribution featured by a fluid stratification in the core of the cavity. Additionally, the concentration and temperature patterns are somehow similar, although the thickness of the concentration boundary layers is much smaller than that of the thermal boundary layers. The profiles of the vertical velocity component V, temperature T and concentration m along the horizontal midplane of the enclosure are displayed in Figs. 3.4 - 3.6, respectively.

In both Figs. 3.4 and 3.5, the corresponding distributions for the pure base liquid are also represented for comparison. It may be seen that when a certain amount of nanoparticles is suspended into the base liquid, the consequent growth of the effective dynamic viscosity leads to a decrease in the motion intensity (see Fig. 3.4).

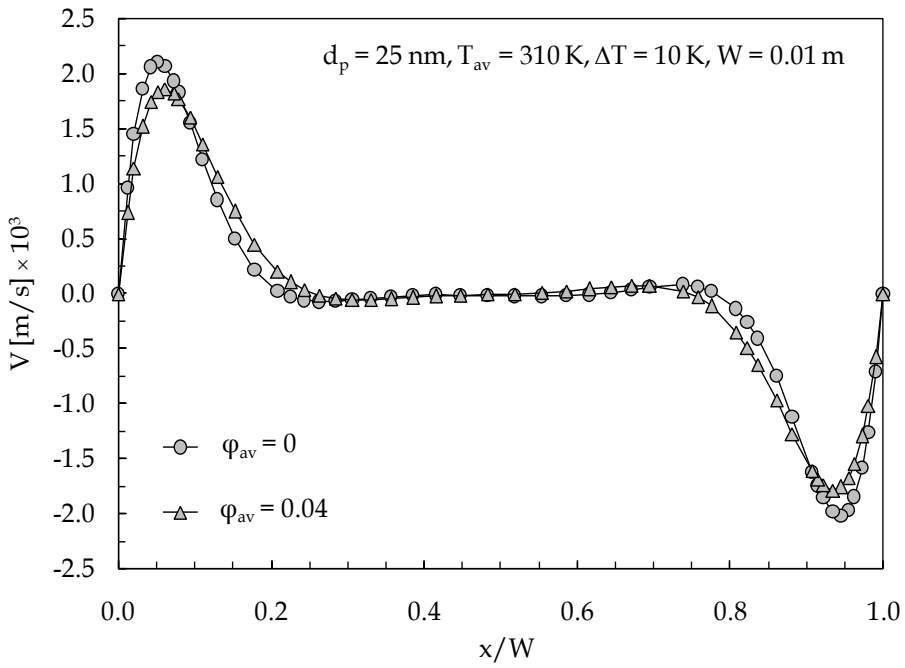

Fig. 3.4 – Distributions of V along the horizontal midplane of the enclosure with φ_{av} as a parameter.

This unavoidably results in a minor compression of the isotherms toward the heated and cooled sidewalls of the enclosure, as reflected by the decrease of the local temperature gradients (see Fig. 3.5).

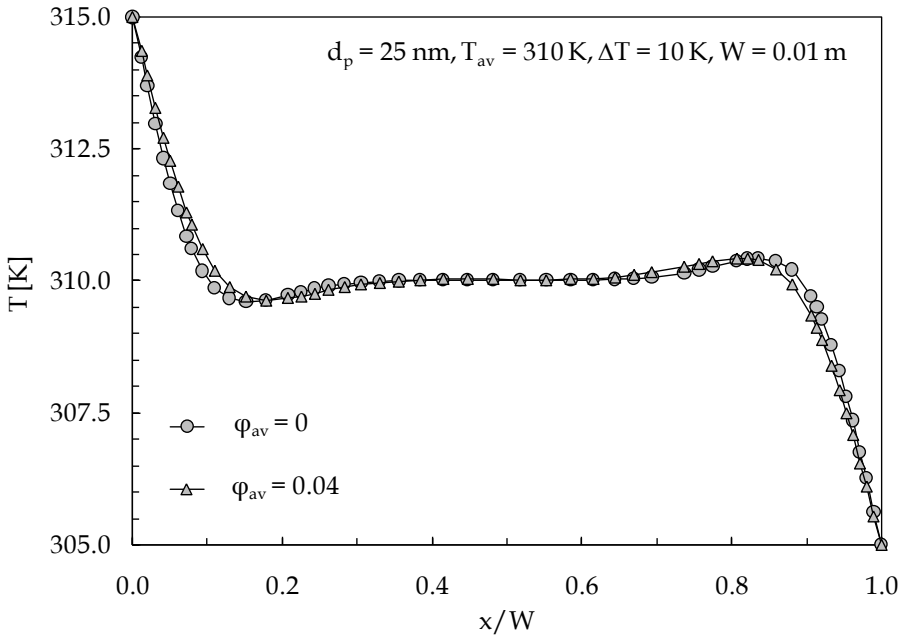

Fig. 3.5 – Distributions of T along the horizontal midplane of the enclosure with φ_{av} as a parameter.

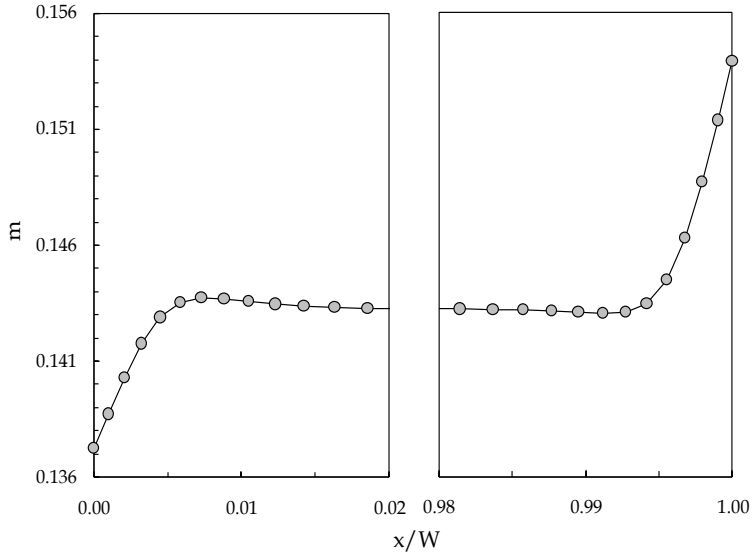

Fig. 3.6 – Distributions of m along the horizontal midplane of the enclosure.

On the other hand, since at same time also the effective thermal conductivity increases, such diminution of the temperature gradients at the cavity sides does not necessarily imply a degradation of the local heat transfer. This is clearly displayed in Fig. 3.7, in which a set of distributions of the heat flux at the cooled side of the cavity is

represented, demonstrating that, fixed d_p = 25 nm, T_c = 305 K, T_h = 315 K, and W = 0.01 m, the heat fluxes at φ_{av} = 0.02 are higher than those for the pure base fluid, whereas at φ_{av} = 0.04 and 0.06 the heat fluxes are lower.

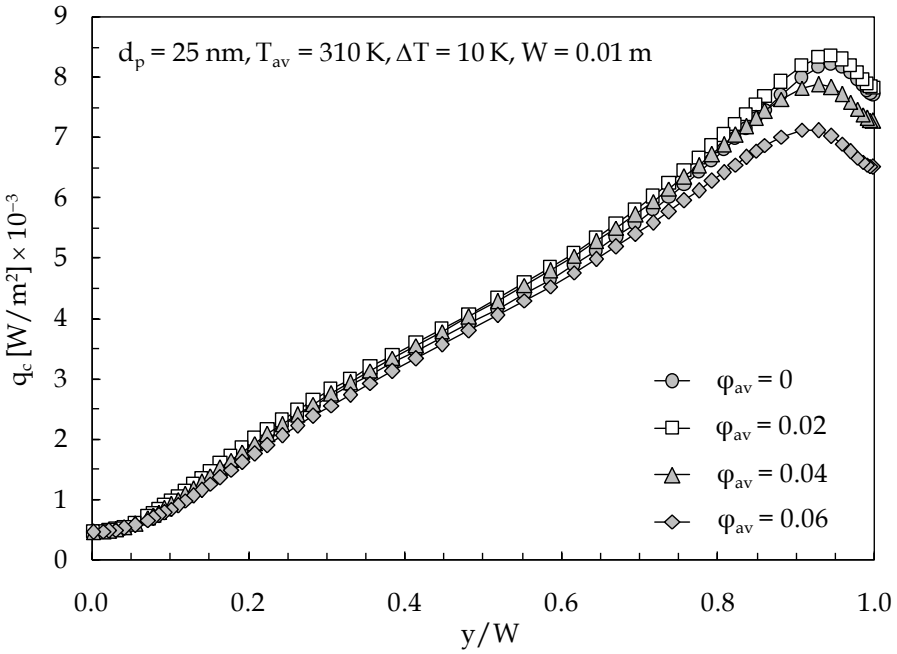

Fig. 3.7 – Distributions of q_c along the cooled sidewall with φ_{av} as a parameter.

Actually, this is perfectly in line with the earlier findings on the existence of an optimal particle loading, whose main features will be discussed at length in the next paragraph dedicated to the overall results.

The overall results are here presented in terms of the heat transfer enhancement relative to the performance of the pure base fluid, E, defined as

$$E = \frac{q_n}{q_f} - 1, \tag{3.17}$$

where q_n and q_f are the heat transfer rates flowing through the nanofluid and the pure base fluid, respectively.

The effects of the nanoparticle size, the cavity width and the nanofluid temperature on the heat transfer enhancement are displayed in Figs. 3.8–3.11.

It is apparent that, owing to the dispersion of a progressively larger amount of solid nanoparticles into the base liquid, E increases up to a point, which is due to the increased effective thermal conductivity. The value of φ_{av} corresponding to the peak of E is defined as the optimal particle loading for maximum heat transfer, denoted as φ_{opt}. As the volume fraction is further increased above φ_{opt}, E decreases, which is due to the excessive growth of the effective dynamic viscosity. Obviously, when the increased viscosity effect outweighs the increased thermal conductivity effect, E becomes negative, which means that the use of the nanofluid brings to a deterioration in the heat transfer rate. The value of φ_{av} relative to E = 0, i.e., the value of φ_{av} over which the thermal performance of the nanofluid starts becoming worse than that of the pure base liquid, is denoted asφ_0. It may be seen that E increases with decreasing d_p, whereas φ_{opt} increases with increasing d_p. In contrast, the dependence of φ_0 on$d_p$is so weak to be negligible. Additionally, E, φ_{opt} and φ_0 increase with increasing W, T_{av} and ΔT. A further peculiarity is that, assigned T_{av}, E is a little more sensitive to increases in ΔT for a fixed value of T_c, rather than increases in T_c for a fixed ΔT.

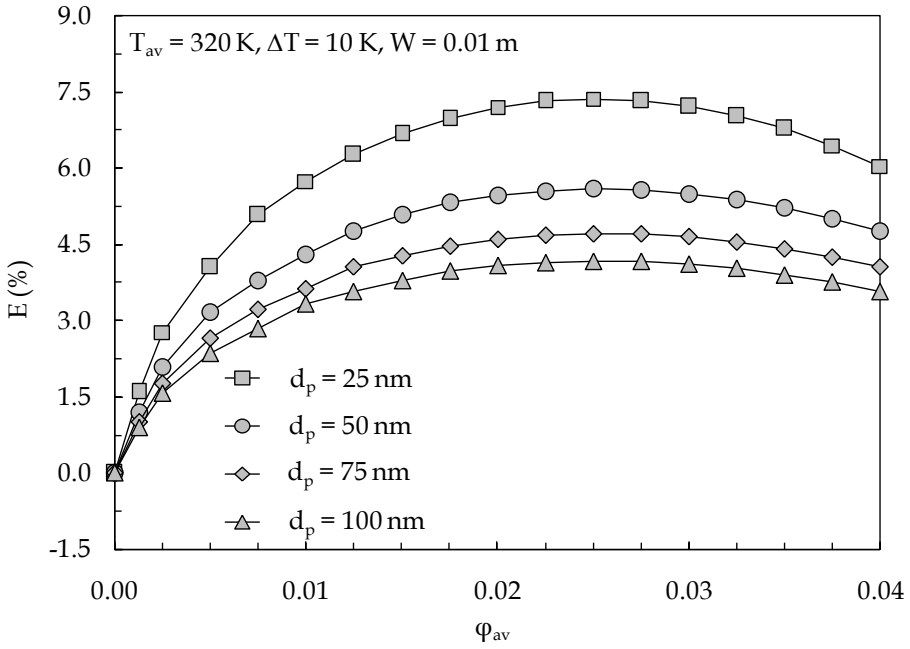

Fig. 3.8 – Distributions of E (%) vs. φ_{av} with d_p as a parameter.

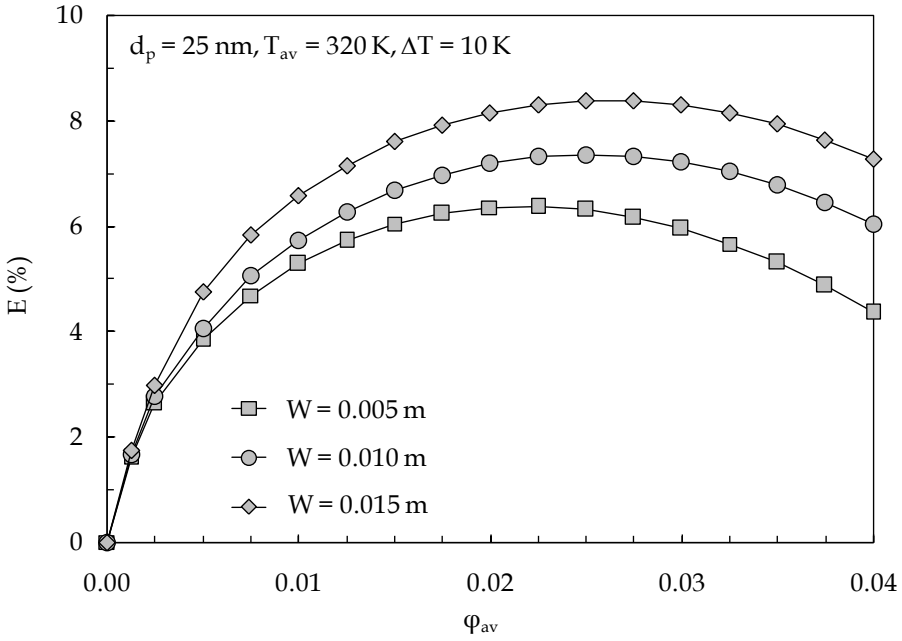

Fig. 3.9 – Distributions of E (%) vs. φ_{av} with W as a parameter.

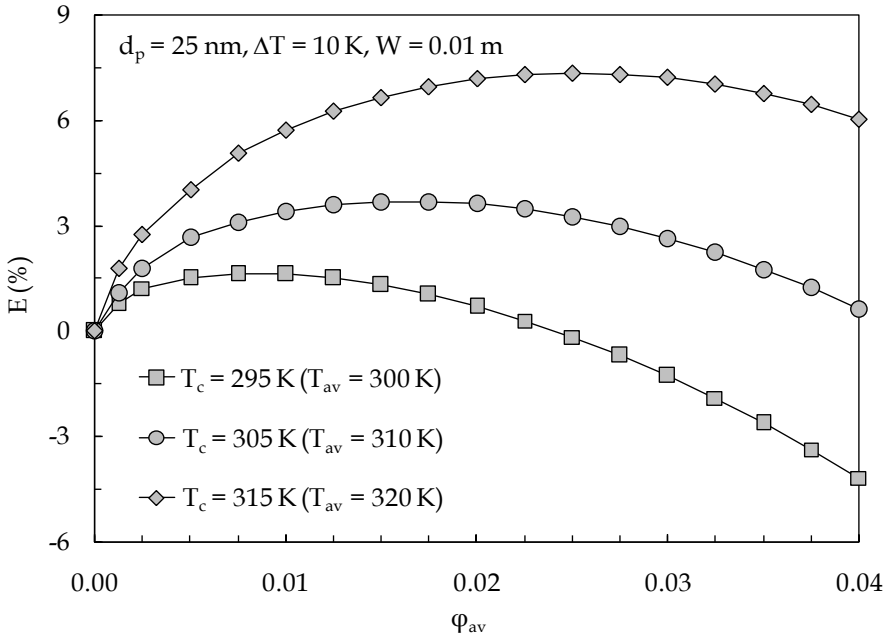

Fig. 3.10 – Distributions of E (%) vs. φ_{av} with T_c as a parameter.

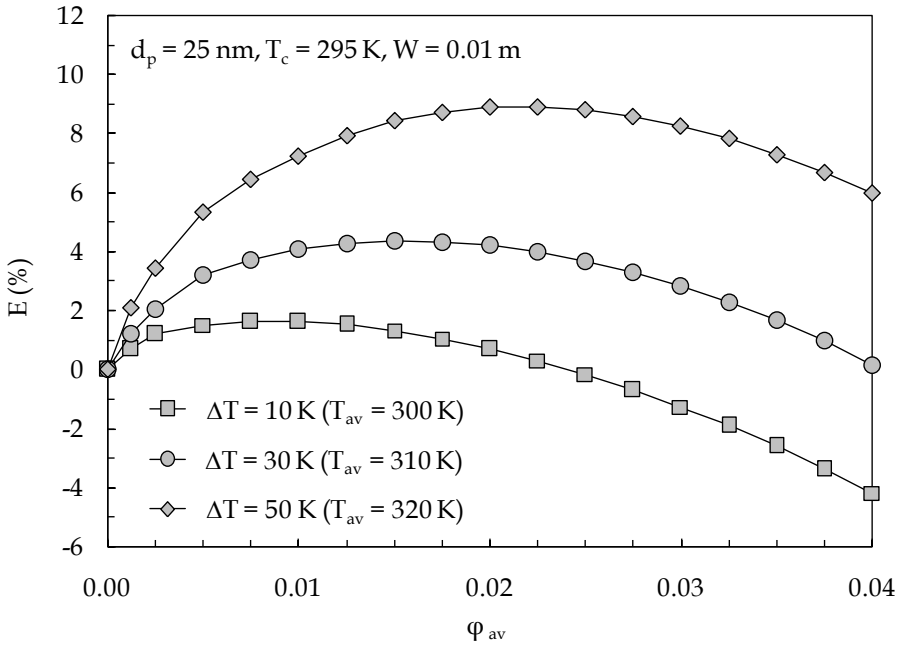

Fig. 3.11 – Distributions of E (%) vs. φ_{av} with ΔT as a parameter.

The whole set of numerical results obtained for the optimal particle loading, φ_{opt}, and the corresponding maximum value of the heat transfer enhancement, denoted as E_{max}, as well as the average particle loading over which the use of the nanofluid is not convenient any more, φ_0, may be correlated through the following dimensional equations derived by a multiple regression method:

$$\varphi_{opt} = (3.7\times10^{-2})\cdot\left[W(m)\right]^{0.12}\cdot\left[d_p(nm)\right]^{0.025}\cdot\left[t_c(^{\circ}C)^{0.174} - 1.612\right]\cdot\Delta T^{0.56} \tag{3.18}$$

with a 3.7% standard deviation of error and a ±10% range of relative error with a 98%level of confidence;

$$E_{max} = (4.2\times10^{-4})\cdot\left[W(m)\right]^{0.19}\cdot\left[d_p(nm)\right]^{-0.395}\cdot\left[t_c(^{\circ}C)\right]^{2.56}\cdot\Delta T^{1.03} \tag{3.19}$$

with a 2.9% standard deviation of error and a ±10% range of relative error with a 95%level of confidence;

$$\varphi_0 = (4.85\times10^{-2})\cdot\left[W(m)\right]^{0.1}\cdot\left[t_c(^{\circ}C)^{0.277} - 2\right]\cdot\Delta T^{0.355} \tag{3.20}$$

with a 2.0% standard deviation of error and a ±10% range of relative error with a 97%level of confidence. In the above equations, d_p(nm) is the nanoparticle diameter in nm, and t_c(°C) = T_c − 273.15 is the temperature of the cooled sidewall in Celsius degrees. The ranges of validity of eqs. (3.18)–(3.20) are 25 nm ≤ d_p ≤ 100 nm, 295 K ≤ T_c ≤ 315 K, 300 K ≤ T_h ≤ 345 K and 0.002 m≤ W≤ 0.05 m.

In addition, a dimensionless correlation is developed for predicting the effective average Nusselt number of the cooled sidewall in the same mentioned ranges of validity:

$$\left(\mathrm{Nu_n}\right)_c = 0.2\left[\frac{\mathrm{Pr_n}}{0.4+\mathrm{Pr_n}}\mathrm{Ra_n}\right]^{0.3}\left(\frac{\Delta T}{T_c}\right)^{0.08}\cdot e^{1.34\varphi_{av}} \tag{3.21}$$

with a 2.8% standard deviation of error and a ±5% range of relative error with a 95% level of confidence, as shown in Fig. 3.12.

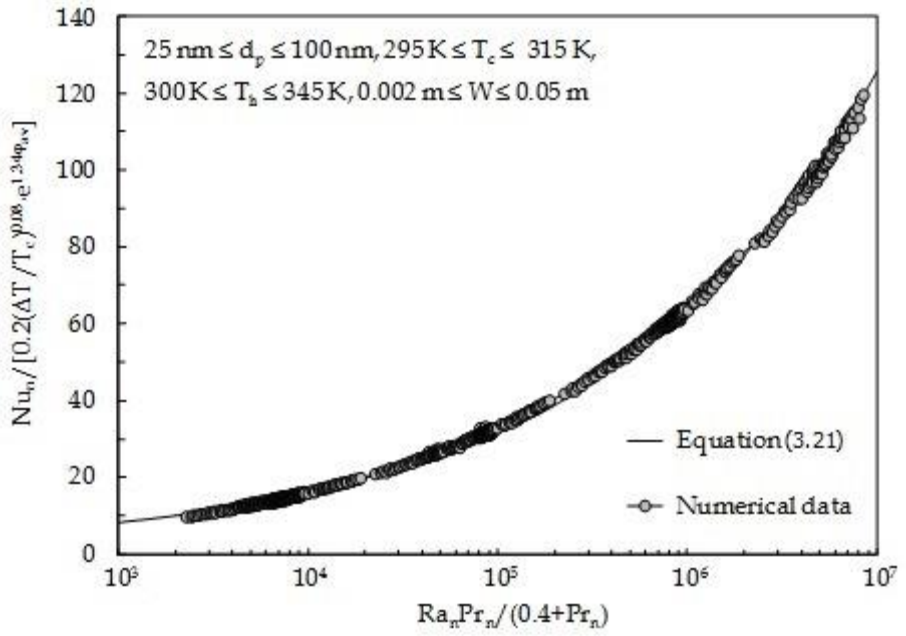

Fig. 3.12 − Comparison between eq. (3.21) and the numerical data.

In eq. (3.21), $\mathrm{Pr_n}$ and $\mathrm{Ra_n}$ are the effective Prandtl and Rayleigh numbers defined using the effective properties:

$$\mathrm{Pr_n} = \frac{(c_n)_c(\mu_n)_c}{(k_n)_c} \tag{3.22}$$

$$Ra_n = \frac{(\rho_n)_c (c_n)_c g[(\rho_n)_c - (\rho_n)_h] W^3}{(k_n)_c (\mu_n)_c}, \tag{3.23}$$

in which the properties with subscript "c" are calculated at temperature T_c, whereas the properties with subscript "h" are calculated at temperature T_h. Notice that Pr_n and Ra_n can be expressed as functions of the Rayleigh and Prandtl numbers of the base fluid, Pr_f and Ra_f, by the following relations:

$$Pr_n = Pr_f \frac{(c_n/c_f)_c (\mu_n/\mu_f)_c}{(k_n/k_f)_c} \tag{3.24}$$

$$Ra_n = Ra_f \frac{(\rho_n/\rho_f)_c (c_n/c_f)_c}{(k_n/k_f)_c (\mu_n/\mu_f)_c} \cdot \frac{(\rho_n)_c - (\rho_n)_h}{(\rho_f)_c - (\rho_f)_h}. \tag{3.25}$$

Obviously, once $(Nu_n)_c$ is known from eq. (3.21), the value of the effective average Nusselt number of the heated sidewall of the enclosure, $(Nu_n)_h$, can be calculated through eq. (3.15).

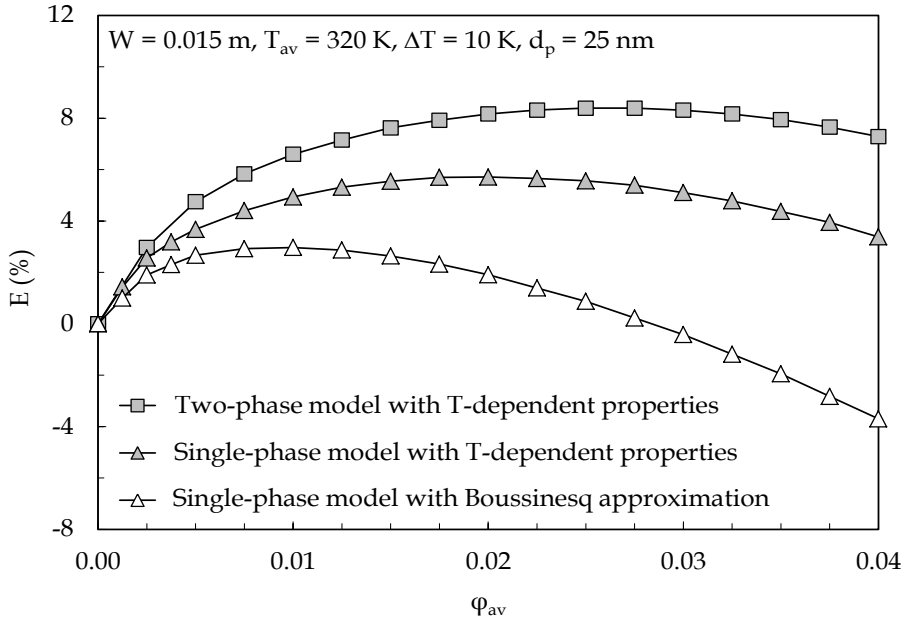

Fig. 3.13 – Comparison between the solutions of the two-phase and single-phase models.

Finally, a comparison between the solutions obtained in the present study and those that would have been derived by using the single-phase model is displayed in Fig. 3.13 for

d_p = 25 nm, T_c = 315 K, T_h = 325 K, and W = 0.015 m, with the aim to point out the combined effect of Brownian motion and thermophoresis on the heat transfer performance.

In the same figure, the results obtained through the single-phase model assuming constant physical properties, which is the typical approach used in most studies available in the literature, are also reported for further comparison. It can be seen that the degree of failure of the simulations based on the single-phase model is absolutely non negligible, especially when the Boussinesq approximation is invoked: as a matter of fact, in the specific case considered here the optimal particle loading obtained using this simplified approach is approximately 0.0075, i.e., less than one third of that obtained through the two-phase approach with temperature-dependent properties, that is, nearly 0.0250. Moreover, also the heat transfer enhancement calculated using the two-phase approach is higher, owing to the non-uniform concentration of particles with a mass density larger than the base fluid, which induces a solutal buoyancy that strengthens the thermal one.

3.5 Summary of the main results

The main result of the study is that :the increase of the effective dynamic viscosity occurring as the average volume fraction of the suspended nanoparticles increases, and their size decreases, leads to a decrease in the motion intensity, and to a corresponding decrease of the local temperature gradients at both sides of the cavity; however, due to the contemporary increase of the effective thermal conductivity, this does not necessarily mean that a heat transfer degradation takes place. Actually, the heat transfer performance consequent to the dispersion of solid nanoparticles into the base liquid increases with increasing the nanoparticle volume fraction up to an optimal particle loading at which the heat transfer performance has a peak. Further volume fraction increases imply a diminution of the heat transfer rate, which can even become lower than that of the pure base liquid.

The impact of the nanoparticle dispersion on the thermal performance decreases as the nanoparticle size is increased, whereas it increases as the width of the cavity, the average temperature and the temperature difference between the cavity sides are increased; in its turn, the optimal particle loading increases as all these independent controlling parameters are increased.

References

[1] L. Godson, B. Raja, D. Mohan Lal, S. Wongwises, Enhancement of heat transfer using nanofluids – An overview, Renewable Sustainable Energy Rev. 14 (2010) 629-641.

[2] J. Buongiorno, Convective transport in nanofluids, J. Heat Transfer 128 (2006) 240-250.

[3] J. C. Maxwell, A Treatise on Electricity and Magnetism, 3rd ed., Dover, New York, 1954.

[4] H. C. Brinkman, The viscosity of concentrated suspensions and solutions, J. Chem. Phys. 20 (1952) 571.

[5] N. Putra, W. Roetzel, S. K. Das, Natural convection of nano-fluids, Heat Mass Transfer 39 (2003) 775-784.

[6] E. Abu-Nada, A. J. Chamkha, Effect of nanofluid variable properties on natural convection in enclosures filled with a CuO-EG-Water nanofluid, Int. J. Thermal Sciences 49 (2010) 2339-2352.

[7] E. Abu-Nada, Z. Masoud, H. F. Oztop, A. Campo, Effect of nanofluid variable properties on natural convection in enclosures, Int. J. Thermal Sciences 49 (2010) 479-491.

[8] J. A. Esfahani, V. Bordbar, Double diffusive natural convection heat transfer enhancement in a square enclosure using nanofluids, J. Nanotechn. Eng. Medicine 2 (2011) 021002.

[9] F. S. Oueslati, R. Bennacer, Heterogeneous nanofluids: natural convection heat transfer enhancement, Nanoscale Res. Lett. 6 (2011) 222.

[10] S. K. Das, N. Putra, P. Thiesen, W. Roetzel, Temperature dependence of thermal conductivity enhancement for nanofluids. J. Heat Transfer 125 (2003) 567-574.

[11] C. H. Li, G. P. Peterson, Experimental investigation of temperature and volume fraction variations on the effective thermal conductivity of nanoparticle suspensions (nanofluids), J. Appl. Phys. 99 (2006) 084314.

[12] W. Yu, H. Xie, L. Chen, Y. Li, Investigation on the thermal transport properties of ethylene glycol-based nanofluids containing copper nanoparticles, Powder Technology 197 (2010) 218-221.

[13] H. Chen, Y. Ding, Y. He, C. Tan, Rheological behaviour of ethylene glycol based titania nanofluids, Chem. Phys. Lett. 444 (2007) 333-337.

[14] J. Chevalier, O. Tillement, F. Ayela, Rheological properties of nanofluids flowing through microchannels, Appl. Phys. Lett. 91 (2007) 233103.

[15] A. G. A. Nnanna, Experimental model of temperature-driven nanofluid, J. Heat Transfer 129 (2007) 697-704.

[16] C. J. Ho, W. K. Liu, Y. S. Chang, C. C. Lin, Natural convection heat transfer of alumina-water nanofluid in vertical square enclosures: An experimental study, Int. J. Thermal Sciences 49 (2010) 1345-1353.

[17] M. Corcione, Heat transfer features of buoyancy-driven nanofluids inside rectangular enclosures differentially heated at the sidewalls, Int. J. Thermal Sciences 49 (2010) 1536-1546.

[18] S. K. Das, N. Putra, W. Roetzel, Pool boiling characteristics of nano-fluids, Int. J. Heat Mass Transfer 46 (2003) 851-862.

[19] R. Prasher, D. Song, J. Wang, P. Phelan, Measurements of nanofluid viscosity and its implications for thermal applications, Appl. Phys. Lett. 89 (2006) 133108.

[20] Y. He, Y. Jin, H. Chen, Y. Ding, D. Cang, H. Lu, Heat transfer and flow behaviour of aqueous suspensions of TiO_2 nanoparticles (nanofluids) flowing upward through a vertical pipe, Int. J. Heat Mass Transfer 50 (2007) 2272-2281.

[21] G. S. McNab, A. Meisen, Thermophoresis in liquids, J. Colloid Interface Science 44 (1973) 339-346.

[22] J. P. Van Doormaal, G. D. Raithby, Enhancements of the simple method for predicting incompressible fluid flows, Num. Heat Transfer 11 (1984) 147-163.

[23] S. V. Patankar, D. B. Spalding, A calculation procedure for heat, mass and momentum transfer in three-dimensional parabolic flows, Int. J. Heat Mass Transfer 15 (1972) 1787-1797.

[24] S. V. Patankar, Numerical Heat Transfer and Fluid Flow, Hemisphere Publ. Co., Washington, DC, 1980.

[25] B. P. Leonard, A stable and accurate convective modelling procedure based on quadratic upstream interpolation, Comp. Meth. in Appl. Mech. Engng. 19 (1979) 59-78.

[26] G. de Vahl Davis, Natural convection of air in a square cavity: a bench mark numerical solution, Int. J. Num. Meth. Fluids 3 (1983) 249-264.

[27] H. S. Mahdi, R. B. Kinney, Time-dependent natural convection in a square cavity: application of a new finite volume method, Int. J. Num. Meth. Fluids 11 (1990) 57-86.

[28] M. Hortmann, M. Peric, G. Scheuerer, Finite volume multigrid prediction of laminar natural convection: bench-mark solutions, Int. J. Num. Meth. Fluids 11 (1990) 189-207.

[29] D. C. Wan, B. S. V. Patnaik, G. W. Wei, A new benchmark quality solution for the buoyancy-driven cavity by discrete singular convolution, Num. Heat Transfer 40 (2001) 199-228.

[30] A. Bejan, Convection Heat Transfer, 3rd ed., John Wiley & Sons, Inc., Hoboken, New Jersey (2004).

[31] F. P. Incropera, D. P. Dewitt, T. L. Bergman, A. S. Lavine, Fundamentals of Heat and Mass Transfer, 6th ed., John Wiley & Sons, Inc., Hoboken, New Jersey (2007).

[32] C. Béghein, F. Haghigat, F. Allard, Numerical study of double-diffusive natural convection in a square cavity, Int. J. Heat Mass Transfer 35 (1992) 833-846.

[33] A. Einstein, Über die von der molekularkinetischen Theorie der Wärme geforderte Bewegung von in ruhenden Flüssigkeiten suspendierten Teilchen (in German), Ann. Phys. 17 (1905) 549-560.

CHAPTER IV
Forced Convection in Nanofluids: Laminar and Turbulent Pipe Flow. A Theoretical Approach

4.1 Introduction

Heat transfer of nanoparticle suspensions in pipe flow is undoubtedly one of the most investigated topics in the field of convection in nanofluids. The main results of prior work clearly show that nanoparticle suspensions offer better thermal performance than the base liquids at same Reynolds number, and that heat transfer increases with increasing the nanoparticle volume fraction – see, e.g., Yu et al. [1], Kakaç and Pramuanjaroenkij [2], and Godson et al. [3].

For the laminar flow regime, due to its wider application at the small scale of new-generation components (this is, e.g., the flow regime occurring in many microfabricated heat exchangers and heat sinks [14]-[18]), it is worth noticing that all the experimental studies performed in this field have reached the common conclusion that nanofluids offer better thermal performance than the corresponding base liquids at same Reynolds number, and that the heat transfer rate increases with increasing the nanoparticle volume fraction. In particular, for Al_2O_3 + H_2O nanofluids with suspended nanoparticles having an average diameter in the range 20–50 nm, enhancements up to 20% with respect to pure water have been reported by Wen and Ding [19], Kim et al. [20], Roberts and Walker [21], Liu and Yu [22], and Ho et al. [23]. The effect of the particle size on the thermal performance of nanofluids was pointed out by Anoop et al. [24], who showed that the dispersion of smaller alumina nanoparticles into pure water led to higher heat transfer rates. Detailed information on the local heat transfer coefficient for water-based nanofluids with

suspended alumina or zirconia nanoparticles with average diameters of 46 nm and 60 nm, respectively, were provided by Rea et al. [25], who detected heat transfer increases up to an order of 30%. Appreciable increases in thermal performance were also observed for very dilute suspensions, i.e., suspensions with a nanoparticle volume fraction lower than 1%, as reported by Hwang et al. [26], Lai et al. [27], and Hung et al. [28]. A summary of the aforementioned experimental works, including details on the nanofluid type, and the size and concentration of the particles used by each group, is reported in Table 4.1. Same results on the nanofluid performance were also achieved by other research teams via numerical investigation [29]-[31].

Literature source	Nanofluid type	Nanoparticle size	Concentration
Wen and Ding	$Al_2O_3 + H_2O$	27-56 nm	≤ 1.6 vol %
Kim et al.	$Al_2O_3 + H_2O$	20-50 nm	3.0 vol %
	amorphous carbon + H_2O	20 nm	3.5 vol %
Roberts and Walker	$Al_2O_3 + H_2O$	20-30 nm	≤ 1.5 vol %
Liu and Yu	$Al_2O_3 + H_2O$	40 nm	≤ 5.0 vol %
Ho et al.	$Al_2O_3 + H_2O$	33 nm	≤ 10.0 wt %
Anoop et al.	$Al_2O_3 + H_2O$	45 nm and 150 nm	≤ 6.0 wt %
Rea et al.	$Al_2O_3 + H_2O$	50 nm	≤ 6.0 vol %
Hwang et al.	$Al_2O_3 + H_2O$	30 nm	≤ 0.3 vol %
Lai et al.	$Al_2O_3 + H_2O$	20 nm	≤ 1.0 vol %
Hung et al.	$Al_2O_3 + H_2O$	20 nm	≤ 1.5 wt %

Table 4.1 – Summary of recent measurements on nanofluids in laminar pipe flow.

For the turbulent flow regime, which our interest is focused on, increased heat transfer data were reported by Pak and Cho [4], Xuan and Li [5], Maïga et al. [6], Behzadmehr et al. [7], Williams et al. [8], and Bianco et al. [9].

However, it must be pointed out that the increase in effective thermal conductivity consequent to the dispersion of nanoparticles into the base liquid is accompanied by a

contemporary growth of the effective dynamic viscosity, which could represent a serious limitation. In fact, an excessive increase in pressure drop may result in an exaggerated pumping power requirement, as detected by Pak and Cho [4], and Williams et al. [8]. This means that the merits of nanofluids need to be evaluated necessarily in terms of global energetic performance, and not simply by the common point of view of the heat transfer enhancement, as discussed by Gosselin and da Silva [10] in a paper on external boundary layer flow, and by Mansour et al. [11] in a study investigating the effects of the different models used to predict the nanofluid physical properties on their thermal and hydraulic performance in pipe flow. Actually, this overall point of view becomes absolutely relevant when the availability of electric energy for pumping purposes is reduced or in case of battery-operated pumps. Two options are possible for such an approach. The first option is aimed at determining how much the heat transfer rate changes as the nanoparticle volume fraction is increased, keeping constant the pumping power. The second option has the scope to evaluate in what measure the pumping power changes with increasing the nanoparticle concentration, for an assigned heat transfer rate. Obviously, the addition of nanoparticles to the base liquid is advantageous in all those cases in which either a heat transfer enhancement occurs at a fixed cost of operation or a lower amount of power is dissipated in friction at same thermal performance.

Framed in this general background, the aim of the present chapter is to undertake a comprehensive theoretical study on the overall energetic performance of nanofluids both in laminar and turbulent pipe flow with the primary scope to determine if and when the dispersion of nanoparticles into a base liquid is beneficial. Both cases of constant driving power and constant heat transfer rate are investigated for different operating conditions, nanoparticle diameters, and solid–liquid combinations.

4.2 Theoretical formulation of the problem

As discussed in Chapter II for natural convection in annular space and from vertical flat plates, also in the case-study of forced convection in pipe flow the hypothesis of a solid–liquid mixture statistically homogeneous, isotropic, in local thermal equilibrium and without slip motion can reasonably be advanced.

Therefore, the heat transfer and friction factor correlations originally developed for single-phase flows can be extended to the corresponding nanofluid applications, provided that the thermophysical properties appearing in them are the nanofluid effective properties calculated at the reference temperature. Certainly, the trustworthiness of the results obtained following this procedure is strongly related to the use of robust theoretical models or empirical equations able to predict with adequate accuracy the nanofluid effective properties.

For laminar pipe flow, such an approach finds experimental confirmation in the study performed by Rea et al. [33], who demonstrated that the heat transfer and friction factor data relative to water-based nanofluids with suspended alumina or zirconia nanoparticles showed good agreement with the predictions of the traditional models/correlations valid for pure fluids, provided that the Nusselt, Reynolds and Prandtl numbers were calculated using the thermophysical properties of the suspension.

Experimental corroborations for turbulent pipe flows come from the data provided by Williams et al. [35], who demonstrated that the traditional correlations valid for turbulent pipe flow of pure liquids are safely applicable to nanofluids. In particular, the heat transfer and friction factor data obtained for $Al_2O_3 + H_2O$ and $ZrO_2 + H_2O$ were predicted with good accuracy by the Dittus–Boelter correlation [36], and the relations developed by Blasius [37] and Moody [38], respectively.

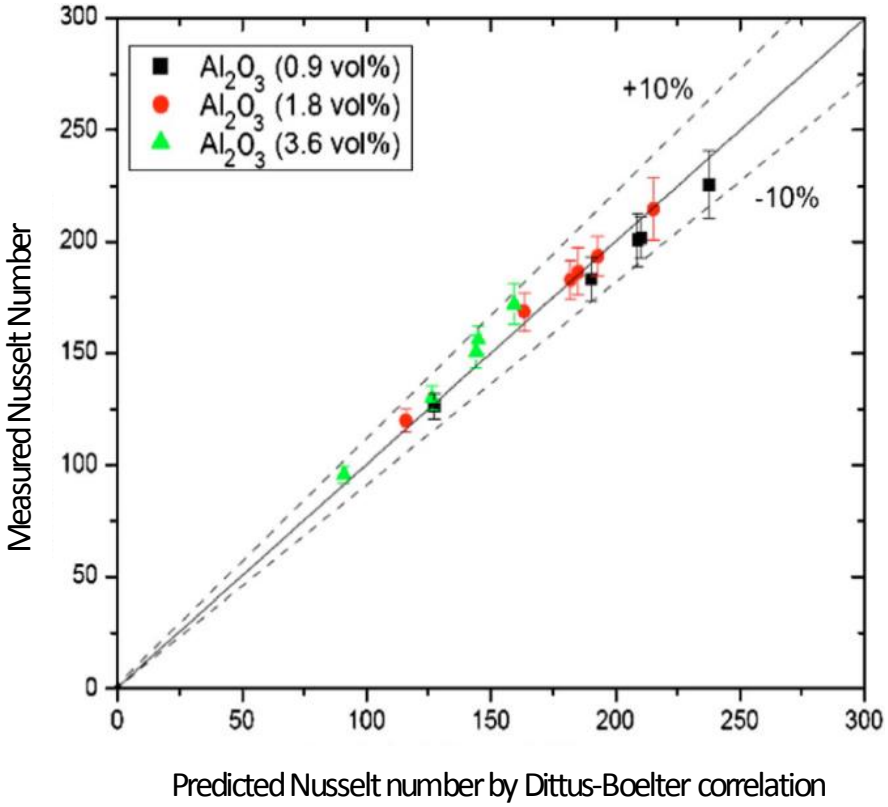

Extracted from Williams et al., *J. Heat Transfer* 130 (2008) 042412

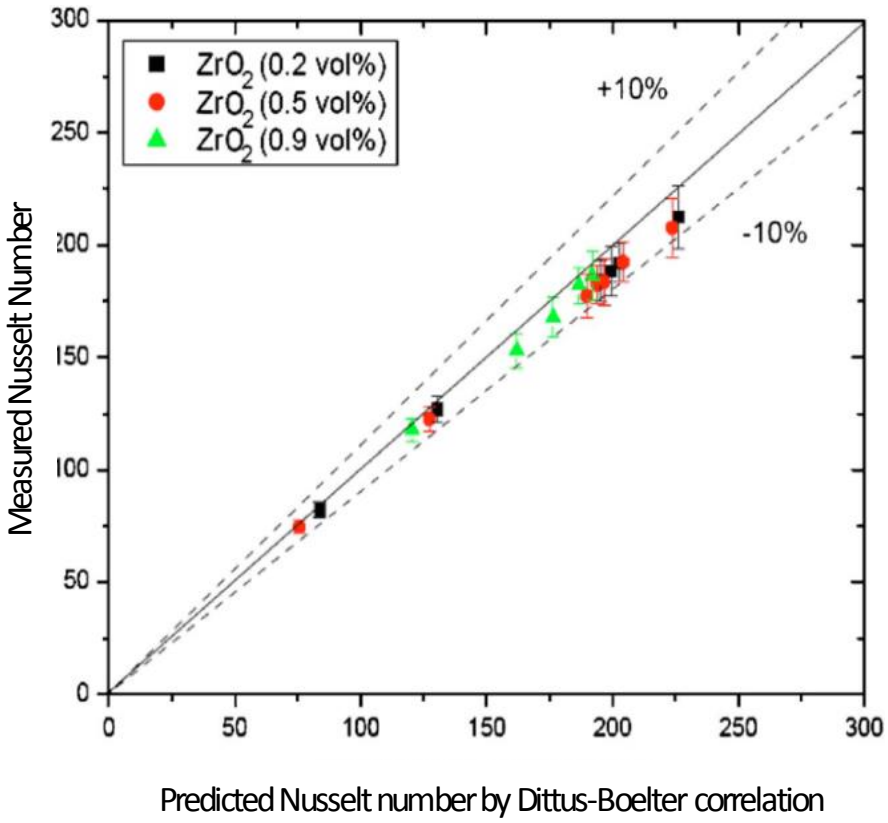

Extracted from Williams et al., *J. Heat Transfer* 130 (2008) 042412

A further evidence of the fact that nanofluids behave as homogeneous mixtures is given by the results of the experiments conducted by Sommers and Yerkes [39] using a propanol suspension of Al_2O_3 nanoparticles, whose heat transfer behaviour in laminar and turbulent pipe flow could be closely reproduced by the Seider–Tate correlation [40], and the Gnielinski correlation [41], respectively.

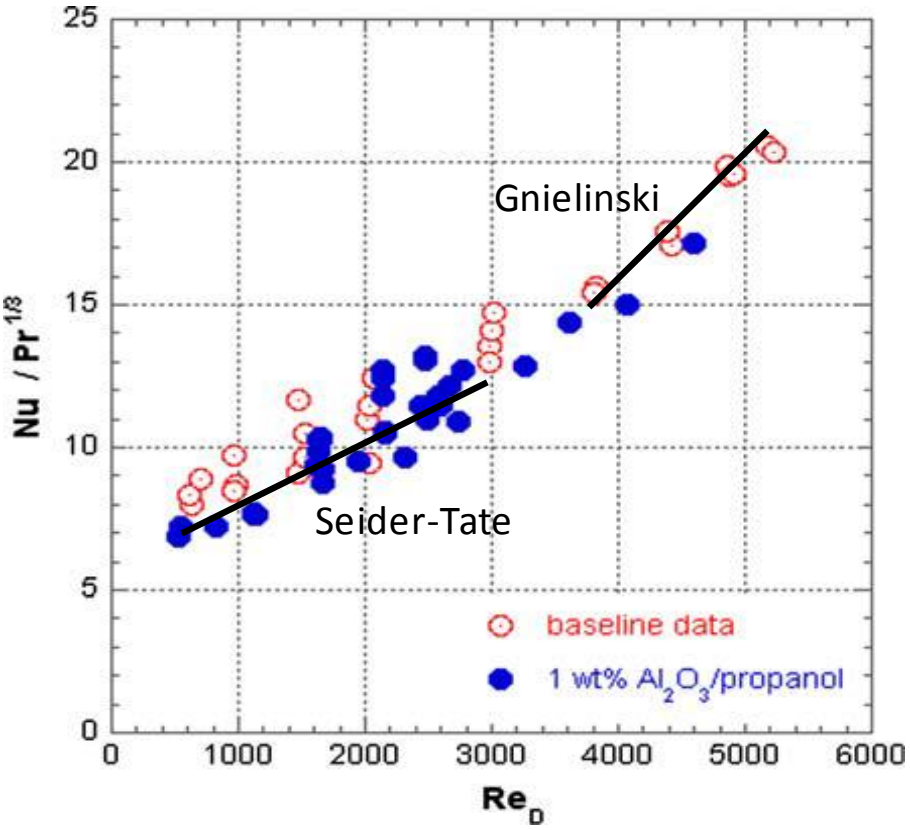

Extracted from Sommers and Yerkes, *J. Nanopart. Res.* 12 (2009) 1003-1014

Finally, Hwang et al. [32] and Pak and Cho [34] found that the friction factor correlations for pure fluids could be extended to water-based nanofluids with excellent approximation, which gives further strength to the single-phase approach. Notice that same type of results mentioned earlier were accomplished also for natural convection flows, such as those reported by Chang et al. [42].

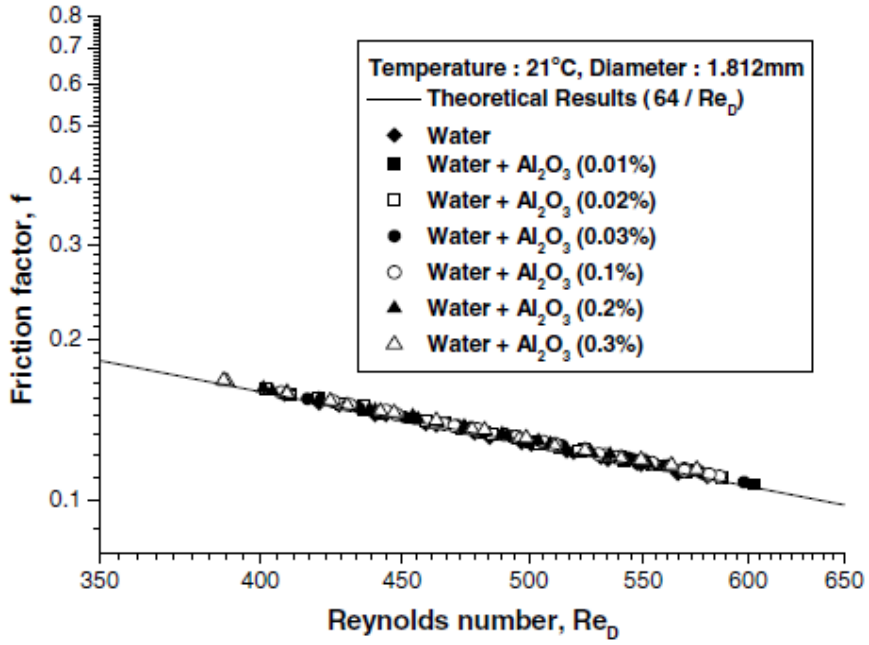

Extracted from Hwang et al., *J. Heat Mass Transfer* 52 (2009) 193-199

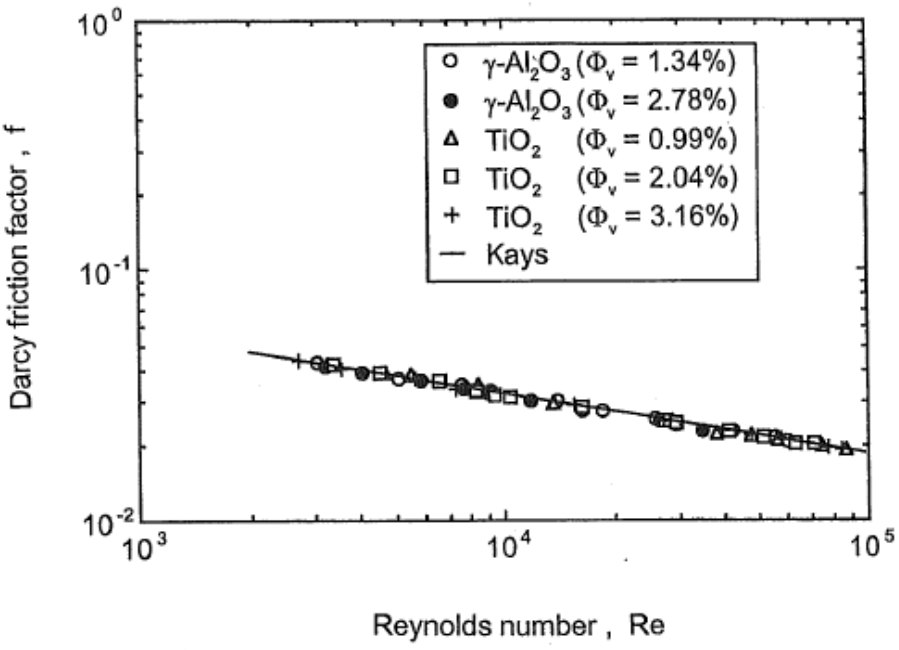

Extracted from Pak and Cho, *Exp .Heat Mass Transfer* 11 (1998) 151-170

For the calculation of the amount of heat transferred to an incompressible single-phase fluid with constant properties flowing through a circular tube having a uniform wall temperature, the Hausen correlation for fully developed laminar flow [43] is typically

recommended:

$$\mathrm{Nu} = 3.66 + \frac{0.19\left[\mathrm{Re\,Pr}(\mathrm{D/L})\right]^{0.8}}{1+0.117\left[\mathrm{Re\,Pr}(\mathrm{D/L})\right]^{0.467}} \tag{4.1}$$

$\mathrm{Re} \le 2300,\ 10^{-1} \le \mathrm{Re\,Pr}(\mathrm{D/L}) \le 10^{4}$

where D and L are the diameter and length of the tube, respectively.

For developed turbulent flow in pipes, the most popular formula is the Dittus−Boelter correlation for smooth-walled tubes [12]:

$$\mathrm{Nu} = 0.023\,\mathrm{Re}^{4/5}\,\mathrm{Pr}^{n} \tag{4.2}$$

$0.7 \le \mathrm{Pr} \le 120,\ 2500 \le \mathrm{Re} \le 1.24\times10^{5},\ \mathrm{L}/\mathrm{D} > 60,$

where L and D are the length and diameter of the tube, respectively, and the characteristic dimension in the Nusselt and Reynolds numbers is the tube diameter D. The Prandtl exponent is n = 0.4 when the fluid is being heated, and n = 0.3 when the fluid is being cooled. The equation can be used for small to moderate temperature differences between the tube wall and the fluid at inlet, $T_w - T_i$, with all the physical properties evaluated at the bulk temperature T_m.

However, since the maximum deviation between experimental data and values predicted by eq. (4.1) is of the order of 40 percent, the more accurate correlation proposed by Gnielinski [13] is usually recommended:

$$\mathrm{Nu} = \frac{(f_F/2)(\mathrm{Re}-10^{3})\mathrm{Pr}}{1+12.7(f_F/2)^{1/2}(\mathrm{Pr}^{2/3}-1)}\left[1+(\mathrm{D/L})^{2/3}\right] \tag{4.3}$$

$2300 < \mathrm{Re} \le 5\times10^{6},\ 0.5 \le \mathrm{Pr} \le 2\times10^{3},$

where D and L are the diameter and length of the tube, respectively, and f_F is the Fanning friction factor defined by the so-called Fanning equation. The above equations can be used

for small to moderate temperature differences between the tube wall and the fluid at inlet, with all the physical properties evaluated at the bulk temperature T_m. In the eq. (4.3), the characteristic length in the Nusselt and Reynolds numbers is the tube diameter D.

As regards the Fanning friction factor f_F, its value for the laminar regime is given by the well-known relation derived from the Hagen–Poiseuille equation for fully developed laminar flow in a circular tube reported in any classic textbook, see e.g. [45]:

$$f_F = 16/\mathrm{Re}. \tag{4.4}$$

Conversely, for the turbulent flow the relation given by Filonenko [46] for isothermal flows in smooth tubes can be used:

$$f_F = 0.25\left(0.79\ln \mathrm{Re} - 1.64\right)^{-2}. \tag{4.5}$$

Notice that the Fanning friction factor f_F, also called friction coefficient, is not to be confused with the Moody (or Darcy) friction factor, whose value is known to be four times that of the Fanning friction factor.

Two simpler alternatives to eq. (4.3), with similar degree of accuracy, are [44]:

$$\mathrm{Nu} = 0.0214\left(\mathrm{Re}^{0.8} - 100\right)\mathrm{Pr}^{0.4}\left[1 + (\mathrm{D}/\mathrm{L})^{2/3}\right], \tag{4.6}$$

$10^4 \leq \mathrm{Re} \leq 5\times10^6$, $0.5 \leq \mathrm{Pr} \leq 1.5$

and

$$\mathrm{Nu} = 0.012\left(\mathrm{Re}^{0.87} - 280\right)\mathrm{Pr}^{0.4}\left[1 + (\mathrm{D}/\mathrm{L})^{2/3}\right], \tag{4.7}$$

$3\times10^3 \leq \mathrm{Re} \leq 10^6$, $1.5 < \mathrm{Pr} \leq 500$.

Also the curve from eq. (4.5) can be reproduced with good accuracy by the Blasius relation [37]:

$$f_F = 0.079\,\mathrm{Re}^{-0.25}, \tag{4.8}$$

$3\times10^3 \le \mathrm{Re} \le 2\times10^4$

and the Moody relation [38]:

$$f_F = 0.046\,\mathrm{Re}^{-0.20}, \tag{4.9}$$

$2\times10^4 < \mathrm{Re} \le 10^6$,

The relations of eqs. (4.4), (4.8) and (4.9) may be synthetized in:

$$f_F = a\,\mathrm{Re}^{-\alpha}, \tag{4.10}$$

with

$a = 16,\ \alpha = 1$ $\quad \mathrm{Re} \le 2300$ (4.10a)

$a = 0.079$ and $\alpha = 0.25$ $\quad 3\times10^3 \le \mathrm{Re} \le 2\times10^4$ (4.10b)

$a = 0.046$ and $\alpha = 0.20$ $\quad 2\times10^4 < \mathrm{Re} \le 10^6$. (4.10c)

The Hausen correlation and the Gnielinski simplified correlation for liquids given by eqs. (4.1) and (4.7), respectively, in conjunction with the condensed Fanning friction factor relation expressed by eq. (4.10), will be used to assess the merits of nanofluids in pipe flow applications by the point of view of the global energetic performance.

The effect of the nanoparticle volume fraction on the heat transfer rate at constant pumping power will be evaluated in terms of relative heat transfer enhancement ε_q defined as:

$$\varepsilon_q = \frac{q_n}{q_f} - 1, \tag{4.11}$$

where q_n and q_f are the heat transfer rates of the nanofluid and the base fluid, respectively, at same cost of operation.

The heat transfer rate q between the wall of a pipe and a fluid flowing through the pipe can be calculated as:

$$q = h\pi DL\Delta T_{LM}, \tag{4.12}$$

in which h is the average coefficient of convection, and the logarithmic mean temperature difference ΔT_{LM} is defined as:

$$\Delta T_{LM} = \frac{(T_w - T_i) - (T_w - T_o)}{\ln[(T_w - T_i)/(T_w - T_o)]}, \tag{4.13}$$

where T_i and T_o are the inlet and outlet fluid temperatures, respectively, and T_w is the temperature of the pipe wall. Hence:

$$q = Gc(T_w - T_i)(1 - e^{\frac{-h\pi DL}{Gc}}), \tag{4.14}$$

where G is the mass flow rate of the fluid, and c is the specific heat at constant pressure of the fluid. After easy calculations the following expression is obtained:

$$q = \frac{\pi D}{4}(T_w - T_i)k\,Re\,Pr\left[1 - e^{-4\left(\frac{L}{D}\right)\frac{Nu}{Re\,Pr}}\right], \tag{4.15}$$

in which k is the thermal conductivity of the fluid, and Nu, Re and Pr are the Nusselt, Reynolds and Prandtl numbers. Accordingly, the relative heat transfer enhancement is given by:

$$\varepsilon_q = \frac{k_n}{k_f} \times \frac{Re_n}{Re_f} \times \frac{Pr_n}{Pr_f} \times \frac{1 - e^{-4\left(\frac{L}{D}\right)\frac{Nu_n}{Re_n Pr_n}}}{1 - e^{-4\left(\frac{L}{D}\right)\frac{Nu_f}{Re_f Pr_f}}} - 1, \tag{4.16}$$

where k_f, Re_f, Pr_f and Nu_f are the thermal conductivity, the Reynolds number, the Prandtl number and the Nusselt number of the base fluid, respectively, and k_n, Re_n, Pr_n and Nu_n are the corresponding effective quantities of the nanoparticle suspension. Indeed, in order to keep constant the driving power, the effective Reynolds number has to be calculated by imposing that the friction loss of the nanofluid must be the same as the friction loss of the

base fluid. According to the Fanning equation, the friction loss is:

$$F = G f_F \frac{2}{D} V^2 L = f_F \frac{\pi D L}{2} \rho V^3, \tag{4.17}$$

in which ρ is the mass density of the fluid, and V is the average velocity of the fluid. If we substitute eq. (4.10) into eq. (4.17) we obtain:

$$F = a Re^{-\alpha} \frac{\pi D L}{2} \rho V^3. \tag{4.18}$$

The required condition $F_n = F_f$ leads to:

$$a_n \, Re_n^{-\alpha} \, \rho_n V_n^3 = a_f \, Re_f^{-\alpha} \, \rho_f V_f^3 \tag{4.19}$$

and then

$$Re_n = Re_f \left[\frac{a_f}{a_n} \frac{(\rho_n/\rho_f)^2}{(\mu_n/\mu_f)^3} \right]^{\frac{1}{3-\alpha}}, \tag{4.20}$$

where a_f and α_f are the coefficient and exponent of eq. (4.11) applied to the base fluid, while V_f, ρ_f and μ_f are the average velocity, the mass density and the dynamic viscosity of the base fluid, respectively, and V_n, ρ_n and μ_n are the corresponding effective quantities of the nanofluid.

Hence:

$$\varepsilon_q = \frac{k_n}{k_f} \times \frac{Pr_n}{Pr_f} \times R_q \times \left[\frac{a_f (\rho_n/\rho_f)^2}{a_n (\mu_n/\mu_f)^3} \right]^{\frac{1}{3-\alpha}} - 1 \tag{4.21}$$

with

$$R_q = \frac{1 - e^{-4\left(\frac{L}{D}\right)\frac{Nu_n}{Re_n Pr_n}}}{1 - e^{-4\left(\frac{L}{D}\right)\frac{Nu_f}{Re_f Pr_f}}}, \tag{4.22}$$

in which Re_n is given by eq. (4.20) and Nu_n is the outcome of eq. (4.7) obtained by replacing Re and Pr with Re_n and Pr_n calculated at the bulk temperature T_m.

The effect of the nanoparticle volume fraction on the pumping power requirement at constant heat transfer rate will be evaluated in terms of relative friction loss diminution δ_{fl} defined as:

$$\delta_{fl} = 1 - \frac{F_n}{F_f}, \tag{4.23}$$

where F_n and F_f are the friction losses of the nanofluid and the base liquid, respectively, at same heat transfer rate.

If we combine eqs. (4.10), (4.17), and (4.23) we obtain:

$$\delta_{fl} = 1 - \frac{a_n Re_n^{-\alpha_n} \rho_n V_n^3}{a_f Re_f^{-\alpha_f} \rho_f V_f^3} \tag{4.24}$$

and then

$$\delta_{fl} = 1 - \frac{a_n}{a_f} \times \frac{\left(Re_n\right)^{3-\alpha_n}}{\left(Re_f\right)^{3-\alpha_f}} \times \frac{\left(\mu_n/\mu_f\right)^3}{\left(\rho_n/\rho_f\right)^2}, \tag{4.25}$$

where a_n and α_f are the coefficient and exponent of eq. (4.10) applied to the base fluid, while V_f, ρ_f, μ_f and Re_f are the average velocity, the mass density, the dynamic viscosity and the Reynolds number of the base fluid, respectively; similarly, a_n, α_n, V_n, ρ_n, μ_n and Re_n are the corresponding effective quantities of the nanoparticle suspension.

Now, with the scope to maintain constant the thermal performance, the effective Reynolds number has to be calculated by imposing that the heat transfer rate of the nanofluid must be the same as the heat transfer rate of the base fluid. Specifically, on account of eq. (4.15), the condition $q_n = q_f$ brings to the equation:

$$Re_n = Re_f \left[\frac{k_n}{k_f} \times \frac{Pr_n}{Pr_f} \times \frac{1 - e^{-4\left(\frac{L}{D}\right)\frac{Nu_n}{Re_n Pr_n}}}{1 - e^{-4\left(\frac{L}{D}\right)\frac{Nu_f}{Re_f Pr_f}}} \right]^{-1}, \tag{4.26}$$

whose solution can easily be obtained numerically by a trial-and-error procedure.

Substituting eq. (4.26) into eq. (4.25) we have:

$$\delta_{fl} = 1 - \left[\frac{k_n}{k_f} \times \frac{Pr_n}{Pr_f} \times R_{fl} \times \frac{(\rho_n / \rho_f)^{2/(3-\alpha)}}{(\mu_n / \mu_f)^{3/(3-\alpha)}} \right]^{-(3-\alpha)}, \quad (4.27)$$

where R_{fl} has the same formal expression of the second member of eq. (4.22), in whichRe_n is given by eq. (4.26) and Nu_{eff} is the outcome of eq. (4.7) obtained by replacing Re and Pr with Re_n and Pr_n calculated at the bulk temperature T_m.

4.3 Results and Discussion - Heat transfer at constant pumping power

The effects of the nanoparticle volume fraction on both the relative heat transfer enhancement ε_q and the relative friction loss diminution δ_{fl} are calculated for different values of the nanoparticle diameter d_p, the bulk temperature of the nanofluid T_m, the Reynolds number of the base fluid Re_f, the length-to-diameter ratio L/D, as well as for a number of combinations between solid and liquid phases.

The results obtained for the relative heat transfer enhancement at constant pumping power produced by suspending Al_2O_3 nanoparticles into pure water are displayed and discussed first. Subsequently, the results pertaining to the relative friction loss diminution at constant heat transfer rate for the same Al_2O_3 + H_2O nanofluid are shown and commented. Finally, the roles played by both the nanoparticle material and the base liquid are analyzed.

4.3.1 Laminar pipe flow

The effects of the size of the suspended nanoparticles and the nanofluid bulk temperature on the heat transfer enhancement at constant driving power are pointed out in Figs. 4.1 and 4.2, where the distributions of the percentage values of ε_q are plotted versus the volume fraction φ for different values of d_p and T_m, respectively.

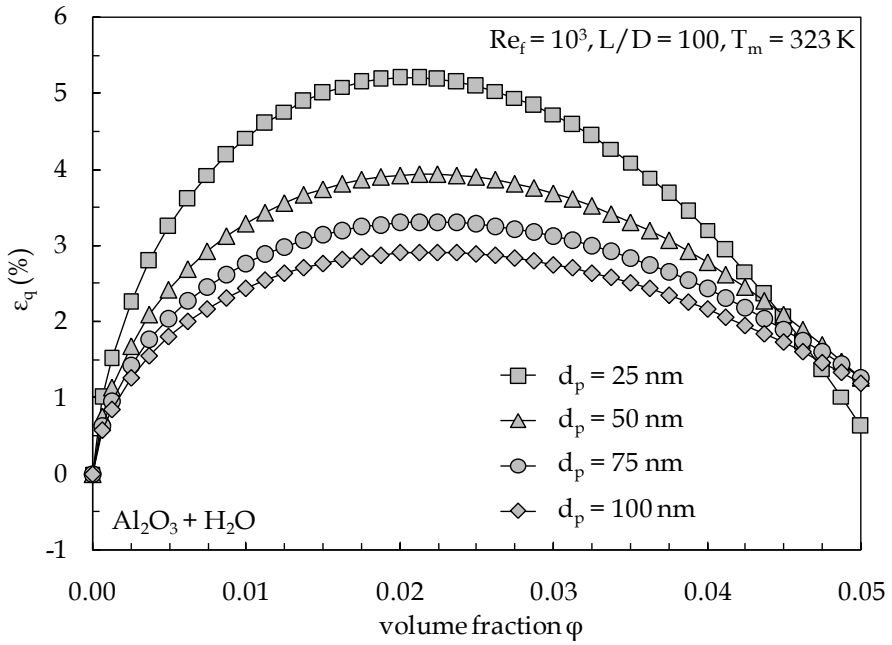

Fig. 4.1 – Distributions of ε_q (%) vs. φ with d_p as a parameter.

It may be seen that, owing to the dispersion of a progressively larger amount of nano-sized particles into the base liquid, the heat transfer enhancement increases up to a point, which is due to the increased effective thermal conductivity of the nanofluid. Notice that the impact of the increased effective thermal conductivity is higher when the diameter of the suspended nanoparticles is smaller and the nanofluid bulk temperature is higher. The value of φ corresponding to the peak of ε_q is defined as the optimal particle loading for maximum heat transfer enhancement at constant pumping power $\varphi_{q\text{-}opt}$. As the volume fraction is further increased above $\varphi_{q\text{-}opt}$, the heat transfer enhancement decreases, which is due to the excessive growth of the nanofluid effective viscosity. In fact, as mentioned earlier, the overall energetic performance of nanofluids is a strict consequence of the two opposite effects that originate from the increase of both the effective thermal conductivity and the effective dynamic viscosity occurring as the nanoparticle concentration is increased. The first effect, which tends to enhance the heat transfer performance, prevails at small volume fractions, whilst the second effect, which tends to increase the friction loss, prevails at large volume fractions. Obviously, when the increased viscosity effect

outweighs the increased thermal conductivity effect, the heat transfer enhancement at constant pumping power becomes negative, which means that the thermal performance of the nanofluid is lower than that of the pure base liquid at same cost of operation.

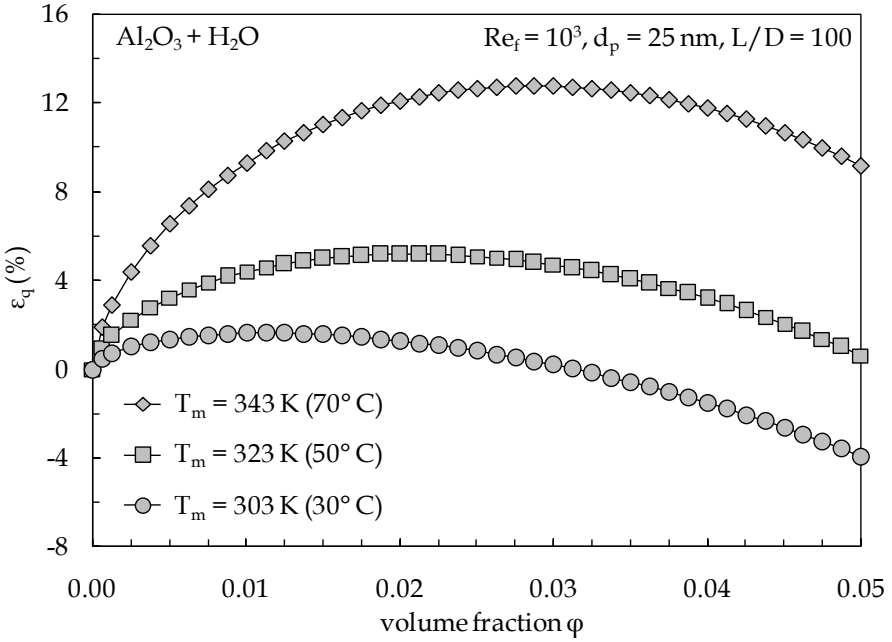

Fig. 4.2 – Distributions of ε_q (%) vs. φ with T_m as a parameter.

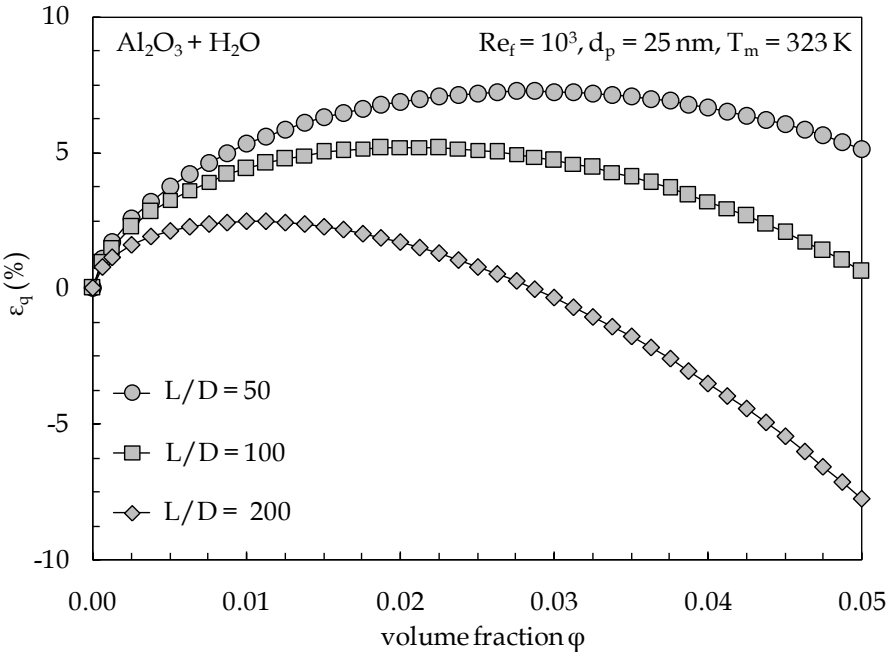

Fig. 4.3 – Distributions of ε_q (%) vs. φ with L/D as a parameter.

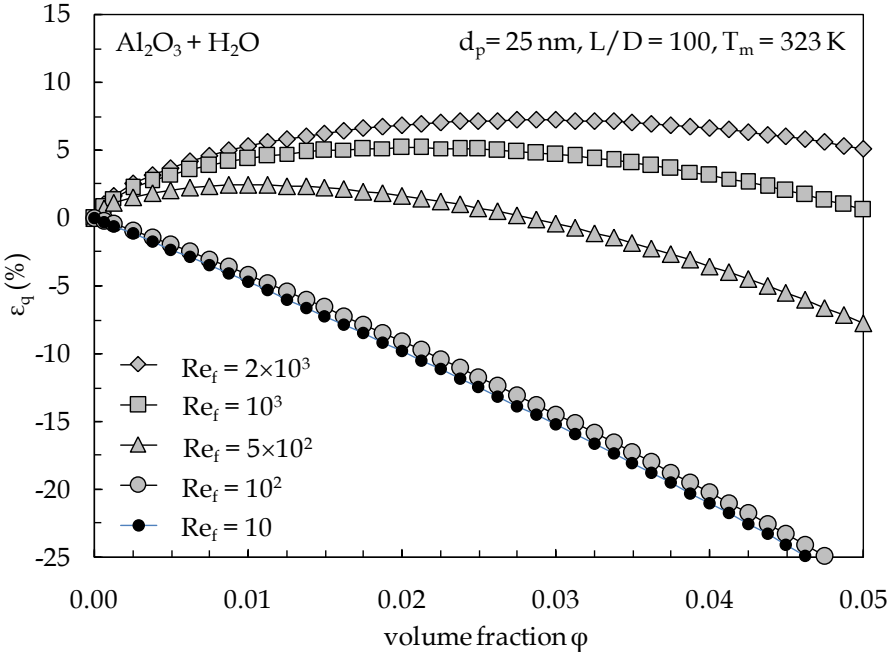

Fig. 4.4 – Distributions of ε_q (%) vs. φ with Re_f as a parameter.

Distributions of ε_q vs. φ with same trends of those reported in Figs. 4.1 and 4.2 are obtained for any investigated length-to-diameter ratio of the pipe, as displayed in Fig. 4.3, and for values of the Reynolds number of the base fluid higher than 10^2–5×10^2 (depending on the values of d_p, T_m and L/D), as shown in Fig. 4.4. In particular, it is apparent that the addition of solid nanoparticles to the base liquid is more beneficial when Re_f is higher and L/D is smaller. In contrast, for Re_f of the order of 10^1–10^2 the dispersion of an increasing amount of nanoparticles into the base liquid becomes progressively more unfavourable in terms of global energetic performance.

Regarding the optimal particle loading, a number of distributions of $\varphi_{q\text{-}opt}$ versus Tm and L/D are represented in Figs. 4.5 and 4.6 for different values of d_p and Re_f, respectively. It may be noticed that $\varphi_{q\text{-}opt}$ increases as the nanofluid bulk temperature increases, the length-to-diameter ratio of the pipe decreases, and the Reynolds number of the base liquid increases. Moreover, $\varphi_{q\text{-}opt}$ is almost independent of the nanoparticle size in the low-temperature range investigated, whilst it increases as the nanoparticle diameter is increased

at higher bulk temperatures.

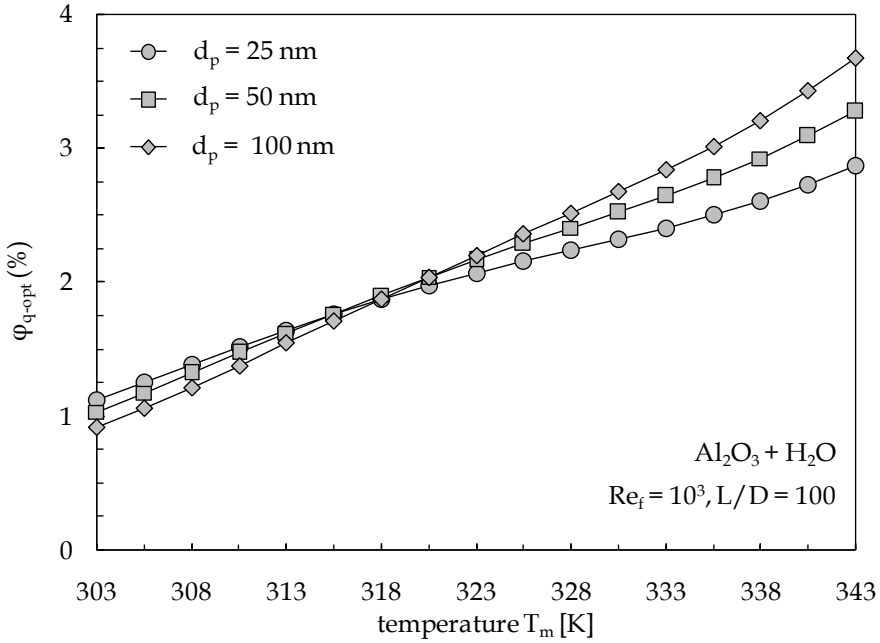

Fig. 4.5 – Distributions of $\varphi_{q\text{-}opt}$ (%) vs. T_m with d_p as a parameter.

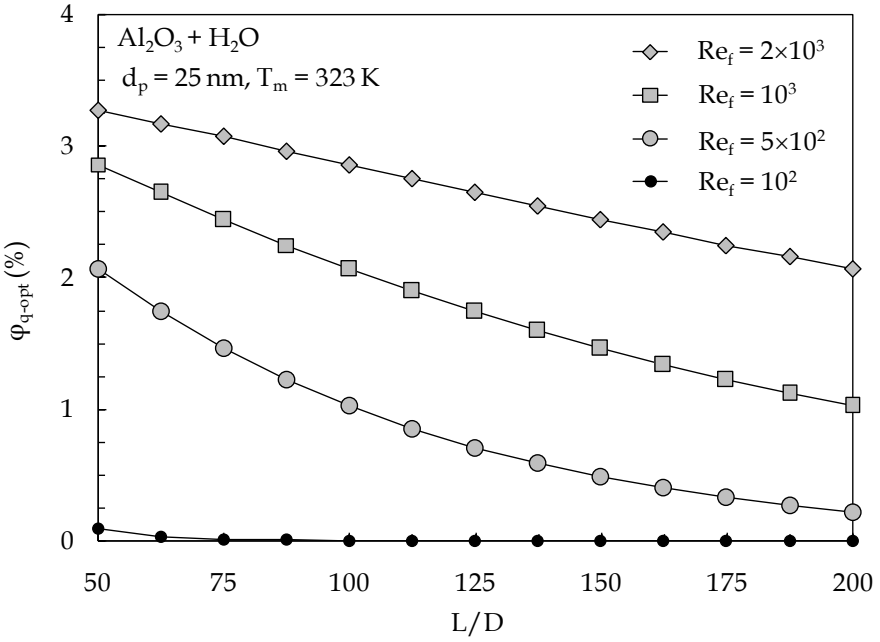

Fig. 4.6 – Distributions of $\varphi_{q\text{-}opt}$ (%) vs. L/D with Re_f as a parameter.

The distributions of the heat transfer enhancement at constant pumping power that corresponds to the optimal particle loading, $\varepsilon_{q\text{-}max}$, plotted versus T_m and L/D for the same values of d_p and Re_f used in Figs. 4.5 and 4.6, are depicted in Figs. 4.7 and 4.8, respectively.

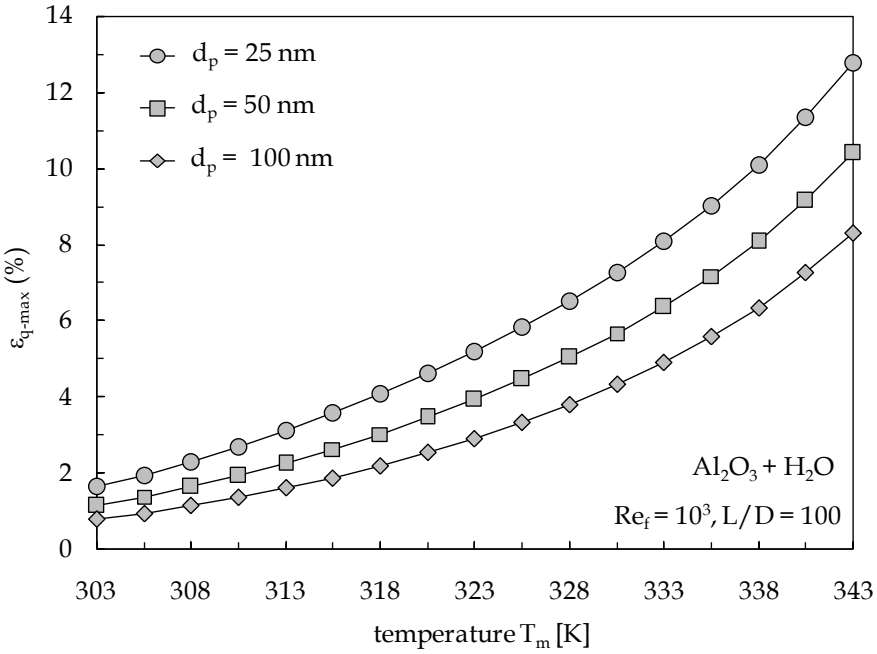

Fig. 4.7 – Distributions of $\varepsilon_{q\text{-}max}$ (%) vs. T_m with d_p as a parameter.

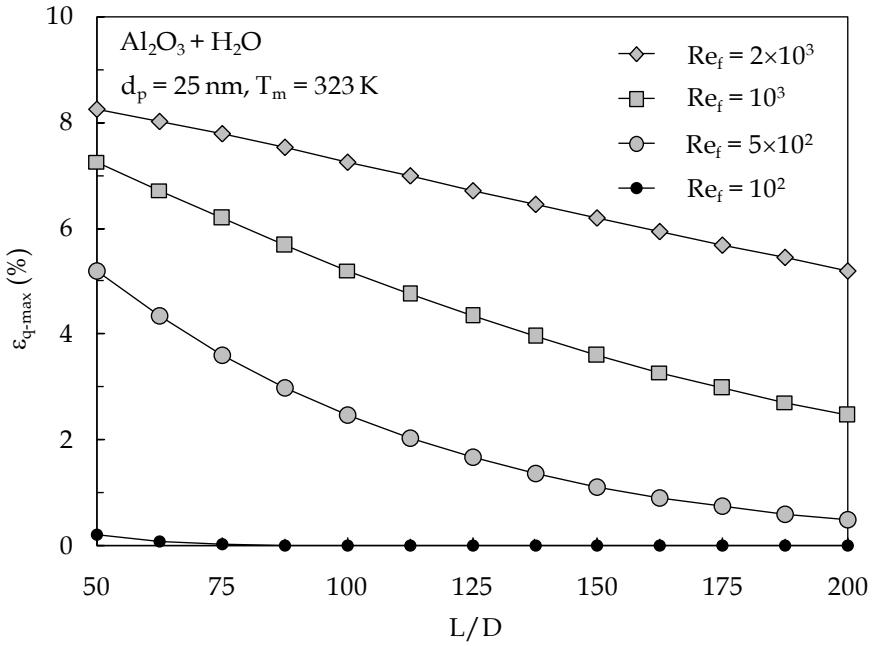

Fig. 4.8 – Distributions of $\varepsilon_{q\text{-}max}$ (%) vs. L/D with Re_f as a parameter.

Notice that, in accordance with the data reported in Fig. 4.4 for $Re_f = 10^2$, both values of $\varphi_{q\text{-}opt}$ and $\varepsilon_{q\text{-}max}$ at such Reynolds number of the base liquid are zero for the majority of the investigated geometries.

For the specific case of laminar pipe flow of a water suspension of alumina nanoparticles (Al_2O_3 + H_2O), that actually is one of the nanofluids most frequently investigated, a multiple regression analysis of the results obtained for the percentage optimal particle loadings produces a pair of empirical dimensional algebraic equations with the same functional structure:

$$\varphi_{opt}(\%) = A\,Re_f^{\alpha} \cdot \exp[(B\,Re_f^{\beta} + C) \times (L/D)][d_p(nm)]^{\gamma}[T_m(K) - 273.15]^{D[d_p(nm)]^{\delta}}, \qquad (4.28)$$

$5\times10^2 \leq Re_f \leq 2300$, $30°C \leq t_m \leq 70°C$,

$25\ nm \leq d_p \leq 100\ nm$, $50 \leq L/D \leq 1000$,

in which $T_m(K)$ is the bulk temperature of the nanofluid expressed in Kelvin degrees, and $d_p(nm)$ is the average diameter of the suspended nanoparticles expressed in nanometers. The values of the coefficients and exponents relative to $\varphi_{q\text{-}opt}$ and $\varphi_{fl\text{-}opt}$ are reported in the first and second line of Table 4.2.

	A	α	B	β	C	γ	D	δ
$\varphi_{q\text{-}opt}$	0.770	-0.074	-6.60	-0.976	0.00090	-0.719	0.693	0.156
$\varphi_{fl\text{-}opt}$	0.860	-0.011	-4.61	-0.926	0.00066	-0.715	0.552	0.180
φ_{opt}	0.818	-0.044	-5.60	-0.954	0.00077	-0.718	0.624	0.167

Table 4.2 – Coefficients and exponents of eq. (4.28) for $\varphi_{q\text{-}opt}$, $\varphi_{fl\text{-}opt}$ and φ_{opt}.

The percentage standard deviation of error is 1.8% for both equations, as shown in Fig. 4.9. Notice that, on account of the results shown further in Figs. 4.25 and 4.26 for different solid–liquid combinations, eq. (4.28) can be used with good approximation to determine the optimal particle loadings of any water-based nanofluid.

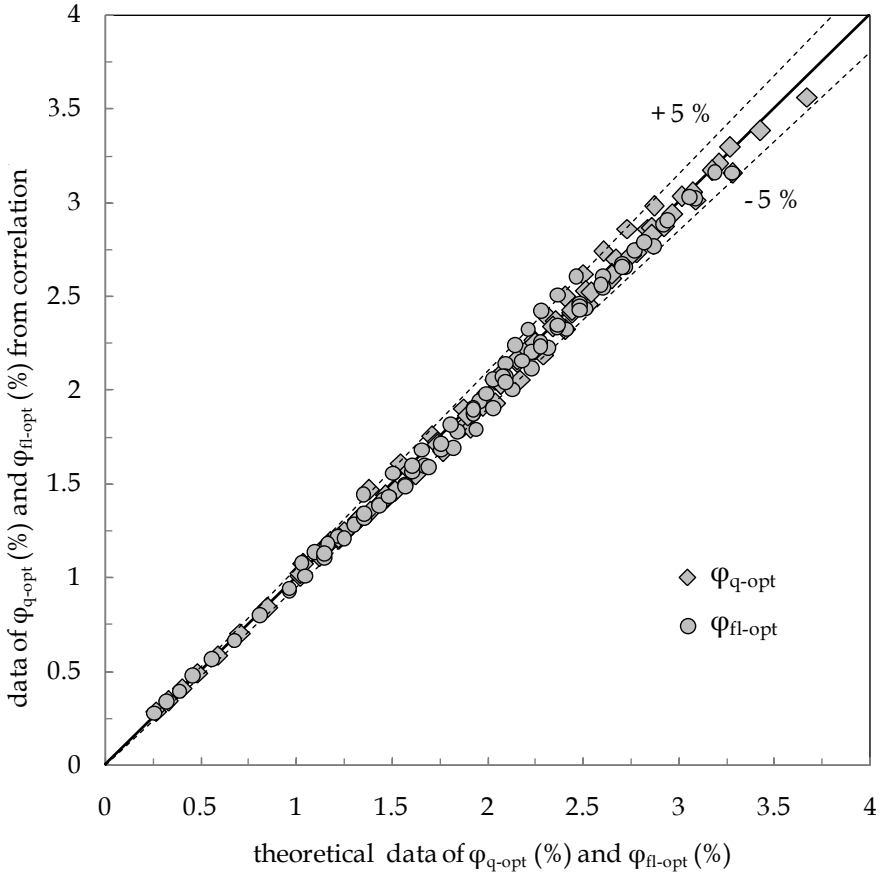

Fig. 4.9 – Comparison between eq. (4.28) and the theoretical data of $\varphi_{q\text{-}opt}$ (%) and $\varphi_{fl\text{-}opt}$ (%).

On the other hand, taking into account that the average percentage difference between $\varphi_{q\text{-}opt}$ and $\varphi_{fl\text{-}opt}$ is very small, as said earlier, and that in most situations the maximum for both ε_q and δ_{fl} is rather smooth, a unique correlation may be produced for a first approach calculation of the "mean" optimal volume fraction φ_{opt}, having the same form of eq. (4.28), whose values of the coefficients and exponents are listed in the third line of Table 4. The corresponding percentage standard deviation of error is 2%.

4.3.2 Turbulent pipe flow

As for laminar pipe flow, same effects of the size of the suspended nanoparticles and the nanofluid bulk temperature on the heat transfer enhancement at constant driving power can be pointed out (Figs. 4.10 and 4.11). In the same figures, the distributions of ε_q vs. φ obtained by using the Maxwell-Garnett and Brinkman models for calculating the effective

thermal conductivity and dynamic viscosity of the nanofluid are also reported, confirming the weakness of these models in capturing the thermo-mechanical main features of nanoparticle suspensions.

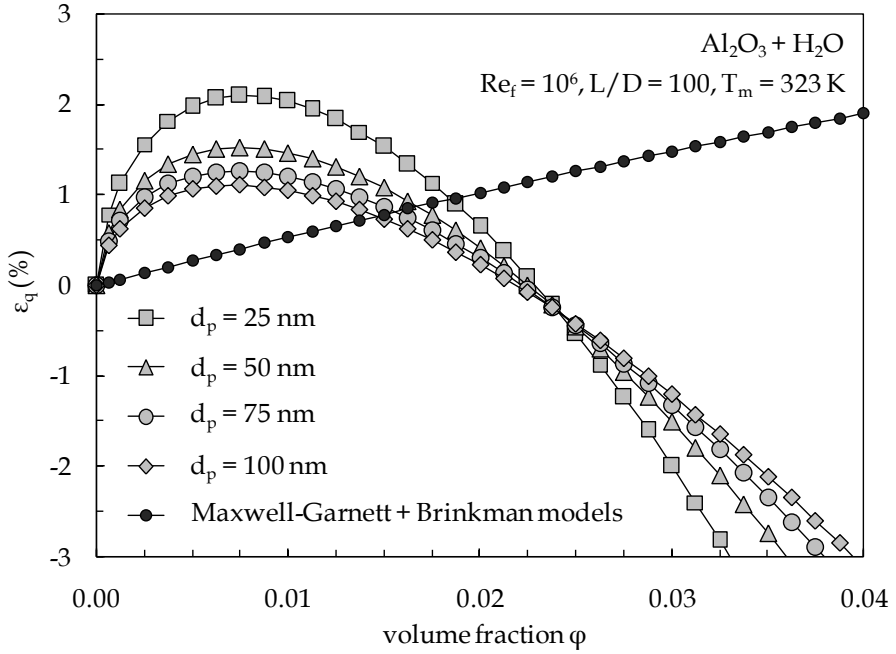

Fig. 4.10 – Distributions of ε_q (%) vs. φ with d_p as a parameter.

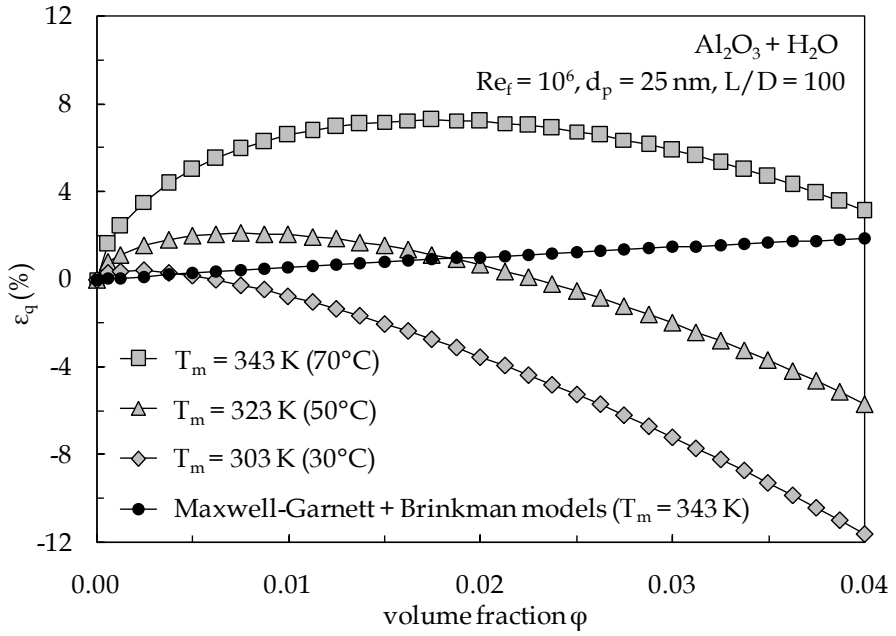

Fig. 4.11 – Distributions of ε_q (%) vs. φ with T_m as a parameter.

A set of distributions of ε_q vs. φ, obtained for any investigated Reynolds number of

the base fluid (Fig. 4.12) and any investigated L/D (Fig. 4.13), and a number of distributions of $\varphi_{q\text{-}opt}$ Vs. T_m for different values of d_p (Fig. 4.14), and $\varphi_{q\text{-}opt}$ vs. L/D for different values of Re_f (Fig. 4.15), are reported. The same conclusions delineated for laminar pipe flow can be drawn.

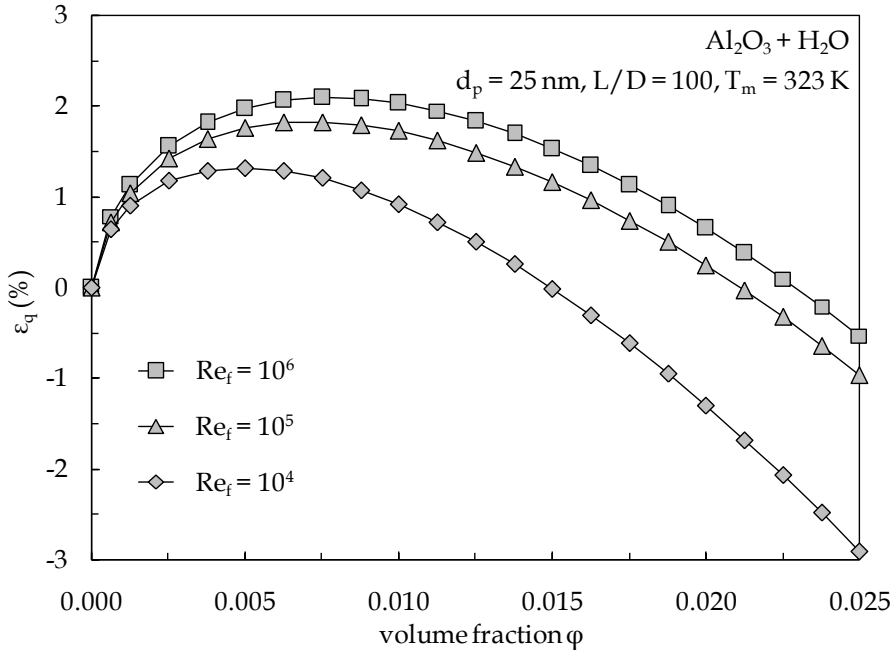

Fig. 4.12 – Distributions of ε_q (%) vs. φ with Re_f as a parameter.

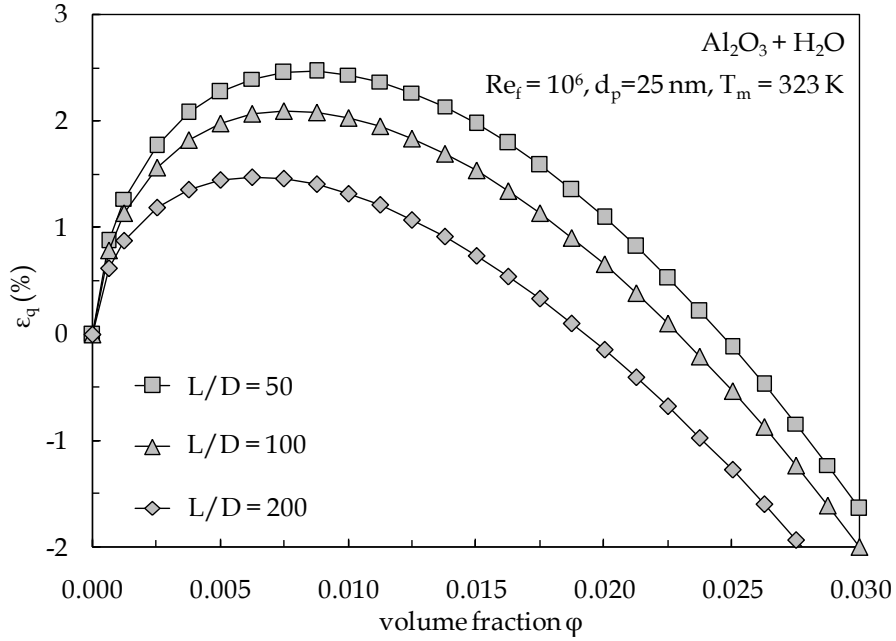

Fig. 4.13 – Distributions of ε_q (%) vs. φ with L/D as a parameter.

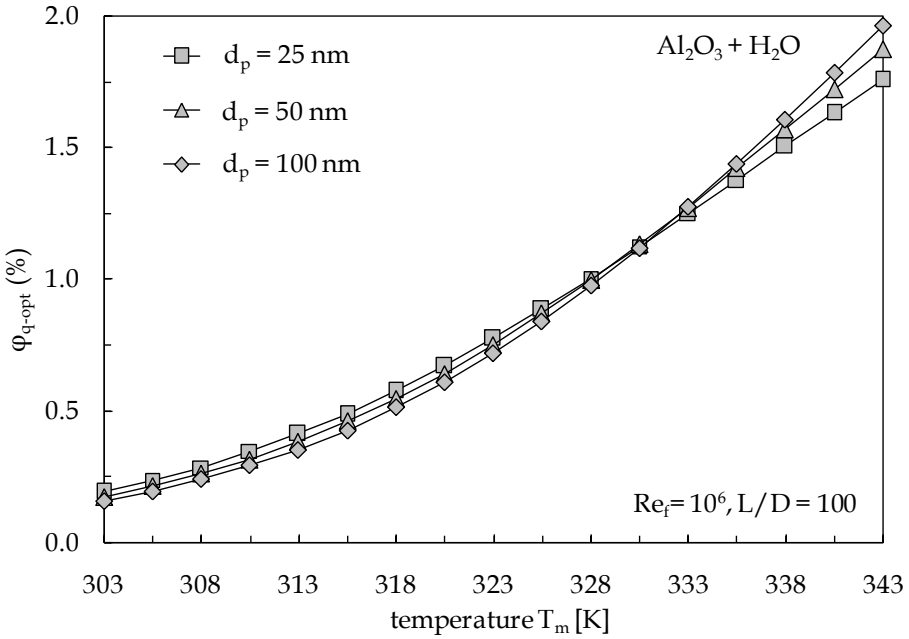

Fig. 4.14 – Distributions of $\varphi_{q\text{-}opt}$ (%) vs. T_m with d_p as a parameter.

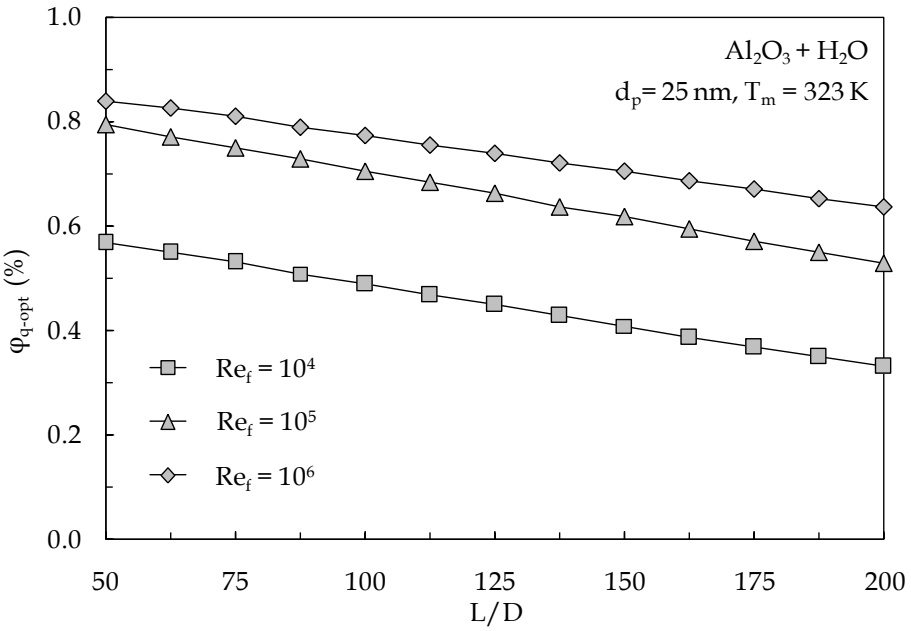

Fig. 4.15 – Distributions of $\varphi_{q\text{-}opt}$ (%) vs. L/D with Re_f as a parameter.

The distributions of the heat transfer enhancement at constant pumping power that corresponds to the optimal particle loading, $\varepsilon_{q\text{-}max}$, plotted versus T_m and L/D for the same values of d_p and Re_f used in Figs. 4.14 and 4.15, are depicted in Figs. 4.16 and 4.17, respectively.

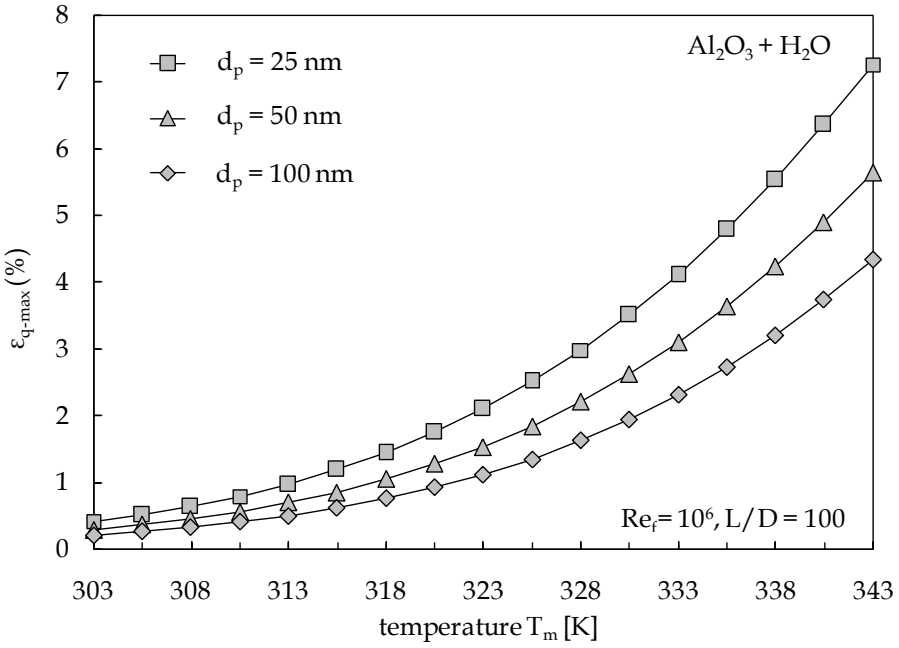

Fig. 4.16 – Distributions of $\varepsilon_{q\text{-}max}$ (%) vs. T_m with d_p as a parameter.

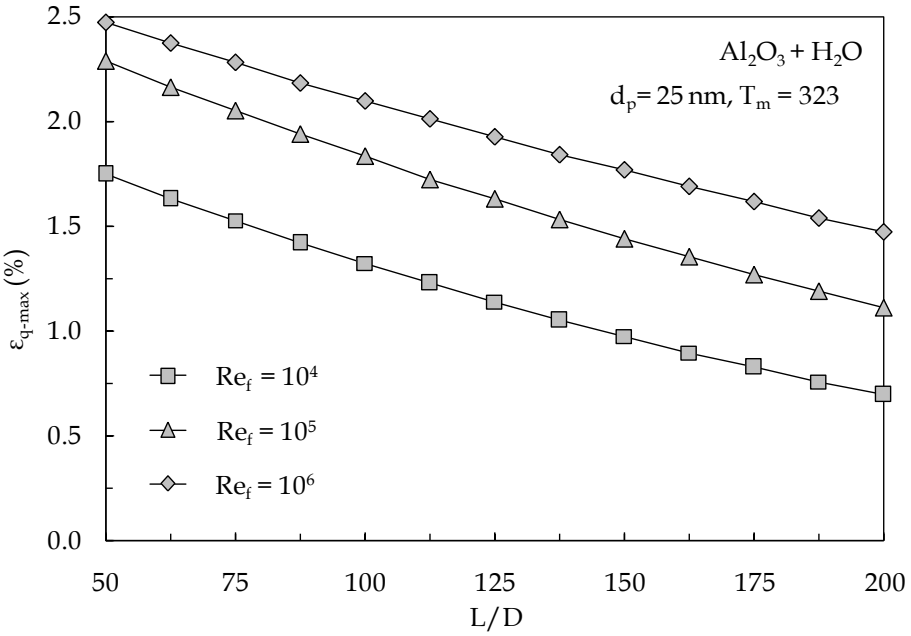

Fig. 4.17 – Distributions of $\varepsilon_{q\text{-}max}$ (%) vs. L/D with Re_f as a parameter.

For the specific case of turbulent pipe flow of a water suspension of alumina nanoparticles (Al_2O_3 + H_2O), the empirical dimensional algebraic equations for the percentage optimal particle loading are expressed as follow:

$$\varphi_{opt}(\%) = (1.32\times10^{-5})\,Re_f^{0.332}(L/D)^{-0.358}[d_p(nm)]^{-0.822}[t_m(°C)]^{2.441[d_p(nm)]^{0.064}}, \qquad (4.29)$$

$2300 \le Re_f \le 10^4$, $30°C \le t_m \le 70°C$

$25\ nm \le d_p \le 100\ nm$, $50 \le L/D \le 1000$

$$\varphi_{opt}(\%) = (6.6\times10^{-4})\,Re_f^{0.043}(L/D)^{-0.228}[d_p(nm)]^{-0.859}[t_m(°C)]^{2.045[d_p(nm)]^{-0.077}}, \qquad (4.30)$$

$10^4 < Re_f \le 5\times10^6$, $30°C \le t_m \le 70°C$

$25\ nm \le d_p \le 100\ nm$, $50 \le L/D \le 1000$

with an overall 5% standard deviation of error, as shown in Fig. 4.18, in which t_m(°C) is the bulk temperature of the nanofluid in Celsius degrees, and d_p(nm) is the average diameter of the suspended nanoparticles in nm. Also in this case, as for laminar regime, on account of the results shown further in Figs. 4.27 and 4.28 for different solid–liquid combinations, eqs. (4.29) and (4.30) can be used with good approximation to determine the optimal particle loading of any water-based nanofluid.

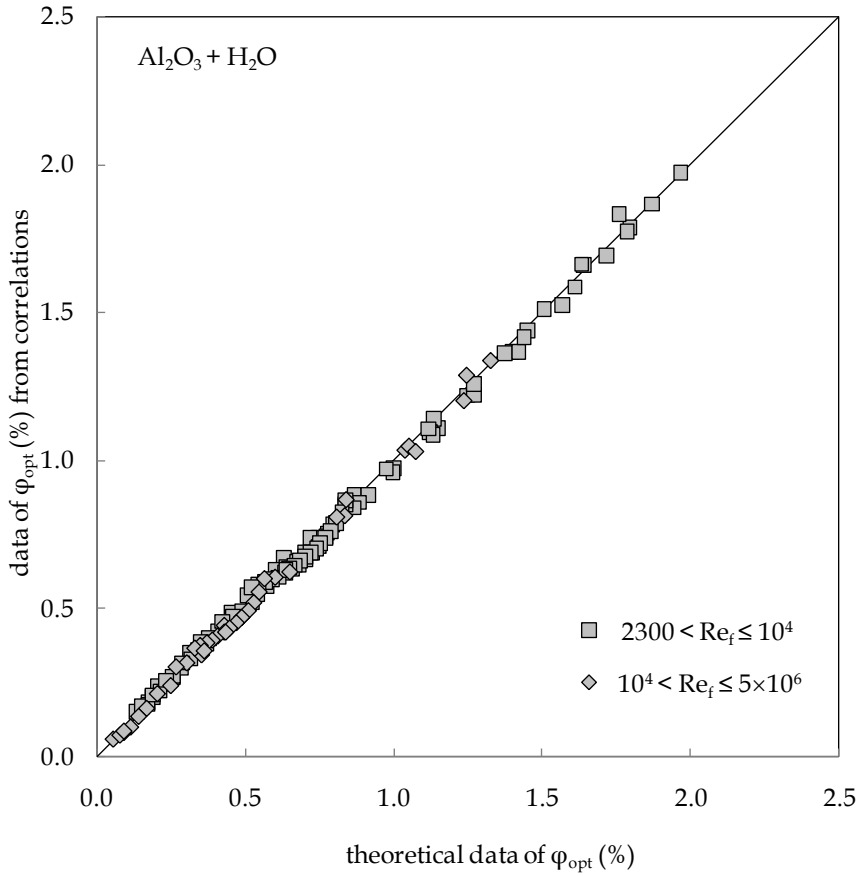

Fig. 4.18 – Comparison between eqs. (4.29)–(4.30) and the theoretical data of φ_{opt} (%).

4.4 Results and Discussion - Friction losses at constant heat transfer rate

The results obtained for the relative friction loss diminution at constant heat transfer rate will now be presented and discussed.

4.4.1 Laminar pipe flow

Four sets of distributions of the percentage values of δ_{fl} vs. φ are displayed in Figs. 4.19–4.22 for different values of d_p, T_m, Re_f and L/D, respectively.

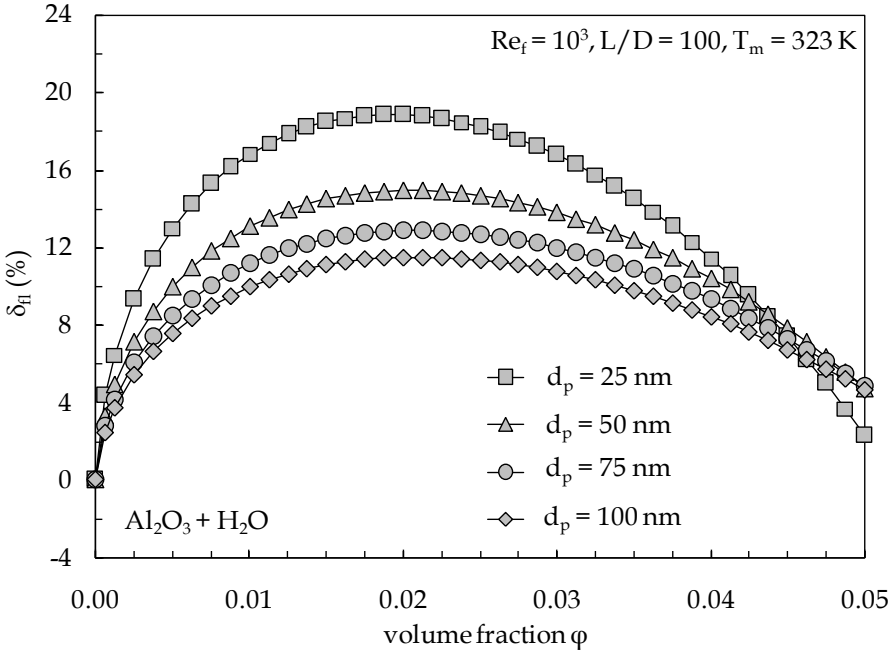

Fig. 4.19 – Distributions of δ_{fl}(%) vs. φ with d_p as a parameter.

Based on these figures, two considerations deserve to be mentioned. First, as expected, the trends of the distributions of δ_{fl} vs. φ are the same as those of the distributions of ε_q vs. φ, which means that the friction loss diminution at constant heat transfer rate has a peak at an optimal particle loading $\varphi_{fl\text{-}opt}$. Moreover, it may be noticed that δ_{fl} is higher than ε_q for $\varepsilon_q > 0$, and lower than ε_q for $\varepsilon_q < 0$. Second, for any fixed situation, i.e., for any assigned combination of the values of the independent variables d_p, T_m, L/D and Re_f, the optimal particle loading $\varphi_{q\text{-}opt}$ is larger than $\varphi_{fl\text{-}opt}$. However, it must

be said that the average percentage difference between $\varphi_{q\text{-}opt}$ and $\varphi_{fl\text{-}opt}$ is of the order of 5%, which leads to the conclusion that the optimal formulation of the nanofluid is almost independent of what criterion is used to evaluate the nanofluid energetic performance.

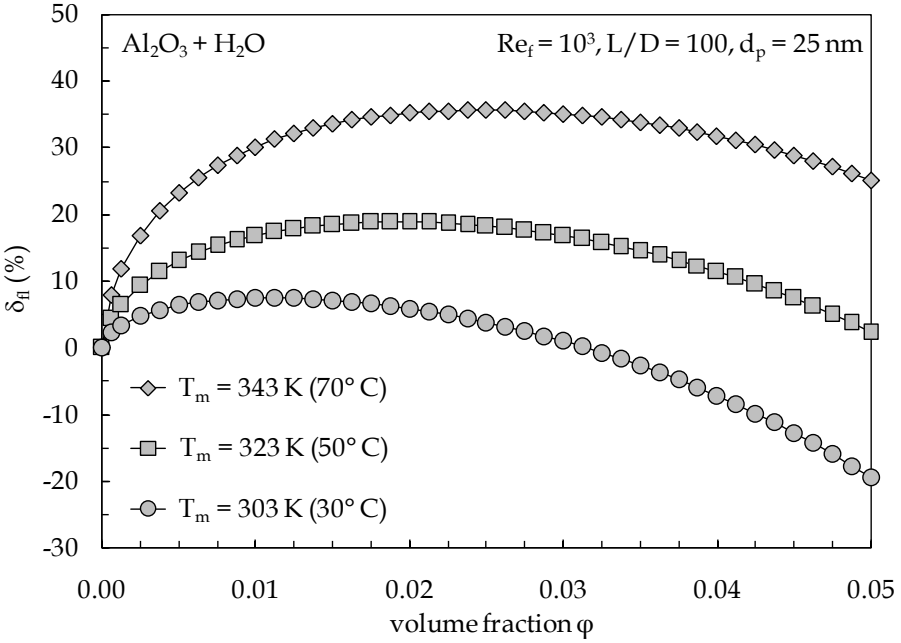

Fig. 4.20 – Distributions of δ_{fl}(%) vs. φ with T_m as a parameter.

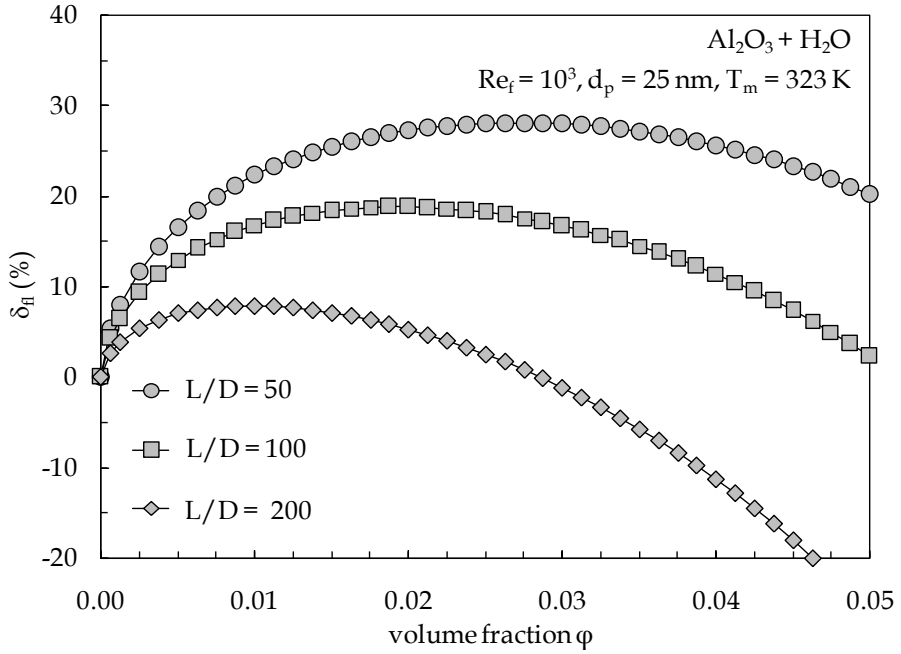

Fig. 4.21 – Distributions of δ_{fl}(%) vs. φ with L/D as a parameter.

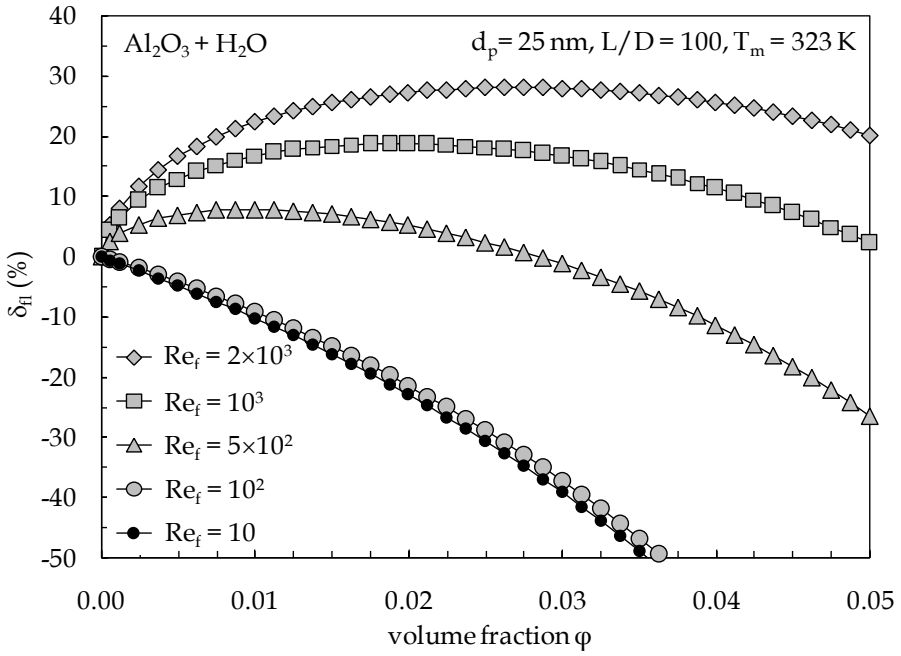

Fig. 4.22 – Distributions of δ_{fl}(%) vs. φ with Re_f as a parameter.

4.4.2 Turbulent pipe flow

The distributions of the percentage values of δ_{fl} vs. φ are displayed in Figs. 4.23–4.26. The analysis of these figures leads at the same conclusions discussed in the previous paragraph.

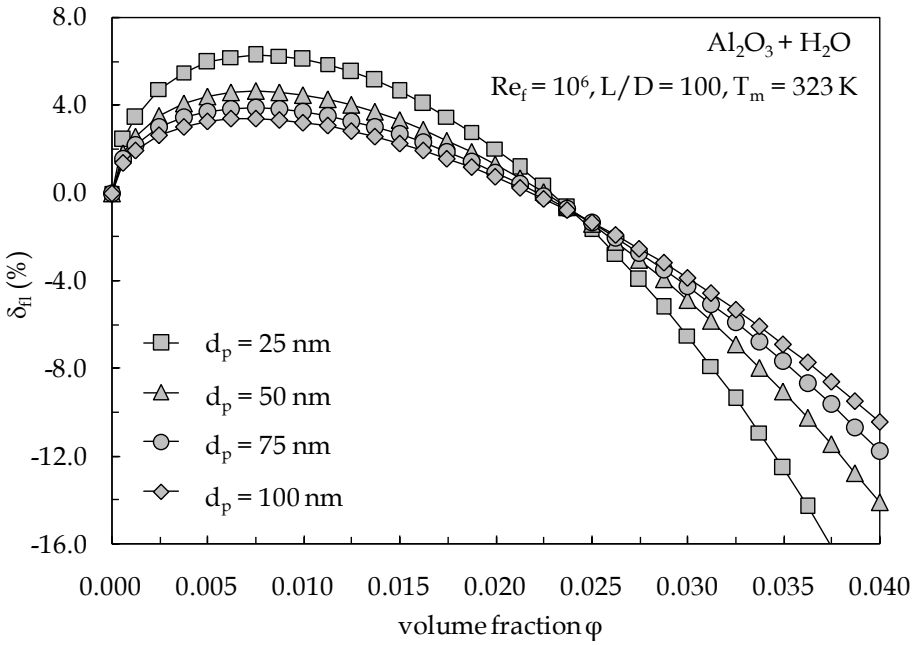

Fig. 4.23 – Distributions of δ_{fl}(%) vs. φ with d_p as a parameter.

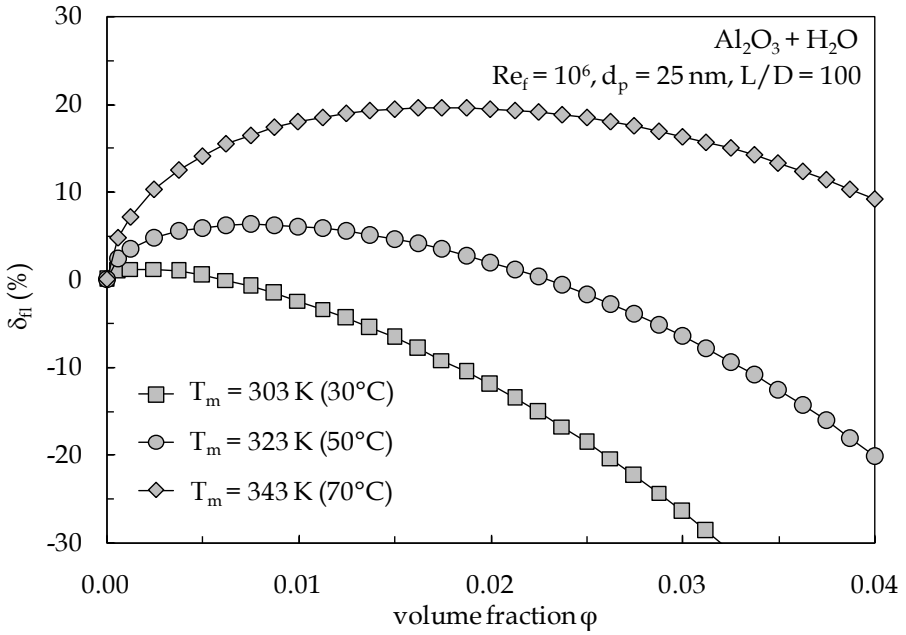

Fig. 4.24 – Distributions of $\delta_{fl}(\%)$ vs. φ with T_m as a parameter.

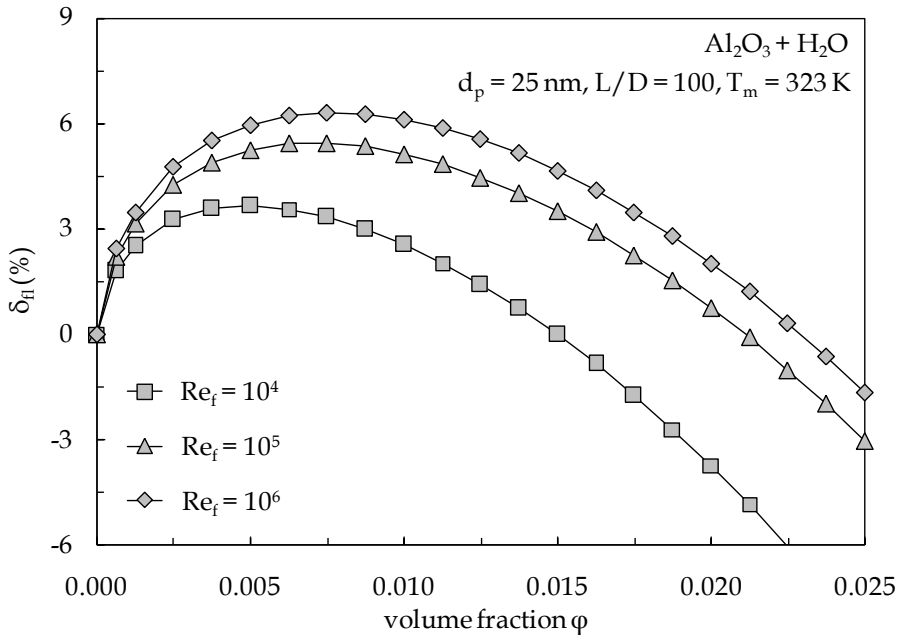

Fig. 4.25 – Distributions of $\delta_{fl}(\%)$ vs. φ with Re_f as a parameter.

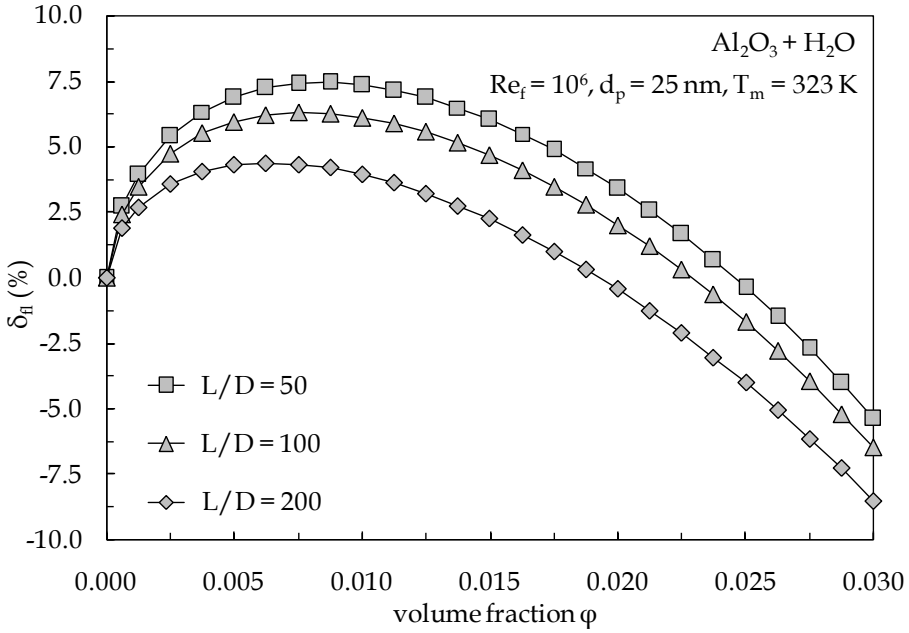

Fig. 4.26 – Distributions of δ_{fl}(%) vs. φ with L/D as a parameter.

At this stage, with the aim to explain these results, it is important to point out that the values of the two parameters R_q and R_{fl} previously introduced in eqs. (4.21)–(4.22) and (4.27) are practically the same whatever are the values of d_p, T_m, Re_f and L/D, as shown in Fig. 4.27 for two given situations. Thus, if we assume $R_q = R_{fl}$, the combination of eqs. (4.21) and (4.27) yields the relation:

$$\delta_{fl} = 1 - \left(\frac{1}{\varepsilon_q + 1} \right)^{(3-\alpha)} , \tag{4.31}$$

according to which, for assigned values of d_p, T_m, Re_f and L/D, at any nanoparticle concentration φ the absolute value of δ_{fl} is higher than the absolute value of ε_q, and the peaks for δ_{fl} and ε_q occur at the same optimal volume fraction, that we can denote as φ_{opt}.

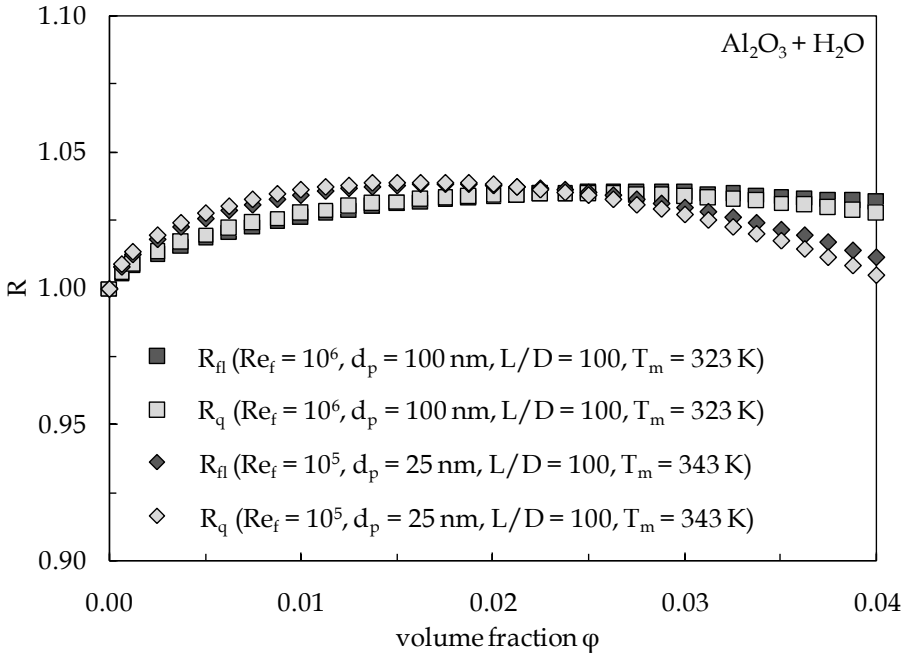

Fig. 4.27 – Distributions of R_q and R_{fl} vs. φ for two different situations.

4.5 Results and Discussion - Effects of the solid–liquid combination

The effects of the solid–liquid combination on the relative heat transfer enhancement at constant driving power and on the relative friction loss diminution at constant heat transfer rate are now discussed.

4.5.1 Laminar pipe flow

The distributions of ε_q(%) vs. φ and δ_{fl}(%) vs. φ for different solid–liquid combinations are displayed in Figs. 4.28 and 4.29 (in both figures EG stands for ethylene glycol). It is apparent that the effect of the base fluid is definitely more pronounced than that of the nanoparticle material. Such major dependence on the base liquid can be explained by recalling that the energetic performance of nanofluids is a consequence of the conflict between the effects of the increased thermal conductivity and the increased dynamic viscosity. This means that the performance of the nanofluid relative to the base liquid depends principally on both the thermal conductivity ratio k_n/k_f and the dynamic viscosity ratio μ_n/μ_f. Hence, taking into account that k_n/k_f depends very little on the

nanoparticle material, whereas μ_n / μ_f is completely independent of the nanoparticle material, we can conclude that ε_q and δ_{fl} are affected much more by the liquid phase than by the solid phase. Obviously, since the thermal conductivity of ethylene glycol is less than one-half of the thermal conductivity of water, the effect produced by the addition of nanoparticles to the base liquid is more marked for ethylene glycol than for water. Moreover, since the dynamic viscosity of ethylene glycol is at least one order of magnitude higher than the dynamic viscosity of water, for ethylene glycol-based nanofluids the growth of the effective viscosity starts becoming excessive in comparison with the growth of the effective thermal conductivity at a larger volume fraction. Therefore, for assigned values of d_p, T_m, Re_f and L/D, the optimal particle loadings of ethylene glycol-based nanofluids are higher than those of water-based nanofluids.

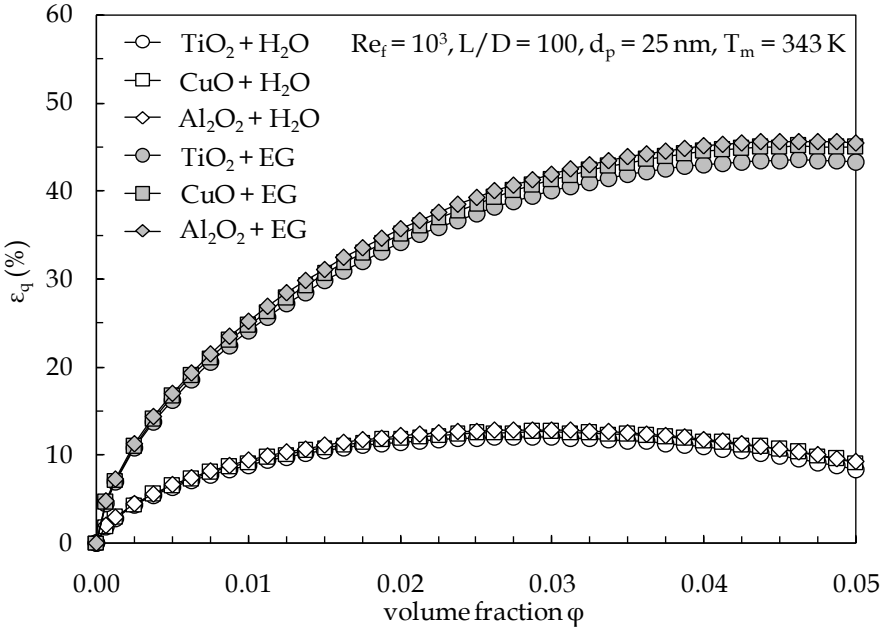

Fig. 4.28 – Distributions of ε_q (%) vs. φ for different solid–liquid combinations.

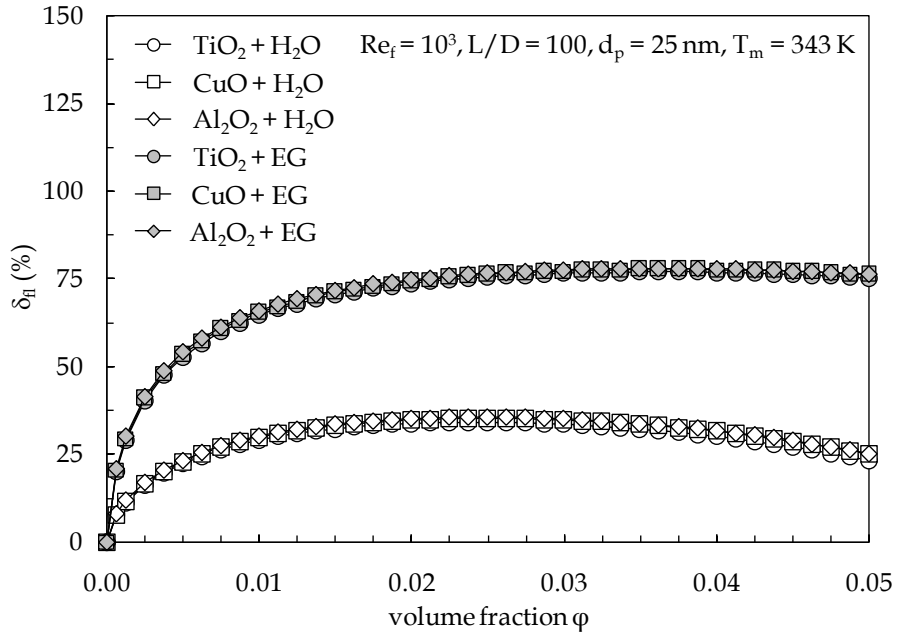

Fig. 4.29 – Distributions of δ_{fl} (%) vs. φ for different solid–liquid combinations.

4.5.2 Turbulent pipe flow

The distributions of ε_q(%) vs. φ and δ_{fl}(%) vs. φ for different solid–liquid combinations are displayed in Figs. 4.30 and 4.31 (in both figures EG stands for ethylene glycol).

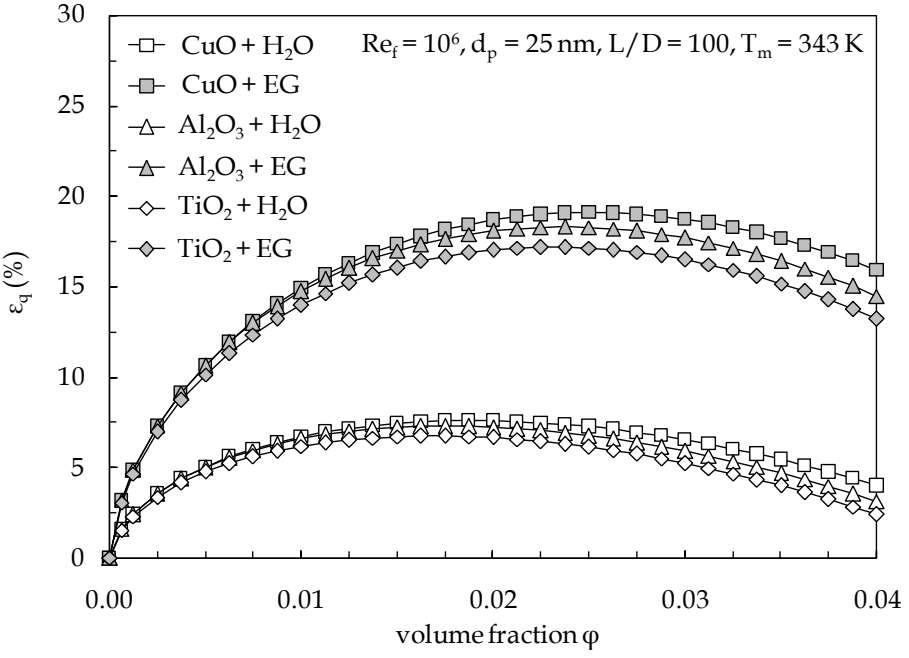

Fig. 4.30 – Distributions of ε_q (%) vs. φ for different solid–liquid combinations.

The curves have the same trends of those obtained for laminar regime, therefore the deductions that can be reached are equivalent.

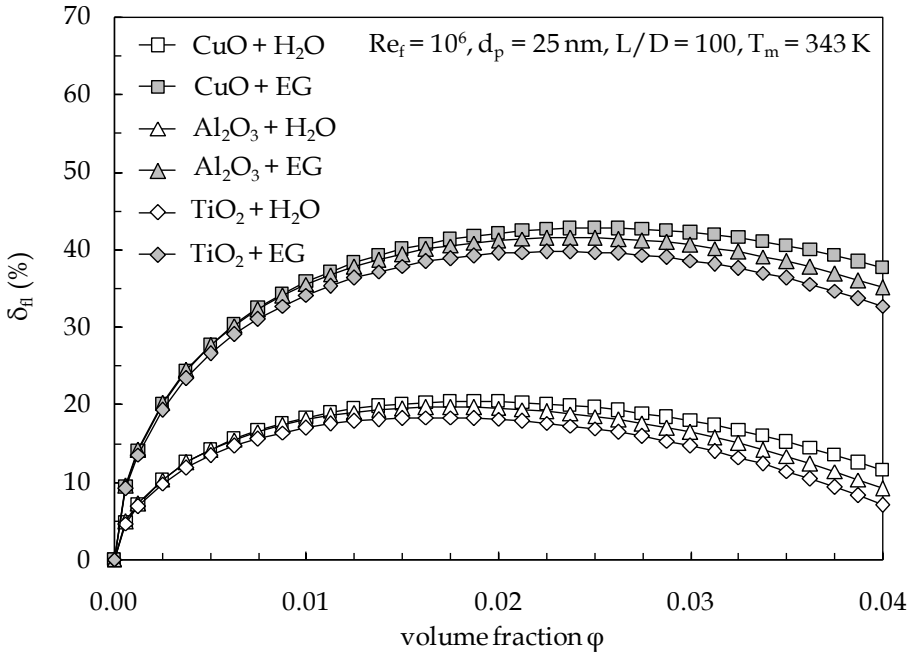

Fig. 4.31 – Distributions of δ_{fl} (%) vs. φ for different solid–liquid combinations.

4.6 Summary of the main results

The main results obtained may be summarized as follows:

(a) The relative heat transfer enhancement at constant driving power and the relative friction loss diminution at constant heat transfer rate increase with increasing the nanoparticle volume fraction up to an optimal particle loading; excessive increases of the volume fraction above such optimal value may bring to remarkable deteriorations of the heat transfer rate or exaggerate magnifications of the friction loss with respect to the reference case of pure base liquid; for the laminar flow regime, when the Reynolds number of the base fluid is as low as 10^1–10^2, the dispersion of

nanoparticles into the base liquid has always a negative effect that increases noteworthy with increasing the concentration of the suspended nanoparticles.

(b) The optimal particle loading for maximum heat transfer at constant driving power is practically the same as that for minimum cost of operation at constant heat transfer rate; for any assigned combination of solid and liquid phases, such optimal volume fractions increase as the nanofluid bulk temperature is increased, the length-to-diameter ratio of the pipe is decreased, and the Reynolds number of the base fluid is increased; as far as the diameter of the suspended nanoparticles is concerned, the optimal volume fraction is practically independent of the nanoparticle size in the turbulent flow regime and in the low-temperature range of the laminar flow regime, whilst it increases with increasing the nanoparticle diameter in the high-temperature range of the laminar flow regime.

(c) When different nanofluids are considered, the relative heat transfer enhancement at constant pumping power and the relative friction loss diminution at constant heat transfer rate, as well as the optimal particle loadings, depend substantially on the base liquid and very little on the nanoparticle material.

References

[1] W. Yu, D. M. France, J. L. Routbort, S. U. S. Choi, Review and comparison of nanofluid thermal conductivity and heat transfer enhancements, Heat Transfer Engineering 29 (2008) 432-460.

[2] S. Kakaç, A. Pramuanjaroenkij, Review of convective heat transfer enhancement with nanofluid, Int. J. Heat Mass Transfer 52 (2009) 3187-3196.

[3] L. Godson, B. Raja, D. Mohan Lal, S. Wongwises, Enhancement of heat transfer using nanofluids – An overview, Renew. Sustain. Energy Reviews 14 (2010) 629-641.

[4] B. C. Pak, Y. I. Cho, Hydrodynamic and heat transfer study of dispersed fluids with submicron metallic oxide particles, Exp. Heat Transfer 11 (1998) 151-170.

[5] Y. Xuan, Q. Li, Investigation on convective heat transfer and flow features of nanofluids, J. Heat Transfer 125 (2003) 151-155.

[6] S. E. B. Maïga, C. T. Nguyen, N. Galanis, G. Roy, Heat transfer behaviours of nanofluids in a uniformly heated tube, Superlattices and Microstructures 35 (2004) 543-557.

[7] A. Behzadmehr, M. Saffar-Avval, N. Galanis, Prediction of turbulent forced convection of a nanofluid in a tube with uniform heat flux using a two phase approach, Int. J. Heat Fluid Flow 28 (2007) 211-219.

[8] W. Williams, J. Buongiorno, L. W. Hu, Experimental investigation of turbulent convective heat transfer and pressure loss of alumina/water and zirconia/water nanoparticle colloids (nanofluids) in horizontal tubes, J. Heat Transfer 130 (2008) paper No. 042412.

[9] V. Bianco, O. Manca, S. Nardini, Numerical investigation on nanofluids turbulent convection heat transfer inside a circular tube, Int. J. Thermal Sciences 50 (2011) 341-349.

[10] L. Gosselin, A. K. da Silva, Combined "heat transfer and power dissipation" optimization of nanofluid flows, Appl. Phys. Lett. 85 (2004) 4160-4162.

[11] R. B. Mansour, N. Galanis, C. T. Nguyen, Effect of uncertainties in physical properties on forced convection heat transfer with nanofluids, Applied Thermal Engineering 27 (2007) 240-249.

[12] P. W. Dittus, L. M. K. Boelter, Heat transfer in automobile radiators of the tubular type, Univ. Calif. Publ. Eng. 2 (1930) 443-461.

[13] V. Gnielinski, Forced convection in ducts, in: G. F. Hewitt (Ed.), Heat Exchanger Design Handbook, Begell House Inc., New York (1998) 2.5.1-1–2.5.1-13.

[14] C.-H. Chen, Forced convection heat transfer in microchannel heat sinks, Int. J. Heat Mass Transfer 50 (2007) 2182-2189.

[15] N. Tsuzuki, M. Utamura, T. L. Ngo, Nusselt number correlations for a microchannel heat exchanger hot water supplier with S-shaped fins, Applied Thermal Engineering 29 (2009) 3299-3308.

[16] T. J. John, B. Mathew, H. Hegab, Parametric study on the combined thermal and hydraulic performance of single-phase micro pin-fin heat sinks part I: Square and circle geometries, Int. J. Thermal Sciences 49 (2010) 2177-2190.

[17] Y. Liu, J. Cui, Y. X. Jiang, W. Z. Li, A numerical study on heat transfer performance of microchannels with different surface microstructures, Applied Thermal Engineering 29 (2009) 3299-3308.

[18] M. Kalteh, A. Abbassi, M. Saffar-Avval, A. Friins, A. Darhuber, J. Harting, Experimental and numerical investigation of nanofluid forced convection inside a wide microchannel heat sink, Applied Thermal Engineering 36 (2012) 260-268.

[19] D. Wen, Y. Ding, Experimental investigation into convective heat transfer of nanofluids at the entrance region under laminar flow conditions, Int. J. Heat Mass Transfer 47 (2004) 5181-5188.

[20] D. Kim, Y. Kwon, Y. Cho, C. Li, S. Cheong, Y. Hwang, J. Lee, D. Hong, S. Moon, Convective heat transfer characteristics of nanofluids under laminar and turbulent flow conditions, Current Appl. Phys. 9 (2009) e119-e123.

[21] N. A. Roberts, D. G. Walker, Convective performance of nanofluids in commercial electronic cooling systems, Applied Thermal Engineering 30 (2010) 2499-2504.

[22] D. Liu, L. Yu, Single-phase thermal transport of nanofluids in a minichannel, J. Heat Transfer 133 (2011) paper No. 031009.

[23] C. J. Ho, J. B. Huang, P. S. Tsai, Y. M. Yang, Water-based suspensions of Al_2O_3 nanoparticles and MEPCM particles on convection effectiveness in a circular tube, Int. J. Thermal Sciences 50 (2011) 736-748.

[24] K. B. Anoop, T. Sundararajan, S. K. Das, Effect of particle size on the convective heat transfer in nanofluid in the developing region, Int. J. Heat Mass Transfer 52 (2009) 2189-2195.

[25] U. Rea, T. McKrell, L.-W. Hu, J. Buongiorno, Laminar convective heat transfer and viscous pressure loss of alumina-water and zirconia-water nanofluids, Int. J. Heat Mass Transfer 52 (2009) 2042-2048.

[26] K. S. Hwang, S. P. Jang, S. U. S. Choi, Flow and convective heat transfer characteristics of water-based Al_2O_3 nanofluids in fully developed laminar flow regime, Int. J. Heat Mass Transfer 52 (2009) 193-199.

[27] W. Y. Lai, S. Vinod, P. E. Phelan, R. Prasher, Convective heat transfer for water-based alumina nanofluids in a single 1.02-mm tube, J. Heat Transfer 131 (2009) paper No. 112401.

[28] Y.-H. Hung, T.-P. Teng, T.-C. Teng, J.-H. Chen, Assessment of heat dissipation performance for nanofluid, Applied Thermal Engineering 32 (2012) 132-140.

[29] Y. He, Y. Men, Y. Zhao, H. Lu, Y. Ding, Numerical investigation into the convective heat transfer of TiO_2 nanofluids flowing through a straight tube under the laminar flow conditions, Applied Thermal Engineering 29 (2009) 1965-1972.

[30] V. Bianco, F. Chiacchio, O. Manca, S. Nardini, Numerical investigation of nanofluids forced convection in circular tubes, Applied Thermal Engineering 29 (2009) 3632-3642.

[31] E. Ebrahimnia-Bajestan, H. Niazmand, W. Duangthongsuk, S. Wongwises, Numerical investigation of effective parameters in convective heat transfer of nanofluids flowing under a laminar flow regime, Int. J. Heat Mass Transfer 54 (2011) 4376-4388.

[32] Hwang, K. S., Jang, S. P., Choi, S. U. S., 2009, "Flow and convective heat transfer characteristics of water-based Al_2O_3 nanofluids in fully developed laminar flow regime", Int. J. Heat Mass Transfer, 52, pp. 193–199.

[33] Rea, U., McKrell, T., Hu, L.-W., Buongiorno, J., 2009, Laminar convective heat transfer and viscous pressure loss of alumina-water and zirconia-water nanofluids, Int. J. Heat Mass Transfer, 52, pp. 2042–2048.

[34] Pak, B. C., Cho, Y. I., 1998, "Hydrodynamic and heat transfer study of dispersed fluids with submicron metallic oxide particles", Exp. Heat Transfer, 11, pp. 151–170.

[35] Williams, W., Buongiorno, J., Hu, L. W., 2008, "Experimental investigation of turbulent convective heat transfer and pressure loss of alumina/water and zirconia/water nanoparticle colloids (nanofluids) in horizontal tubes", J HEAT TRANS-T ASME, 130, 042412.

[36] Dittus, P. W., Boelter, L. M. K., 1930, "Heat transfer in automobile radiators of the tubular type", Univ. Calif. Publ. Eng., 2, pp. 443–461.

[37] Blasius, H., 1913, Forschungsarb. Ver. Deutsch. Ing., 131.

[38] Moody, L. F., 1944, "Friction factors for pipe flow", Trans. ASME, 66, pp. 671–684.

[39] Sommers, A. D., Yerkes, K. L., 2009, "Experimental investigation into the convective heat transfer and system-level effects of Al_2O_3-propanol nanofluid", J. Nanopart. Res., 12, pp. 1003–1014.

[40] Seider, E. N., Tate, G. E., 1936, "Heat transfer and pressure drop of liquids in tubes", Ind. Eng. Chem., 28, pp. 1429–1436.

[41] Gnielinski, V., 1976, "New equations for heat and mass transfer in turbulent pipe and channel flow", Int. Chem. Eng., 16, pp. 359–368.

[42] Chang, B. H., Mills, A. F., Hernandez, E., 2008, "Natural convection of microparticle suspensions in thin enclosures", Int. J. Heat Mass Transfer, 51, pp. 1332–1341.

[43] Hausen, H., 1959, "Neue Gleichungen fur die Warmeubertragung bei freier oder erzwungener Stromung", Allg. Waermetech., 9, pp. 75–79.

[44] Gnielinski, V., 1998, "Forced convection in ducts", in: G. F. Hewitt (Ed.), Heat Exchanger Design Handbook, Begell House Inc., New York, pp. 2.5.1-1–2.5.1-13.

[45] Bejan, A., 2004, Convection Heat Transfer, 3rd ed., Wiley, Hoboken, NJ.

[46] Filonenko, G. K., 1954, "Hydraulic resistance in pipes", Teploenergetika, 1, pp. 40–44.

CONCLUSIONS

The energetic performance of nanofluids has been studied both theoretically and numerically for a number of situations involving either buoyancy-induced convection flows or forced convection pipe flows. To do this, I relied on a pair of new equations to predict the nanofluid effective thermal conductivity and dynamic viscosity, which were developed by the research team which I collaborated with during my PhD internship, and I further validated by means of relations and experimental data available in the literature.

The main results achieved for natural convection flows can be summarized as follows:

1) the heat transfer enhancement increases with increasing the nanoparticle concentration up to an optimal particle loading at which the heat transfer rate has a peak;
2) excessive increases of the nanoparticle concentration above the optimal value may bring to remarkable deteriorations of the heat transfer rate with respect to the reference case of the pure base liquid;
3) the optimal particle loading is not so much sensitive to the nanoparticle average size, while increases markedly as the nanofluid average temperature increases;
4) the maximum heat transfer enhancement increases as the nanoparticle size decreases and the nanofluid average temperature increases;
5) when different combinations of solid and liquid phases are considered, the effects of the base fluid on both the heat transfer enhancement and the optimal particle loading are much more pronounced than those of the nanoparticle material.

The main results obtained for forced convection pipe flows can be condensed as follows:

1) the heat transfer enhancement at constant driving power and the friction loss diminution

at constant heat transfer rate increase with increasing the nanoparticle concentration up to an optimal particle loading;

2) excessive increases of the nanoparticle concentration above the optimal value may bring to remarkable deteriorations of the heat transfer rate or exaggerate magnifications of the friction loss with respect to the reference case of the pure base liquid, with the exception of situations featured by values of the Reynolds number of the base fluid as low as 10^1–10^2, for which the dispersion of nanoparticles into the base liquid has always a negative effect that increases noteworthy with increasing the concentration of the suspended nanoparticles;
3) the optimal particle loading for maximum heat transfer at constant driving power is practically the same as that for minimum cost of operation at constant heat transfer rate;
4) for any assigned combination of solid and liquid phases, the optimal particle loading increases as the nanofluid bulk temperature is increased, the length-to-diameter ratio of the pipe is decreased, and the Reynolds number of the base fluid is increased;
5) for any assigned combination of solid and liquid phases, the optimal particle loading is practically independent of the nanoparticle size in the turbulent flow regime and in the low-temperature range of the laminar flow regime, while it increases with increasing the size of the suspended nanoparticles in the high-temperature range of the laminar flow regime;
6) when different combinations of solid and liquid phases are considered, the relative heat transfer enhancement at constant pumping power and the relative friction loss diminution at constant heat transfer rate, as well as the optimal particle loading, depend substantially on the base liquid and very little on the nanoparticle material.

In conclusion, I think that a lot of work has still to be done on nanofluids, new theories have to be developed and further measurements have to be executed to properly define their effective properties, as well as many more numerical and experimental studies have to be

performed to understand how beneficial is their use as heat transfer fluids. Indeed, I believe that my researches contributed to open the way to the possibility of determining an optimal formulation of nanofluids in relation to their specific cooling application, which may will have its own importance in the promotion of new strategies for the rational use of energy.

Nomenclature

b gap width

c specific heat at constant pressure

D diameter

D_B Brownian diffusion coefficient

D_E Einstein diffusion coefficient

D_T thermophoretic diffusion coefficient

d_f equivalent diameter of a base fluid molecule

d_p nanoparticle diameter

E heat transfer enhancement

F friction loss

f_F Fanning friction factor

G mass flow rate

g gravity vector

h coefficient of convection

I unit tensor

J_p nanoparticle diffusion mass flux

k thermal conductivity

k_b Boltzmann constant = $1.38066 \cdot 10^{-23}$ $J K^{-1}$

L tube lenght

Le Lewis number

M molecular weight of the base fluid

m nanoparticle mass fraction

N Avogadro number = $6.022 \cdot 10^{23}$ mol^{-1}

Nu Nusselt number

p pressure

Pr Prandtl number

Q heat flux

q heat transfer rate

Ra Rayleigh number

Ra_b Rayleigh number based on the gap width

Re_p nanoparticle Reynolds number

Sh Sherwood number

T temperature

T_i inner fluid temperature

T_o outlet fluid temperature

T_w wall temperature

T_m bulk temperature

t time

u_B nanoparticle Brownian velocity

U_{max} maximum horizontal velocity component

V velocity vector

V average fluid velocity

V_{max} maximum vertical velocity component

W width of the enclosure

x horizontal Cartesian coordinate

y vertical Cartesian coordinate

Greek symbols

δ_{fl} relative friction loss diminution

ε_q relative heat transfer enhancement

β coefficient of thermal expansion

φ nanoparticle volume fraction

μ dynamic viscosity

ρ mass density

τ stress tensor

τ_D time required to cover a distance d_p moving at velocity u_B

Subscripts

av average

c cooled sidewall, at the temperature of the cooled sidewall

f base fluid

fr freezing point of the base fluid

h heated sidewall, at the temperature of the heated sidewall

i inner cylinder

max maximum value

min minimum value

n nanofluid

o outer cylinder

opt optimal value

ref reference state for the calculation of the thermophysical properties

S solute

s solid phase

T thermal

w plate surface

∞ undisturbed fluid reservoir